

CONTROL OF A HELICOPTER DURING AUTOROTATION

A THESIS SUBMITTED TO
THE GRADUATE SCHOOL OF NATURAL AND APPLIED SCIENCES
OF
MIDDLE EAST TECHNICAL UNIVERSITY

BY

KAAN ŞANSAL

IN PARTIAL FULFILLMENT OF THE REQUIREMENTS
FOR
THE DEGREE OF MASTER OF SCIENCE
IN
MECHANICAL ENGINEERING

JUNE 2018

Approval of the thesis:

CONTROL OF A HELICOPTER DURING AUTOROTATION

submitted by **KAAN ŞANSAL** in partial fulfillment of the requirements for the degree of **Master of Science in Mechanical Engineering Department, Middle East Technical University** by,

Prof. Dr. Halil Kalıpçılar
Dean, Graduate School of **Natural and Applied Sciences**

Prof. Dr. M. A. Sahir Arıkan
Head of Department, **Mechanical Engineering**

Assoc. Prof. Dr. E. İlhan Konukseven
Supervisor, **Mechanical Engineering Dept., METU**

Asst. Prof. Dr. Volkan Nalbantoğlu
Co-Supervisor, **School of Civil Aviation, Atılım University**

Examining Committee Members:

Assoc. Prof. Dr. Yiğit Yazıcıoğlu
Mechanical Engineering Dept., METU

Assoc. Prof. Dr. E. İlhan Konukseven
Mechanical Engineering Dept., METU

Asst. Prof. Dr. Ali Emre Turgut
Mechanical Engineering Dept., METU

Asst. Prof. Dr. A. Buğra Koku
Mechanical Engineering Dept., METU

Asst. Prof. Dr. Volkan Nalbantoğlu
School of Civil Aviation, Atılım University

Date: 25.06.2018

I hereby declare that all information in this document has been obtained and presented in accordance with academic rules and ethical conduct. I also declare that, as required by these rules and conduct, I have fully cited and referenced all material and results that are not original to this work.

Name, Last Name: KAAN ŞANSAL

Signature :

ABSTRACT

CONTROL OF A HELICOPTER DURING AUTOROTATION

Şansal, Kaan

M.S., Department of Mechanical Engineering

Supervisor: Assoc. Prof. Dr. Erhan İlhan Konukseven

Co-Supervisor: Asst. Prof. Dr. Volkan Nalbantoğlu

June 2018, 105 pages

Autorotation is a maneuver that requires no power and it is used in rotorcrafts when last operating engine is lost. It is an extremely complex state of flight and landing successfully after total power loss requires considerable skill. Main idea behind autorotation is that, by descending with a controlled rate, available potential energy is used as a source that turns main rotor at desired speed for providing thrust and flight control. Just before touchdown, ground speed and descent rate must be reduced for safe landing which can only be possible by managing available energy effectively.

In this study, an autonomous autorotation controller is developed and implemented to a real-time high fidelity mathematical model of a full-scale light utility helicopter. For developing autorotation controller that consists of a standard inner-outer loop architecture, full linear and reduced order linear models are used which are obtained by linearizing and reducing the order of non-linear helicopter model around different trim points. While designing the outermost loop, autorotation maneuver is divided into five different phases (steady state descent, preflare, flare, landing and touchdown) and different controllers are developed for each of these phases. Collective commands

generated from these controllers are blended using fuzzy transitions. These outer-loop controllers also generate references for velocity tracking controllers which provides attitude references to the inner loop attitude hold controllers. While designing attitude and heading hold controllers, Aeronautical Design Standard 33E-PRF (ADS-33E-PRF) specifications are used as a guideline for evaluation of helicopter handling qualities. Details of linearization and model order reduction techniques that are used during the study are expressed. Comparison results of non-linear and linearized models are presented together with details of control law formation. For assessing performance of the autorotation controller, real-time simulation results of integrated high-fidelity model are provided from different initial flight conditions. Results demonstrate the capability of the proposed controller for achieving safe power-off landings.

Keywords: Helicopter Flight Dynamics, Autorotation Controller, Power-off Landing, Linearization, Model Order Reduction, ADS-33

ÖZ

HELİKOPTERİN OTOROTASYON SIRASINDA KONTROLÜ

Şansal, Kaan

Yüksek Lisans, Makina Mühendisliği Bölümü

Tez Yöneticisi: Doç. Dr. Erhan İlhan Konukseven

Ortak Tez Yöneticisi: Dr. Volkan Nalbantoğlu

Haziran 2018, 105 sayfa

Otorotasyon güç gerektirmeyen bir manevradır ve rotorlu araçlarda çalışan son motorun kaybedilmesi durumunda kullanılır. Oldukça zor bir uçuş koşuludur ve güç kaybından sonra yere başarıyla inmek önemli ölçüde yetenek gerektirir. Otorotasyonun arkasındaki ana fikir, kontrollü bir hızla çökerken, mevcut potansiyel enerjiyi ana rotoru istenen hızda döndüren bir kaynak olarak kullanarak, itki ve uçuş kontrolü sağlamaktır. Yere değmeden hemen önce, yer hızı ve çöküş hızı güvenli bir iniş yapabilmek adına azaltılmalıdır ve bu sadece mevcut enerjiyi etkili bir şekilde kullanarak mümkündür.

Bu çalışmada, otonom bir otorotasyon kontrolcüsü geliştirilmiş ve gerçek zamanlı çalışan yüksek doğruluk oranına sahip tam ölçekli hafif genel maksat helikopterinin matematiksel modeline uygulanmıştır. Standard iç ve dış çevrim mimarisine sahip otorotasyon kontrolcüsü geliştirilirken, doğrusal olmayan helikopter modelini farklı denge noktaları etrafında doğrusallaştırarak ve indirgeyerek elde edilen tam doğrusal ve indirgenmiş doğrusal modeller kullanılmıştır. En dış çevrim tasarlanırken, otorotasyon manevrası 5 farklı faza ayrılmış (kararlı durumda çöküş, flare öncesi,

flare, yere iniş, yere dokunuş) ve her bir faz için ayrı kontrolcüler tasarlanmıştır. Bu kontrolcüler tarafından yaratılan kolektif komutları, bulanık geçişler kullanılarak harmanlanmaktadır. Bu dış çevrim kontrolcüleri ayrıca hız takip kontrolcüsüne referans üretmekte ve bunlar da durum açılarını tutan iç çevrim kontrolcülerine açı referansları sağlamaktadır. Durum açılarını ve baş açısını tutan kontrolcüler tasarlanırken, Havacılık Dizayn Standartları 33E-PRF (ADS-33E-PRF) gereksinimleri, helikopterin uçuş kalitesini değerlendirebilmek adına kılavuz olarak kullanılmıştır. Çalışmada kullanılan doğrusallaştırma ve model derecesi indirgeme tekniklerinin detayları anlatılmaktadır. Doğrusal olmayan ve doğrusallaştırılmış modellerin karşılaştırma sonuçlarıyla birlikte kontrol yasalarının formasyonu sunulmaktadır. Otorotasyon kontrolcüsünün performansını değerlendirmek için, entegre edilmiş yüksek doğruluk oranına sahip modelin farklı başlangıç koşullarındaki gerçek zamanlı simülasyon sonuçları verilmiştir. Sonuçlar, önerilen kontrolcünün güç olmadan emniyetli bir şekilde yere inişler başarabildiğini göstermektedir.

Anahtar Kelimeler: Helikopter Uçuş Dinamiği, Otorotasyon Kontrolcüsü, Güç Olmadan İniş, Doğrusallaştırma, Model Derecesini İndirgeme, ADS-33

To my family and love,

ACKNOWLEDGMENTS

The author would like to express his deepest gratitude to his thesis supervisor Assoc. Prof. Dr. E. İlhan Konukseven and co-supervisor Asst. Prof. Dr. Volkan Nalbantođlu for their guidance and feedbacks throughout this thesis work.

The author wishes to express his special thanks to his supervisor Volkan Kargin at Turkish Aerospace Industries, for his support, motivation, technical assistance, and suggestions on the thesis subject.

The author is also grateful to his colleagues Ilgaz Dođa Okçu, İsmail Hakkı Şahin, Umut Türe, Göktuđ Koçak, Arda Çalıřkan and Mustafa Gürler for their friendship, support and advices.

Finally, the author would like to thank to his wife Selay Fırtına Şansal and to his parents Cornelia Maria and Erol Şansal, for their endless love, encouragement, patience and support.

TABLE OF CONTENTS

ABSTRACT	v
ÖZ.....	vii
ACKNOWLEDGMENTS	x
TABLE OF CONTENTS	xi
LIST OF TABLES	xiv
LIST OF FIGURES	xv
LIST OF SYMBOLS & ABBREVIATIONS	xix
CHAPTERS	
1 INTRODUCTION.....	1
1.1 Background and Motivations of Research (Literature review)	1
1.2 Helicopter Flight Control System.....	4
1.3 Indications of Power Failure	6
1.4 Aerodynamics of Autorotation	8
1.5 Research Objectives	11
1.6 Outline of Thesis	12
2 TOROS.....	13
3 LINEARIZATION AND MODEL ORDER REDUCTION	17
3.1 Linearization.....	17
3.2 Model Order Reduction.....	20

3.2.1	Modal Truncation	21
3.2.2	Matched DC Gain Method	22
3.3	Comparison of Non-linear, Full-Linear and Reduced Linear Models.....	22
4	AUTOROTATION CONTROLLER	29
4.1	Introduction	29
4.2	Flight Control Requirements	30
4.2.1	Small-Amplitude Pitch (Roll) Attitude Changes	30
4.2.2	Small-Amplitude Yaw Attitude Changes.....	33
4.2.3	Character of Attitude and Heading Hold Response Types	33
4.2.4	Transient Response of Attitude Hold Response Types	33
4.3	Control Law Formulation	34
4.3.1	Inner Loop Controller Design	34
4.3.2	Attitude Command Attitude Hold (ACAH) and Heading Hold (HH) Controllers Design	49
4.3.3	Longitudinal Speed Controller Design.....	63
4.3.4	Gain Scheduling	66
4.3.5	Autorotation Controller Design.....	67
5	SIMULATION RESULTS	77
5.1	Effect of Wind during Autorotation	80
5.2	Effect of Pilot Reaction Time during Autorotation Entry	83
5.3	Effect of Entry Speed	86
5.4	Pilot in the Loop Simulation Comparison	87

6	CONCLUSION	89
6.1	Conclusion.....	89
6.2	Future Work	90
	REFERENCES.....	91
APPENDICES		
A.	AUTOROTATIVE INDEX	97
B.	HEIGHT VELOCITY DIAGRAM (DEADMAN’S CURVE).....	99
C.	REDUCED ORDER MODEL STATE AND CONTROL MATRICES	101
D.	CONTROLLER GAINS USED IN THE STUDY	103
E.	TRAPEZOIDAL MEMBERSHIP FUNCTION	105

LIST OF TABLES

TABLES

Table 4-1 6-DoF Helicopter Modes	36
Table 4-2 Pitch Channel ACAH Stability Margins.....	53
Table 4-3 Roll Channel ACAH Stability Margins	57
Table 4-4 Yaw Channel HH Stability Margins	61
Table 4-5 Longitudinal Speed Controller Stability Margins.....	65
Table 5-1 Conditions for Successful and Marginal Landings.....	77

LIST OF FIGURES

FIGURES

Figure 1-1 Cyclic Stick [5].....	4
Figure 1-2 Collective Pitch Control Stick [5]	5
Figure 1-3 Tail Rotor Pitch Angles [5]	5
Figure 1-4 Tail Rotor Pedals [5]	6
Figure 1-5 Dual Engine Failure [4].....	6
Figure 1-6 S-76 Powertrain [4]	7
Figure 1-7 Freewheel Unit [4].....	7
Figure 1-8 Rotor blade section aerodynamics in autorotation [3].....	8
Figure 1-9 Blade regions during autorotation [5]	9
Figure 1-10 Force vectors in vertical autorotation descent [5]	10
Figure 2-1 Real-Time Flight Simulator.....	13
Figure 2-2 Principle Model Structure of TOROS	14
Figure 3-1 Control Inputs.....	24
Figure 3-2 Variation of Body Angular Velocities and Euler Angles.....	25
Figure 3-3 Variation of Body Accelerations and Body Translational Velocities	26
Figure 3-4 Variation of Main Rotor Flapping, Lead-Lag and Inflow States	27
Figure 3-5 Variation of Main Rotor Speed, Engine States and Total Power.....	28
Figure 4-1 Definition of handling qualities Levels [33]	29

Figure 4-2 Definitions of bandwidth and phase delay [33].....	31
Figure 4-3 Requirements for small-amplitude pitch (roll) attitude changes [33]	32
Figure 4-4 Limits on pitch (roll) oscillations – hover and low speed [33].....	32
Figure 4-5 Requirements for small-amplitude heading changes [33]	33
Figure 4-6 Control System Block Diagram.....	34
Figure 4-7 Open Loop Eigenvalues (Longitudinal)	37
Figure 4-8 Collective to Vertical Velocity	38
Figure 4-9 Longitudinal Cyclic to Pitch Rate	38
Figure 4-10 Longitudinal Cyclic to Forward Velocity.....	39
Figure 4-11 Open Loop Eigenvalues (Lateral)	41
Figure 4-12 Lateral Cyclic to Roll Rate	42
Figure 4-13 Lateral Cyclic to Body Lateral Velocity	42
Figure 4-14 Pedal to Yaw Rate	43
Figure 4-15 LQR controller design flowchart.....	45
Figure 4-16 Pitch (Roll) bandwidth assessment – hover and low speed.....	47
Figure 4-17 Roll bandwidth assessment – forward flight	47
Figure 4-18 Pitch bandwidth assessment – forward flight.....	48
Figure 4-19 Pitch (roll) oscillations assessment.....	48
Figure 4-20 Pitch Attitude Command Attitude Hold Controller Structure	50
Figure 4-21 ACAH Responses to Reference Pitch Attitudes.....	50
Figure 4-22 ACAH Responses to Pitch Attitude Pulse Inputs.....	51

Figure 4-23 Loop Transfer Function.....	51
Figure 4-24 Stability margins [37].....	52
Figure 4-25 Nyquist Plots Pitch Channel ACAH	52
Figure 4-26 Pitch bandwidth assessment – hover and low speed	53
Figure 4-27 Pitch bandwidth assessment – forward flight.....	54
Figure 4-28 Roll Attitude Command Attitude Hold Controller Structure	54
Figure 4-29 ACAH Responses to Reference Roll Attitudes.....	55
Figure 4-30 ACAH Responses to Roll Attitude Pulse Inputs	56
Figure 4-31 Nyquist Plots Roll Channel ACAH.....	56
Figure 4-32 Roll bandwidth assessment – hover and low speed	57
Figure 4-33 Roll bandwidth assessment – forward flight	58
Figure 4-34 Heading Hold Controller Structure	58
Figure 4-35 HH Responses to Reference Yaw Attitudes.....	59
Figure 4-36 HH Response to Yaw Attitude Pulse Input.....	60
Figure 4-37 Nyquist Plots Yaw Channel HH.....	60
Figure 4-38 Yaw bandwidth assessment – hover and low speed.....	61
Figure 4-39 Yaw bandwidth assessment – forward flight	62
Figure 4-40 ACAH + HH Controllers Structure	62
Figure 4-41 ACAH + HH controllers oscillations assessment.....	63
Figure 4-42 Longitudinal Speed Hold Controller Structure	64
Figure 4-43 ACAH Responses to Reference Longitudinal Ground Speeds	64

Figure 4-44 Nyquist Plots Longitudinal Speed Controller.....	65
Figure 4-45 1-D Lookup Tables Used for Gain Scheduling	66
Figure 4-46 Phases of Autorotation Landing Flight.....	67
Figure 4-47 Autorotation Controller Phase Diagram [22]	67
Figure 4-48 State flow of Autorotation Controller Phase Transitions	68
Figure 4-49 Steady State Controller Structure	69
Figure 4-50 Integrator Anti Wind-Up Block.....	70
Figure 4-51 Flare trajectory assuming constant vertical acceleration.....	73
Figure 5-1 Control Inputs and Helicopter Attitude during Power-off Landing	78
Figure 5-2 Other Autorotation Related Parameters.....	79
Figure 5-3 Effect of Wind during Power-off Landing - 1	80
Figure 5-4 Effect of Wind during Power-off Landing – 2	81
Figure 5-5 Effect of Severe Turbulence during Power-off Landing – 1	82
Figure 5-6 Effect of Severe Turbulence during Power-off Landing – 2.....	83
Figure 5-7 Effect of pilot delay during autorotation entry	84
Figure 5-8 Effect of pilot delay during autorotation entry	85
Figure 5-9 Effect of Initial Speed during Power-off Landing.....	86
Figure 5-10 Pilot in the Loop Simulations Comparison	88
Figure A-1 Autorotative index of various helicopters [40].....	98
Figure B-1 Representative height-velocity curves for a single-engine and multi-engine helicopters [26].....	99
Figure E-1 Example of MATLAB trapmf function	105

LIST OF SYMBOLS & ABBREVIATIONS

Symbols

D	Aerodynamic drag force, N
g_m	Gain margin, dB
h	Height above ground level, m
\dot{h}	Vertical velocity, m/sec
\ddot{h}	Vertical acceleration, m/sec ²
L	Aerodynamic lift force, N
I_R	Main rotor polar moment of inertia, kg.m ²
J	LQR Cost function
K_{LQR}	LQR gain matrix
K_i	Integrator gain
K_p	Proportional gain
$LonSpd$	Longitudinal Ground Speed, knots
M	Helicopter mass, kg
p, q, r	Body rotational velocities at body fixed reference frame, deg/sec
Q	Rotor torque, Nm
R	Main rotor radius, m
s_m	Stability margin, nd
u, v, w	Translational velocities at body fixed reference frame, m/sec
$w_{ss_descent}$	Weight of steady state phase autorotation controller, nd
$w_{preflare}$	Weight of preflare phase autorotation controller, nd

w_{flare}	Weight of flare phase autorotation controller, nd
$w_{landing}$	Weight of landing phase autorotation controller, nd
w_{tdown}	Weight of touchdown phase autorotation controller, nd
ζ	Damping Ratio, nd
θ_0	Collective command, %
θ_{0TR}	Pedal command, %
θ_{1s}	Longitudinal cyclic command, %
θ_{1c}	Lateral cyclic command, %
τ_p	Phase delay, sec
ϕ, θ, ψ	Helicopter Euler angles (roll, pitch, yaw), deg
Φ_m	Phase margin, deg
Ω	Main rotor rotation speed, rad/sec
ω_{bw}	Bandwidth, rad/sec
ω_{gc}	Gain crossover frequency, rad/sec
ω_{ms}	Stability margin crossover frequency, rad/sec
$\omega_{pc}, \omega_{180}$	Phase crossover frequency, rad/sec

Abbreviations

ACAH	Attitude Command Attitude Hold
ADS	Aeronautical Design Standard
AFCS	Automatic Flight Control System
AGL	Above Ground Level
AHRS	Attitude and Heading Reference System
HH	Heading Hold
HQ	Handling Quality

KE	Kinetic Energy, W
KIAS	Indicated Airspeed, knots
LQR	Linear Quadratic Controller
NR	Nominal Rotor Speed, %
RPM	Revolutions per Minute
TAI	Turkish Aerospace Industries Inc.
TOROS	TAI Originated Rotorcraft Simulation
TTI_F	Time to impact during flare phase, sec
$TTI_{\dot{h}=0}$	Time to impact assuming zero vertical acceleration, sec
TTI_L	Time to impact during landing phase, sec
$TTLE$	Time to landing phase entry, sec
UCE	Useable Cue Environment

Subscripts

$()_{cmd}$	Reference command
$()_{des}$	Desired value
$()_{err}$	Error between reference command and plant output
$()_k$	k^{th} linear model
$()_{lat}$	Lateral dynamics
$()_{lon}$	Longitudinal dynamics
$()_{ss}$	Steady state

Superscripts

$()^{MDC}$	Linear model obtained using matched DC gain method
$()^{trun}$	Linear model obtained using truncation method

CHAPTER 1

INTRODUCTION

Even though reliability of helicopter technology has significantly improved in recent years, major system and component failures (or malfunctions) still occur. Engine loss is regarded as one of the most critical failure scenarios and according to [1], 28.5% of total 8436 U.S. civil rotorcraft accidents reported between years 1963 and 1997, are associated with loss of engine power. Moreover, 31% of the accidents, which result in helicopter structure damage (or even possible serious injury), are caused by complete power loss [2]. In literature, the state of flight with no net power requirement [3] is known as “autorotation”.

For a helicopter, autorotation refers to a descending maneuver where the rotor system is disengaged from the inoperative engine(s) [4] and is turned by the action of air moving through the rotor [5]. The main idea behind autorotation is that, the decrease of potential energy of the helicopter is used as a power source to the rotor. This power is used to produce the required thrust and to keep the rotor RPM within allowable design limits.

1.1 Background and Motivations of Research (Literature review)

Even though each helicopter has its own autorotation capability that depends on various design parameters (see Appendix A), making best use of those capabilities depends highly on pilot skill. Humans are nondeterministic systems, which makes it hard to gather consistent results. In other words, autorotation performance varies in each maneuver as it requires considerable pilot skill.

Starting from 1970’s several studies were conducted about autonomous autorotation controllers to reduce pilot workload and potentially the deadman’s curve (see Appendix B). Johnson’s work [6] is one of the earliest of these studies to introduce

nonlinear optimal control theory for solving power loss of a helicopter in hover. In his work, he used a point mass model of an OH-58A helicopter with a High Energy Rotor System (HERS) [7]. He used a weighted sum of squared vertical and horizontal velocity components at touchdown as the cost function for calculating control inputs as a function of altitude.

Lee et al. ([8] - [9]) extended the work of Johnson, by adding path inequality constraints on rotor thrust (to prevent rotor stall) and maximum sink rate (i.e. high rotor speeds). Using the Sequential Gradient Restoration Algorithm (SGRA) developed by Miele et al. [10], control inputs are calculated.

Floros [11] extended the models of Johnson [6] and Lee et al. ([8] - [9]) with rate controls and some additional constraints to better represent helicopter physics and pilot's reactions. Analytical solutions were compared with the flight test results of the OH-58A helicopter given in [12]. By using commercial optimization package SNOPT, Floros also applied sequential quadratic programming for obtaining optimum flight path after a partial or complete power loss [13].

Okuno et al. [14], investigated the differences between the optimal control theory solutions and pilot's control usage especially just before touchdown. He also worked on analytical prediction of H-V diagram using optimal control theory [15].

Abbeel et al. [16] collected several autorotation flight data to obtain and idealize the target trajectory during autorotation. Dynamics of the helicopter model are obtained from flight data and using differential dynamic programming method a reinforcement learning controller for autonomous autorotation is designed.

Dalamagkidis et al. [17] proposed a nonlinear model predictive controller for autorotation control. This controller is augmented with a recurrent neural network to safely land unmanned helicopters hovering at relatively low altitudes. The developed controller is applied to a vertical autorotation model only.

Tierney et al. [18] focused on real-time flare-phase trajectory planning. They computed optimal trajectories between designated touchdown points and a region of

the vehicle's state space from which a safe, feasible path to landing is guaranteed to exist.

Yomchinda [19] et al. [20] worked on real-time path planning of helicopters during autorotation by dividing whole trajectory into three different states (entry, descent, flare). Different optimization algorithms are used for each of these states in order to generate optimal trajectories. In order to maneuver the helicopter along the desired trajectory, PID compensators are used on longitudinal, lateral and vertical axes.

Z. Sunberg et al. [21]- [22] designed a multiphase expert control system for helicopter autorotation. Transitions between fuzzily defined autorotation phases are based on helicopter height above ground and predicted time to impact information. Unlike optimal control and neural network algorithms, this expert control system avoids significant computational cost. Simulations of the proposed controller are performed using Bell AH-1G Cobra and Align TREX 600 (small sized R/C controlled) helicopters.

Mengotti et al. [23] presented their work for certifying AW189 helicopter with a flight mechanics simulator by using pilot in the loop simulations.

Recently, Rogers et al. [24] designed autorotation controllers based on time to contact control laws and integrated these controllers to a full-motion flight simulator. Outputs of the autorotation controllers are turned into visual aids in the simulator which helps test pilots during power-off landings.

All researches mentioned above share a common point and that is, improving autorotation performance can only be achieved by managing the available energy.

Controlling the available energy, narrows the regions given in height-velocity (dead man's) curve. Hence, controlling helicopters during autorotation makes it possible to successfully land from a region where it is considered to be very difficult or impossible to make a safe landing.

1.2 Helicopter Flight Control System

In a helicopter, major controls are provided by the help of 4 different primary flight control systems which are;

- Lateral cyclic control
- Longitudinal cyclic control
- Collective pitch control
- Tail rotor control

Control inputs given from the cockpit or automatic flight control system (AFCS) are transferred to the rotor blades by mechanical linkages and servos (either hydraulic or electrical).

Cyclic Stick. Cyclic stick, which is usually located between pilot's legs, is used to control lateral and longitudinal motion of the helicopter. Pitch and roll movements of the helicopter is controlled by this stick. Inputs given to the stick simply tilts the plane of main rotor blades in the desired direction.



Figure 1-1 Cyclic Stick [5]

Collective Stick. Being located on the left hand side of pilot's, this control stick is used to change pitch angle of main rotor blades simultaneously. Changing pitch angle of the blades, changes the incidence angle of blades, which in return causes variations in lift and drag forces. Raising the collective not only increases generated thrust but also

the drag force, which causes rotor revolution speed to decrease. For keeping rotor rpm constant, engine governors (generally PI type controllers) or twist grip throttles, usually mounted at the end of collective lever, are used.



Figure 1-2 Collective Pitch Control Stick [5]

Tail Rotor (Anti-torque) Pedals. Tail rotor pedals, which are located on the cabin floor, are used to compensate the torque generated by rotation of main rotor blades. Anti-torque pedals determine helicopter heading by generating thrust.

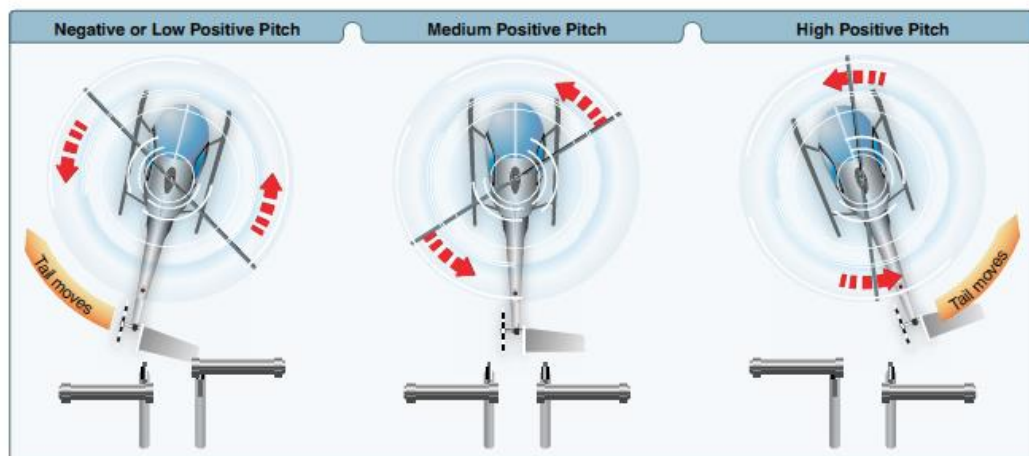


Figure 1-3 Tail Rotor Pitch Angles [5]



Figure 1-4 Tail Rotor Pedals [5]

1.3 Indications of Power Failure

In helicopters, power failure may be caused by either drive system or engine failure and it is usually indicated by low RPM horn [25]. Upon engine failure, rotor speed and power turbine speed of engine(s) start to decrease and percent torque indicator of engine(s) goes to zero. Sample rotor/engine rpm indicator and percent torque indicator during dual-engine failure of a Sikorsky S76 helicopter is given in Figure 1-5. Due to reduction in engine torque, helicopter yaws towards left which requires immediate right pedal and collective pitch reduction to prevent rotor RPM from reducing to an unrecoverable state.

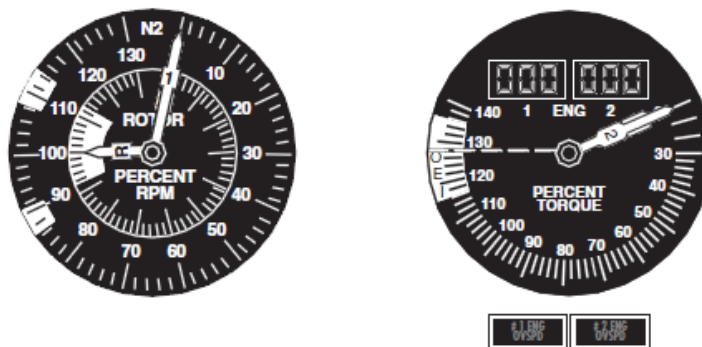


Figure 1-5 Dual Engine Failure [4]

When there is no failure, engine torque is transmitted to main and tail rotors by powertrain (Figure 1-6) which consists of main, intermediate and tail gearboxes together with connecting drive shafts. Connection between main gearbox and each

engine is made by freewheel units (i.e. overrunning clutches) (Figure 1-7). Whenever the engine attempts to rotate faster than the rotor, rollers are forced against the outer drum, which permits instantaneous engagement. In the event of engine failure, freewheel unit permits engine disengagement. This allows rotation main and tail rotor systems together with other modules without drag from the inoperative engine(s).

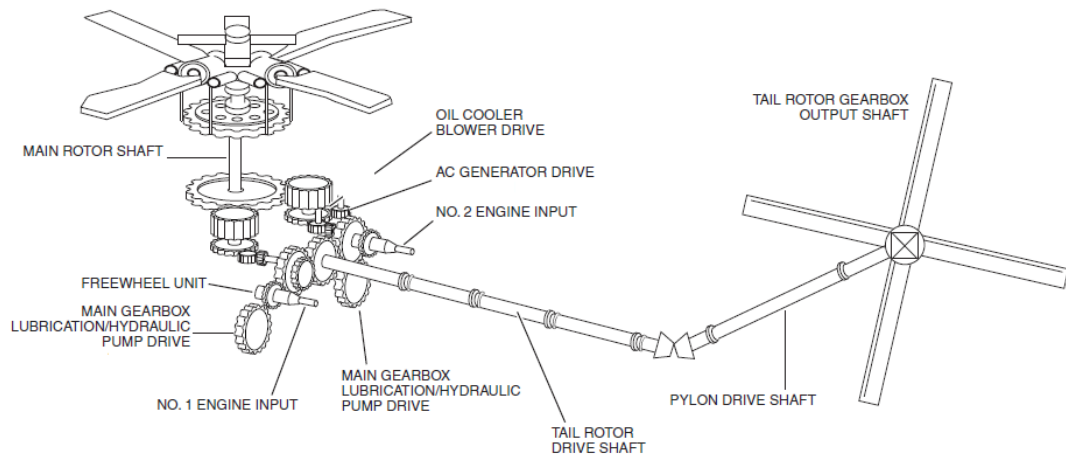


Figure 1-6 S-76 Powertrain [4]

During autorotation, drive shafts and accessory module (electrical generators and hydraulic pumps) are driven continuously by the inputs from the main rotor. Therefore, hydraulic and electric systems continue to work even if there is no power input from the engines. Hence, maintaining main rotor rpm within allowable limits is essential not only for preventing rotor blades stall but also for maintaining other subsystem operations.

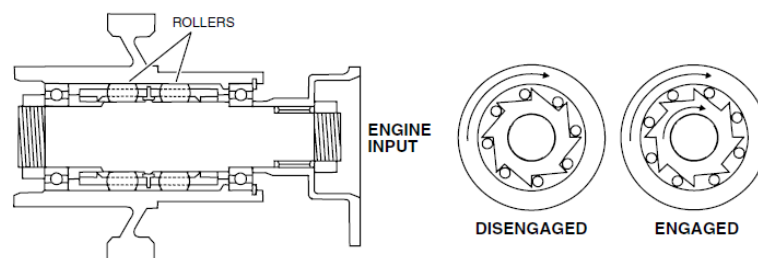


Figure 1-7 Freewheel Unit [4]

1.4 Aerodynamics of Autorotation

Autorotation maneuver is already defined in Section 1 as the state of rotation operation without application of any power from the engine. Torque required for turning the rotor is generated from the relative airstream upward through the rotor as the helicopter descends through the air [26].

Although autorotation's are mostly performed with some forward speed, aerodynamics of vertical autorotative descent is considered first for simplicity. This assumption simplifies the approach by removing the effect of dissymmetry of lift caused by forward speed during flight.

Figure 1-8 shows the aerodynamics of a rotor blade section during autorotation where ϕ is the inflow angle, θ is the blade pitch angle, $\alpha = \theta + \phi$ is the angle-of-attack, Ωr is the in-plane velocity at blade radial station r , V and v are the climb and induced velocities respectively. During autorotation, inflow angle is such that, net in-plane force (i.e. change of rotor torque) calculated by (1-2) is zero.

$$dQ = (D - \phi L)rdr = 0 \quad (1-1)$$

However, this equilibrium condition can exist at most at two radial stations on a rotor blade.

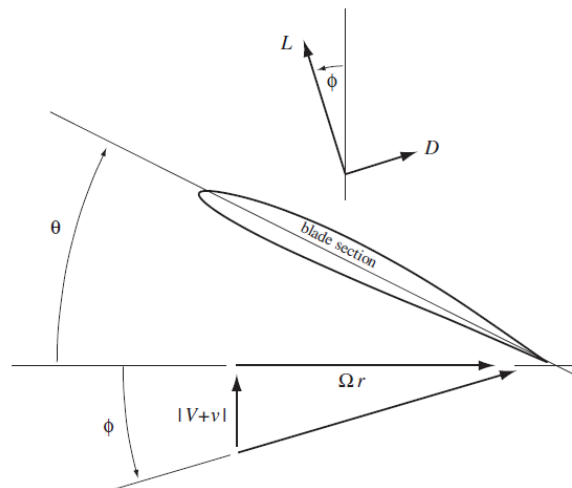


Figure 1-8 Rotor blade section aerodynamics in autorotation [3]

Assuming uniform inflow over the rotor disc, inflow angle can be computed as;

$$\phi = \tan^{-1} \left(\frac{|V + v|}{\Omega r} \right) \quad (1-2)$$

Therefore, inflow angle at the inboard part of the blade are high and decreases toward the tip. Then from (1-1), $dQ < 0$ on the inboard sections which indicates that this blade element absorbs power from air to rotor, hence generates accelerating torque on the rotor. On the other hand, on the outboard sections as ϕ decreases, $dQ > 0$ and power is delivered from rotor to air, which results in decelerating torque. Blade regions on a rotor disk together with force vectors during autorotational descent are illustrated in Figure 1-9 and Figure 1-10 respectively.

The inboard section (~25%) is referred as stall region where the local angle of attack values are above the stall angle of attack. Angle-of-attack values increase towards inboard region because of the inflow angle increase. Moreover, in order to improve the efficiency of the rotor during hover and forward flight, blades generally have negative twist, which further increases the angle of attack of the inboard sections. This behavior at the root section (i.e. stall) therefore causes increased drag, which slows down the rotation of the blade.

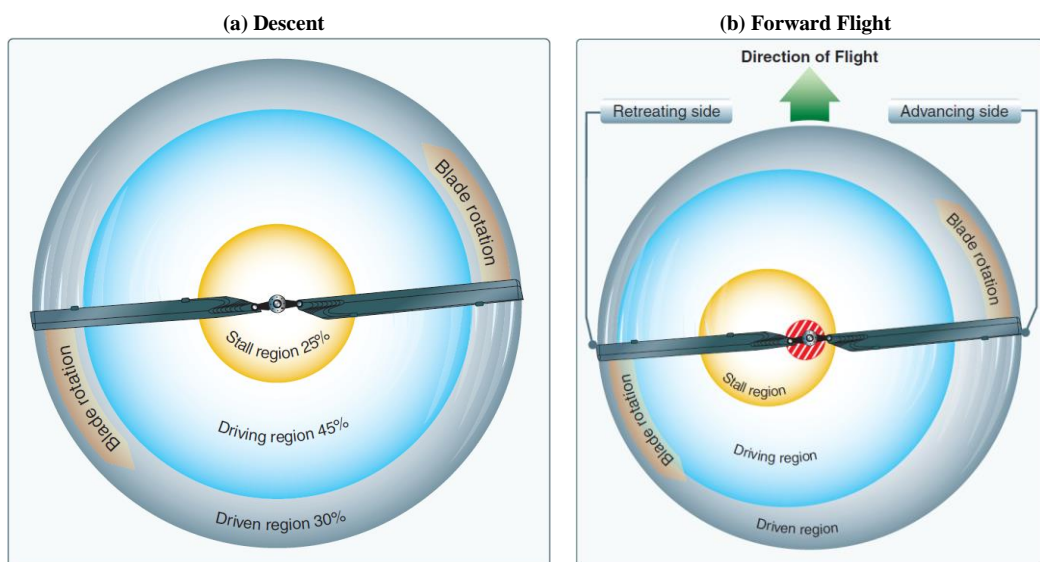


Figure 1-9 Blade regions during autorotation [5]

In the driving (autorotative) region, total aerodynamic force is tilted towards forward of the axis of rotation (see Figure 1-10), which tends increase the rotor speed to hold it near the normal value.

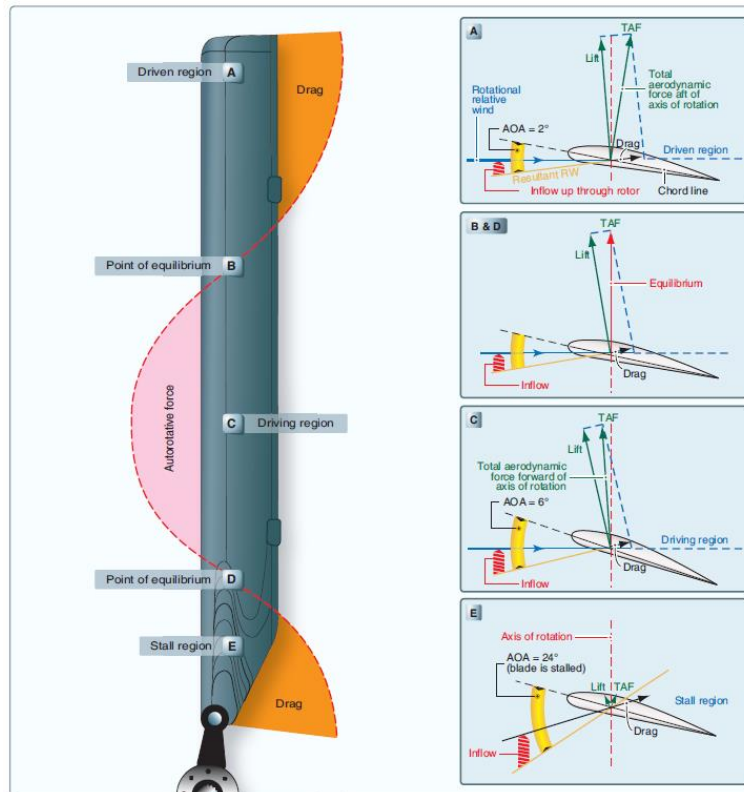


Figure 1-10 Force vectors in vertical autorotation descent [5]

Getting close to the tip of the blade, angle of attack is reduced because of blade twist and higher resultant wind. At a certain point, the driving force (forward component of the lift produced at the blade section) becomes lower than the drag force. This causes rotation of the blade to decelerate. This region is called as the driven region where total aerodynamic force is tilted towards aft of the axis rotation.

Between these three regions, there are at most two radial stations on the rotor blade, where total aerodynamic force is aligned with the axis of rotation. These points are called equilibrium points (Figure 1-10), which do not produce any accelerating or decelerating torque on the blade.

During autorotation, a pilot can control the rotor rpm by simply changing the pitch angles of the blades. For instance, raising the collective will increase the pitch angles of the blades simultaneously, which will increase the size of driven and stall regions. As a consequence, rotor speed will decrease. If collective pitch is lowered, pitch angle of blades will decrease in all regions. Since driving region increases, rotor blade accelerates and its rpm increases.

Autorotation is stable equilibrium point after adjusting the collective pitch so that a desired (or equilibrium) rpm is achieved. If the rotor speed is decreased from the equilibrium, the inflow angle increases, which increases the region accelerating torque outboard. This accelerating torque increases the rotor speed back to its equilibrium value. Conversely, when rotor speed is increased, inflow angle decreases which in return decreases the region of accelerating torque inboard.

The basic physics of the autorotation problem is the same during autorotation in forward flight. The only difference is the loss of axial symmetry due to induced velocity and angle of attack change over the rotor disk. Forward speed causes increased angle of attack values on the retreating side of the blade, which results in a shift of blade regions towards retreating side as shown in Figure 1-9.

1.5 Research Objectives

First objective of this study is to develop a flight control system that can be integrated to a non-linear mathematical model of a full-scale helicopter, by using full and reduced order linear model approximations. For this to be successful, validation studies are carried out between non-linear and linear models. Another objective is to gain insight into the Aeronautical Design Standard Performance Specifications (ADS-33) which are widely used in helicopter industry for measuring flying and handling qualities of helicopters. For that aspect, Attitude Command Attitude Hold (ACAH) type controllers are developed and their handling quality levels are evaluated using ADS-33 requirements. Besides these objectives, main target of this study is to develop a real-time autonomous autorotation controller which can perform successful landings after total engine power loss. This controller is intended to be integrated into a high-

fidelity light utility helicopter model to perform nonlinear simulations from various initial conditions. Using the approaches described in this study, this controller can be implemented to any type of full-authority rotorcraft simply by tuning certain controller parameters.

1.6 Outline of Thesis

In the first chapter, background and motivations of the research are provided together with an overview of helicopter flight control system. Besides, indications of power failure are given and aerodynamics of autorotation is briefly explained. Finally, objectives of the research are given.

In Chapter 2, TAI Originated Rotorcraft Simulation (TOROS), which is a non-linear rotorcraft modeling tool being developed by Turkish Aerospace Industries Helicopter Group, is explained in detail.

In the third chapter, explanations of linearization and model reduction techniques that are used during the study are given. Comparison of non-linear, high order linear and reduced linear system responses are also provided in this chapter.

In the fourth chapter, autorotation controller structure is described in detail. Designing of inner and outer loop control laws, which are used during the study, are briefly explained.

Fifth chapter includes nonlinear simulation results. Starting from various trim conditions, flight simulations are performed to test control law performance under different conditions.

In the last chapter, conclusions of the study together with possible future work recommendations are provided.

CHAPTER 2

TOROS

TAI Originated Rotorcraft Simulation (TOROS), built in MATLAB-Simulink® environment, is an in-house rotorcraft design tool that is used in Turkish Aerospace Industries for constructing high fidelity non-linear rotorcraft models. Other than performing flight mechanics analysis, this tool can also be used for designing automatic flight control systems and making handling quality analyses. Models generated using TOROS can also be integrated into a real-time flight simulator, as in Figure 2-1, for performing pilot in the loop simulations. High fidelity non-linear mathematical models constructed in TOROS are also validated with commercially available FLIGHTLAB® software in terms of trim, linearized system and nonlinear response results [27].



Figure 2-1 Real-Time Flight Simulator

In TOROS, each rotorcraft component is modelled separately using physics-based approach. Contributions of all these components on 6-DoF rotorcraft model are then calculated. During design phase, high complexity level of the rotorcraft model developed in TOROS allows it to be used for predicting the behavior of rotorcraft in its operating envelope. Nevertheless, flight test data is always required to validate the rotorcraft model developed in TOROS.

Principle model structure of TOROS is shown in Figure 2-2.

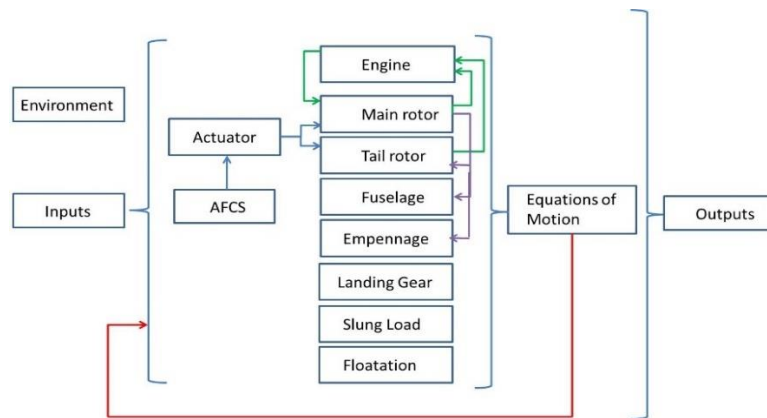


Figure 2-2 Principle Model Structure of TOROS

All modules given in Figure 2-2, are implemented using m-files. Definitions of these modules can be given as follows [28];

- Equations of motion: Using 6-DoF rigid body dynamics in body axis, motion of the rotorcraft is calculated by this module. Equations of motion are solved with respect to a fixed point on the body, which is close to aircraft cg. It is also possible to generate 3-DoF (lateral or longitudinal) or even 1-DoF (for drop test simulations) models.
- Main rotor: This module is used to model forces and moments generated by the main rotor. Forces can be calculated by using either momentum theory or blade element method. Different inflow solution methods are implemented in TOROS which can be selected by the user. Flapping and lead-lag motions with position limits are modelled. Calculations can be made either in Multi or Individual Blade Coordinates. Effect of main rotor interference on different components (ex: Empennage, Fuselage etc.) can be added by lookup tables or analytical finite state model.
- Tail rotor: Similar to the main rotor module, different methods can be selected for tail rotor force and moment calculations. Default solution method is blade element formulation however, for real-time simulations, reduced solution methods (like Bailey) can be used.
- Fuselage: This module is used to calculate aerodynamics forces and moments generated by the fuselage. Aerodynamic coefficient tables, which are obtained either

from CFD analyses or wind tunnel tests are used during calculations. These tables are interpolated with respect to fuselage angle of attack, angle of sideslip, Mach number and landing gear configuration.

- **Empennage:** This module is used to add auxiliary aerodynamic surfaces to the rotorcraft model. Horizontal and vertical tails are modeled separately from the fuselage. Any other aerodynamic component can also be integrated to the rotorcraft model structure. Aerodynamic coefficients obtained from CFD analyses or wind tunnel tests can be entered either in wind frame or local surface body frame.

- **Engine:** This module is used to model the dynamics of power plant and drive train. Dynamics of engine governor is also included by using a PID controller with a collective feed forward term. Using this module, simulations can be performed using multiple engines. Other than user defined generic engine model, any high-fidelity power plant model can be integrated.

- **Actuators:** Different servoactuator models can be implemented using this module. Main rotor servoactuators, which are used for transmitting control inputs to the main rotor swashplate, are modeled as first order linear systems with position and rate saturations (see Figure 3-1). First order full authority parallel servoactuators with dead zone and second order limited authority series servoactuators, for disturbance rejection, can be modelled using this module.

- **Landing Gears:** Different landing gear configurations (single-stage, two-stage or articulated) can be modeled using this module. Rolling degree of freedom of tires is user selectable and can be included during simulations for increasing model fidelity. Strut stiffness and damping properties can either be linear or non-linear whereas linear tire dynamics are used. Preload of struts can be included in calculations, below which tire vertical forces are not transmitted to the rotorcraft body. Tire ground plane forces, which are limited by maximum available friction forces, are modeled as a spring damper system. Brakes can be included to the landing gears and each landing gear can be selected either as locked or unlocked (castor) by the user.

- Slung Load: Both 3-DoF and 6-DoF rigid body load models are available. Similar to fuselage and empennage modules, aerodynamic coefficients of the slung load can be entered using tables. For higher fidelity simulations, 6-DoF model can be integrated with flexible cables, where damping and stiffness values of the cables are given as inputs to the module. There is also an input switch which enables slung load to be released during simulations.
- Floatation: Rotorcrafts may have emergency floatation systems for achieving safe landings after ditching. This module is used to calculate forces and moments generated by the floats in case of water landings.
- Weight and Balance: By the help of this module, effect of fuel change is included during flight simulations. Moreover, weight and cg shift due to icing or extension/retraction/jettison of external bodies (ex: landing gear, floatation, launchers etc.) can also be observed.
- Environment: Simulations can be performed under steady wind, turbulence, gust (sharp edge or “1-cos”) and downburst using this module. Two different turbulence models can be chosen. One of these models is Von Karman turbulence model and other one is based on empirical results and it is applied to the model through control inputs. Intensity of the generated turbulences can vary.
- Failure: This module is used to inject different failure scenarios to the rotorcraft model. Actuator failures (hard-over, jam, soft-over etc.) together with hydraulics and engine failures can be simulated by the help of this module.
- Control System: All modules except control system, are used for modelling open loop rotorcraft dynamics. This module enables users to develop different control laws in MATLAB Simulink® environment and implement it to the rotorcraft model. Any type of lower (disturbance rejection, attitude hold etc.) or upper mode (airspeed hold, position hold etc.) controllers may be designed. If required, this module can be replaced with any type of Automatic Flight Control System.

CHAPTER 3

LINEARIZATION AND MODEL ORDER REDUCTION

3.1 Linearization

A high-fidelity helicopter model contains several nonlinearities. Therefore, superposition principle cannot be applied. In other words, response of a nonlinear system cannot be calculated by adding the responses given to different inputs, which are treated one at a time [29]. Thus, in control applications, linearized models are much more convenient when analyzing and synthesizing control laws.

A nonlinear system can be approximated by a linear system around an equilibrium point if deviations are small enough. In aviation, these equilibrium points correspond to the trim points. As stated in [30], trim refers to the process of manipulating pilot controls and Euler angles for holding helicopter in equilibrium. Helicopter might be flying at different conditions (hover, descent, turn etc.) with fixed controls but if translational velocity components are constant (i.e. sum of forces and moments about each body axis is equal to zero), then the aircraft is said to be in trim.

Generalized non-linear aircraft dynamic equations can be represented as;

$$\dot{x} = F(x, u, t) \quad (3-1)$$

F term given in (3-1) represents a vector of non-linear functions whereas u represents control (input) vector, x represents state vector and \dot{x} represents state derivative vector, which is equal to zero for some values of u .

When helicopter is trimmed, all force and moment functions as well as all its derivatives are known at a point. Using Taylor series expansion, behavior of these functions anywhere in their analytic range can be estimated [31].

Considering a nonlinear system with two inputs x_1 and x_2 and an output function of y , input-output relationship can be given in general form as;

$$y = f(x_1, x_2) \quad (3-2)$$

Writing Taylor series expansion of Equation (3-2) about an equilibrium point x_{1e}, x_{2e}, y_e

$$\begin{aligned} y = f(x_{1e}, x_{2e}) &+ \left[\frac{\partial f}{\partial x_1} (x_1 - x_{1e}) + \frac{\partial f}{\partial x_2} (x_2 - x_{2e}) \right] \\ &+ \frac{1}{2!} \left[\frac{\partial^2 f}{\partial x_1^2} (x_1 - x_{1e})^2 \right. \\ &+ 2 \frac{\partial^2 f}{\partial x_1 \partial x_2} (x_1 - x_{1e})(x_2 - x_{2e}) \\ &\left. + \frac{\partial^2 f}{\partial x_2^2} (x_2 - x_{2e})^2 \right] + \dots \end{aligned} \quad (3-3)$$

Where the partial derivatives are evaluated at $x_1 = x_{1e}$ and $x_2 = x_{2e}$. Using small perturbation theory and assuming variations $\delta x_1 = (x_1 - x_{1e})$ and $\delta x_2 = (x_2 - x_{2e})$ to be small, higher order terms can be neglected and (3-3) reduces to;

$$\begin{aligned} y - y_e &= K_1(x_1 - x_{1e}) + K_2(x_2 - x_{2e}) \\ &= \frac{\partial f}{\partial x_1} \delta x_1 + \frac{\partial f}{\partial x_2} \delta x_2 \end{aligned} \quad (3-4)$$

Equation (3-4) simply represents the linear mathematical model of the nonlinear system given in (3-2) around equilibrium point x_{1e}, x_{2e}, y_e .

Using this information, nonlinear equations of motion of a helicopter represented in (3-1), can be represented by linearized equations about a general trim condition as;

$$\dot{x} = Ax + Bu \quad (3-5)$$

Where partial derivatives of F are used to derive system and control matrices.

$$A = \left(\frac{\partial F}{\partial x} \right)_{x=x_e} \quad (3-6)$$

$$B = \left(\frac{\partial F}{\partial u} \right)_{u=u_e} \quad (3-7)$$

Assuming that deviations of variables from the trim points are small (i.e. using small perturbation theory), perturbed states can be written as;

$$x = x_e \pm \delta x \quad (3-8)$$

For calculation of state matrix, free states and states which have fixed state derivatives are perturbed in both positive and negative directions (two-sided perturbation). Using each perturbed state x_j , new state vector \vec{x}_j is formed;

$$\vec{x}_j = \begin{Bmatrix} \dots \\ x_{e_{j-2}} \\ x_{e_{j-1}} \\ x_{e_j} \pm \delta x_j \\ x_{e_{j+1}} \\ x_{e_{j+2}} \\ \dots \end{Bmatrix} \quad (3-9)$$

After forming \vec{x}_j , function F is evaluated using new state vector and new state derivative vector, $\dot{\vec{x}}_j$ is found. Using numerical differentiation, j^{th} columns of A_P and A_N matrices, which are related to j^{th} perturbed state are found using (3-10).

$$A_{P_j} = \frac{\dot{\vec{x}}_j - \dot{\vec{x}}_e}{\delta x_j}, A_{N_j} = -\frac{\dot{\vec{x}}_j - \dot{\vec{x}}_e}{\delta x_j} \quad (3-10)$$

$\dot{\vec{x}}_e$ term given in (3-10) represents the state derivative vector obtained during trim condition (i.e. using state vector, \vec{x}_e). The subscripts P and N represents positive and negative perturbations respectively. Notice that, if j^{th} state is not perturbed, $\vec{x}_j = \vec{x}_e$, which makes the corresponding columns of A_P and A_N matrices to be zero.

After calculating all columns of A_P and A_N matrices, system matrix can simply be found as;

$$A = \frac{A_P + A_N}{2} \quad (3-11)$$

For the calculation of control (input) matrices, free inputs are perturbed both in positive and negative directions. Using small perturbation theory as before, perturbed inputs can be written as;

$$u = u_e \pm \delta u \quad (3-12)$$

Using each perturbed input u_j , new input vector \vec{u}_j is formed and new state derivative vector is calculated similar to the previous case. Control (input) matrix can then be calculated as;

$$B = \frac{B_P + B_N}{2} \quad (3-13)$$

Where B_P and B_N matrices are obtained by replacing δx_j terms given in (3-10) by δu_j .

Similar to the state equation given in (3-5), output equation of a linearized system can be represented as a single first order matrix differential equation;

$$y = Cx + Du \quad (3-14)$$

C and D matrices given in (3-14) are called as output and feedforward matrices respectively that can be calculated using the same approach used for system and control matrix calculations.

3.2 Model Order Reduction

To represent actual behavior of a helicopter accurately, high fidelity mathematical model is required. However, increasing fidelity level of a model also increases the number of variables and resources to be handled, at the price of a high and expensive computational cost. In the control systems area, complex models result in large

control-engineering problems, which significantly increases simulation time and make it difficult to analyze the models' properties.

Model order reduction (MOR) has become an important tool in the design of complex systems as low order models are easier to analyze and faster to simulate. These techniques can be used for finding a low-order model which approximates original high-order model behavior, while preserving input-output relationship as much as possible.

In literature, various MOR methods are available. In some of these methods, physical interpretations of the states are lost which is not desired in this study. Retaining physical interpretations of the states and obtaining a reduced order model that approximates the original model within the desired frequency range is considered adequate. Among several alternatives, in order to reduce the full-linearized helicopter model, modal truncation and matched DC gain methods are used together.

3.2.1 Modal Truncation

In modal truncation method, states, which do not affect dynamics of the system and slow dynamics, are simply truncated. Partitioning a state vector into x_1 to be kept, and x_2 to be eliminated

$$\begin{bmatrix} \dot{x}_1 \\ \dot{x}_2 \end{bmatrix} = \begin{bmatrix} A_{11} & A_{12} \\ A_{21} & A_{22} \end{bmatrix} \begin{bmatrix} x_1 \\ x_2 \end{bmatrix} + \begin{bmatrix} B_1 \\ B_2 \end{bmatrix} u \quad (3-15)$$

$$y = [C_1 \ C_2] \begin{bmatrix} x_1 \\ x_2 \end{bmatrix} + Du \quad (3-16)$$

Truncated system becomes

$$\dot{x}_1 = A_{11}x_1 + B_1u \quad (3-17)$$

$$y = C_1x_1 + Du \quad (3-18)$$

Notice that, in modal truncation, only the lowest-energy states are truncated and eigenvalues of the truncated model are a subset of full model. Therefore, it is expected for the truncated model to differ slightly from the original model at low frequencies.

3.2.2 Matched DC Gain Method

In matched DC gain method [32], state-space matrices are recomputed and DC gains (static gains), which represent the ratio of the steady state output of a system to its constant input, are preserved. Similar to the modal truncation method, state vector is partitioned into x_1 and x_2 (as in (3-15) and (3-16)) where x_1 is a (k)-dimensional vector which represents the states to be kept and x_2 is a (n-k) dimensional vector which represents the states to be eliminated.

In this method, it is assumed that x_2 states reach steady state immediately. Therefore, derivatives of these states (\dot{x}_2) are set to zero.

$$\dot{x}_2 = 0 = A_{21}x_1 + A_{22}x_2 + B_2u \quad (3-19)$$

From equation (3-19), assuming A_{22} to be invertible, x_2 can be found as

$$x_2 = -A_{22}^{-1}A_{21}x_1 - A_{22}^{-1}B_2u \quad (3-20)$$

The remaining equation can then be solved for x_1 by eliminating the x_2 states. Inserting (3-20) into (3-15) will give the reduced system equations as

$$\dot{x}_1 = [A_{11} - A_{12}A_{22}^{-1}A_{21}]x_1 + [B_1 - A_{12}A_{22}^{-1}B_2]u \quad (3-21)$$

$$y = [C_1 - C_2A_{22}^{-1}A_{21}]x_1 + [D - C_2A_{22}^{-1}B_2]u \quad (3-22)$$

Notice that, in matched dc gain method, low frequencies are preserved at the expense of high frequency accuracy.

3.3 Comparison of Non-linear, Full-Linear and Reduced Linear Models

High order linear models represent the behavior of nonlinear helicopter model around specified trim conditions quite well however, for controller design purposes, they are

still computationally expensive. Therefore, an approximation of the high order (full-linear) model is required. As stated in [31], for linear analysis, classical 6-DoF motion is adequate and as a general approach, this level of approximation is sufficient for handling qualities and low to moderate frequency analysis. In 6-DoF theory, it is assumed that rotor and inflow dynamics are much faster than fuselage dynamics. Therefore, they can be residualized onto the rigid body dynamics using the approach described in section 3.2.2.

For getting high order linear helicopter model, nonlinear model is trimmed for different flight conditions. Full linear model is then reduced to a simpler model that contains only 6-DoF rigid body states and 4 control inputs. Motion states are

$$x = \{u, w, q, \theta, v, p, \phi, r\}$$

Here u , v and w are longitudinal, lateral and vertical translational velocities in body fixed frame; p , q , r are the angular velocities about the body fixed frame center and θ and ϕ are the Euler angles that defines the orientation of body axes relative to the earth. Main rotor collective, longitudinal cyclic, lateral cyclic and tail rotor collective (pedal), are the four control inputs of the reduced linear model, which can be represented as;

$$u = \{\theta_0, \theta_{1S}, \theta_{1C}, \theta_{0TR}\}$$

State (A) and input (B) matrices of the reduced order model at 80 knots forward flight trim is provided in Appendix C.

Figure 3-1 to Figure 3-5 illustrates comparison of non-linear model response with the responses of full and reduced linear models. Starting from 80-knots forward flight trim condition, doublet inputs are given in all four-control channels and responses of three models are plotted. Inputs are given to the open-loop systems and simulations are limited to 5 seconds since open loop model of the helicopter is naturally unstable. As linearized models are defined around specified trim points, only amount of deviations from control inputs, state and output variables are obtained. Therefore, before comparing linearized model response with the nonlinear model, output values of the initial trim condition are added to the simulated linear model outputs.

TOROS

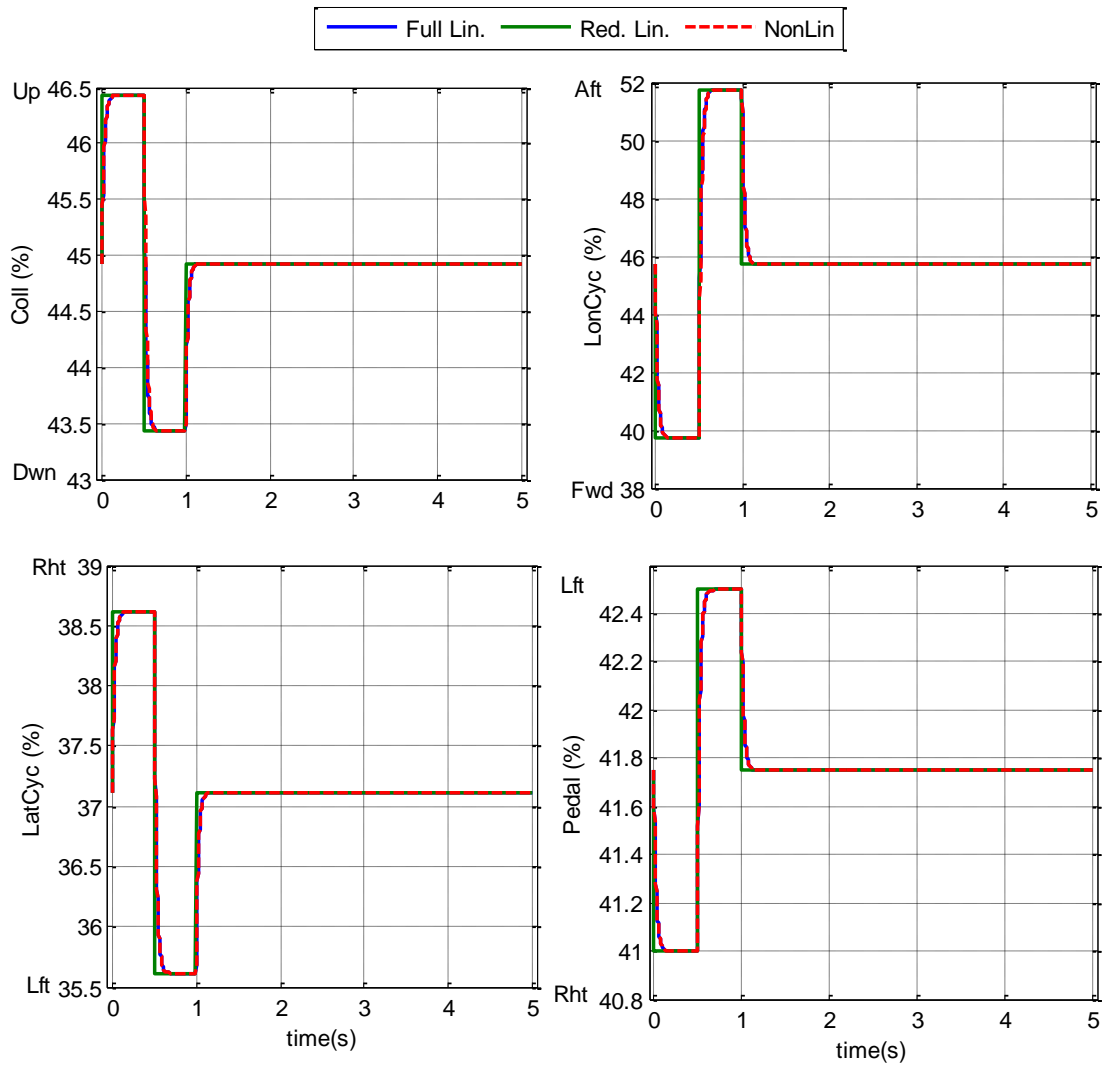


Figure 3-1 Control Inputs

Notice that, in reduced linear system, since actuator dynamics are truncated, doublet inputs are transmitted directly to the main and tail rotor. On the other hand, in non-linear and full linear systems, doublet inputs are limited by the 1st order actuator dynamics which can be seen in Figure 3-1.

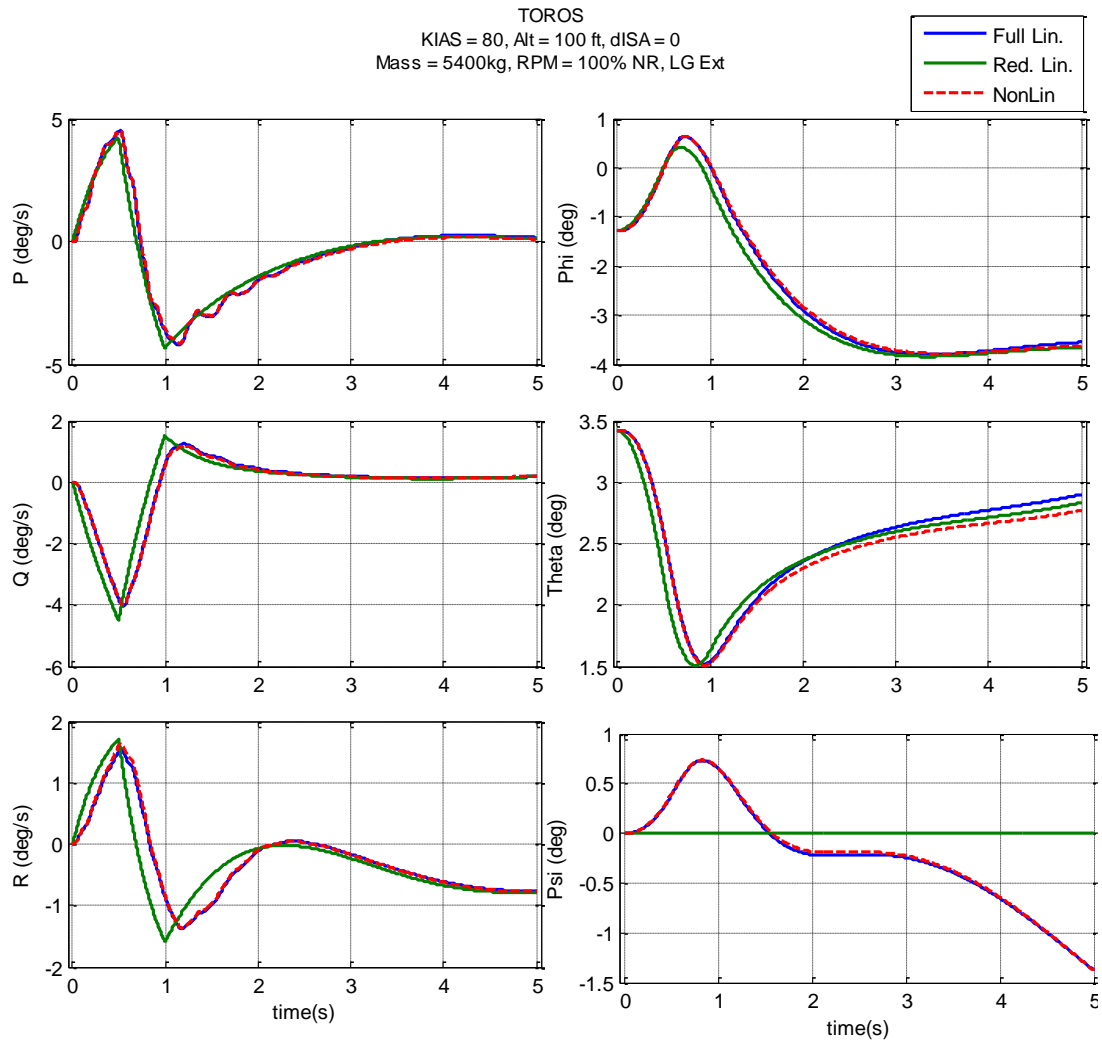


Figure 3-2 Variation of Body Angular Velocities and Euler Angles

It can be seen in Figure 3-2 that, first and second peaks of the body angular velocities match and both full and reduced order models represent the behavior of non-linear model. Euler angles also show similar trend. It is expected for Euler angles to diverge faster than the body angular rates due to error build-up after integration. There is no change in the yaw angle (ψ) of the reduced linear model as it is truncated during model reduction.

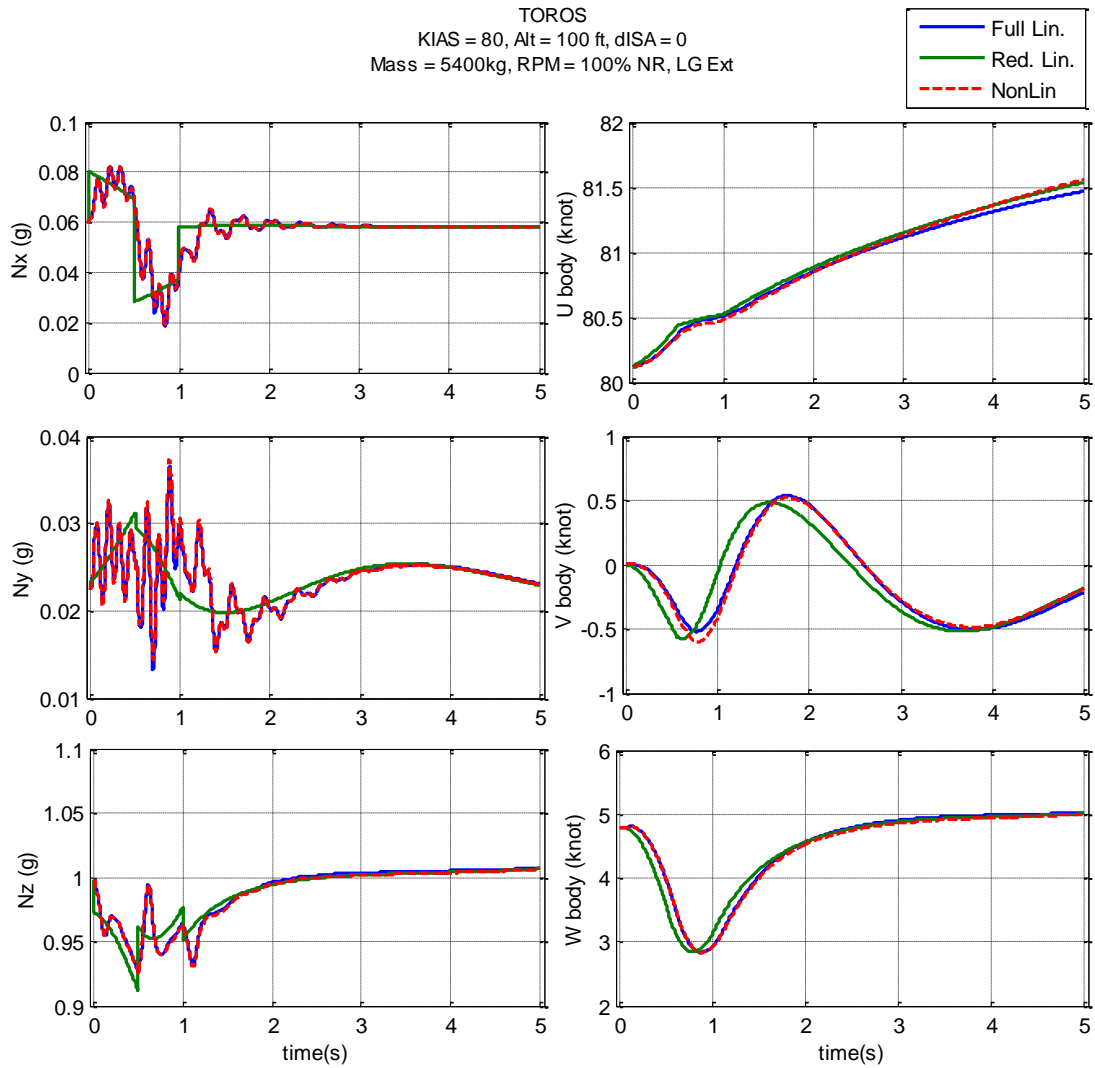


Figure 3-3 Variation of Body Accelerations and Body Translational Velocities

Changes in body accelerations and translational velocities of the non-linear model can be correctly represented by the high and low order linear models around the specified trim condition.

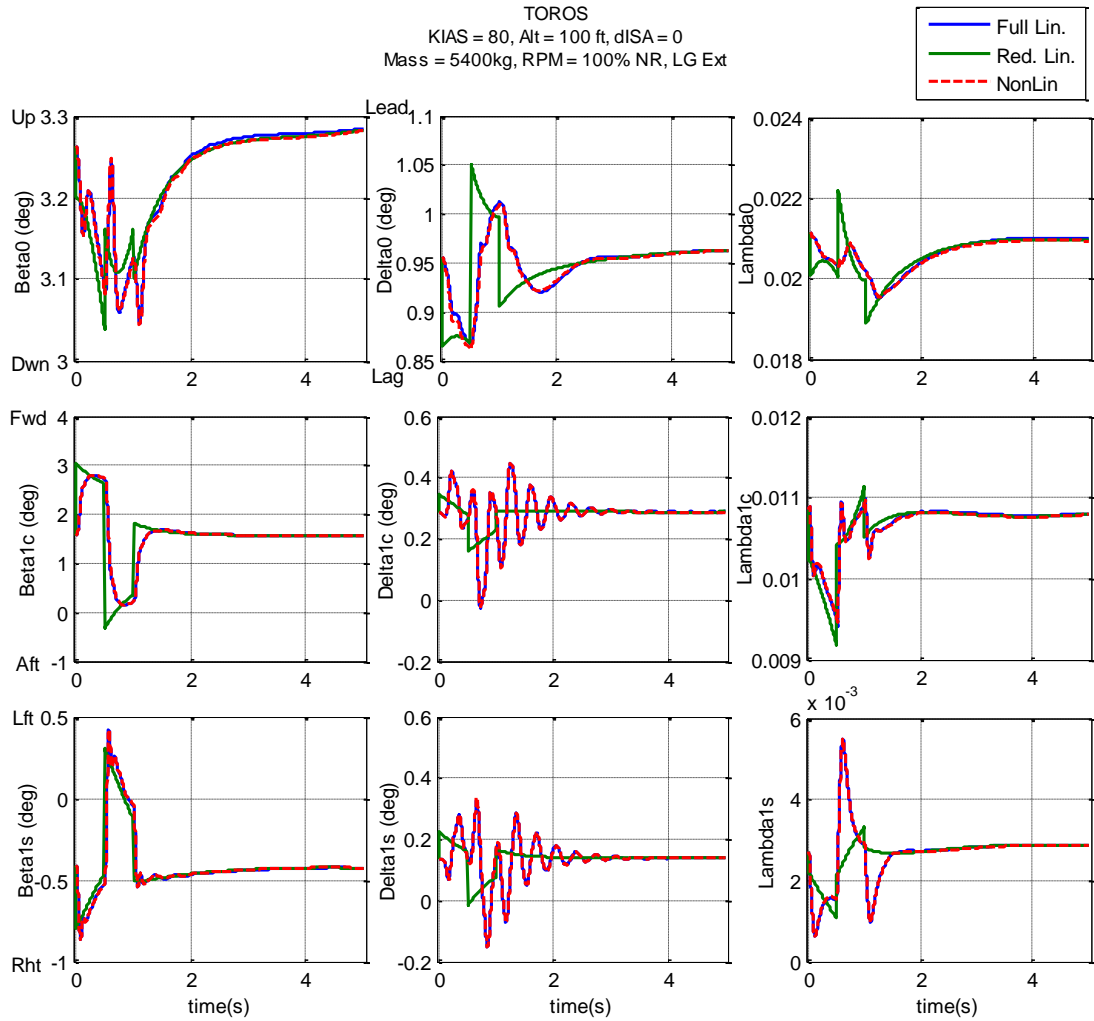


Figure 3-4 Variation of Main Rotor Flapping, Lead-Lag and Inflow States

Main rotor flapping, lead-lag and inflow states show similar behavior in all three models which means that rotor dynamics are correctly residualized onto the 6-DoF rigid body states.

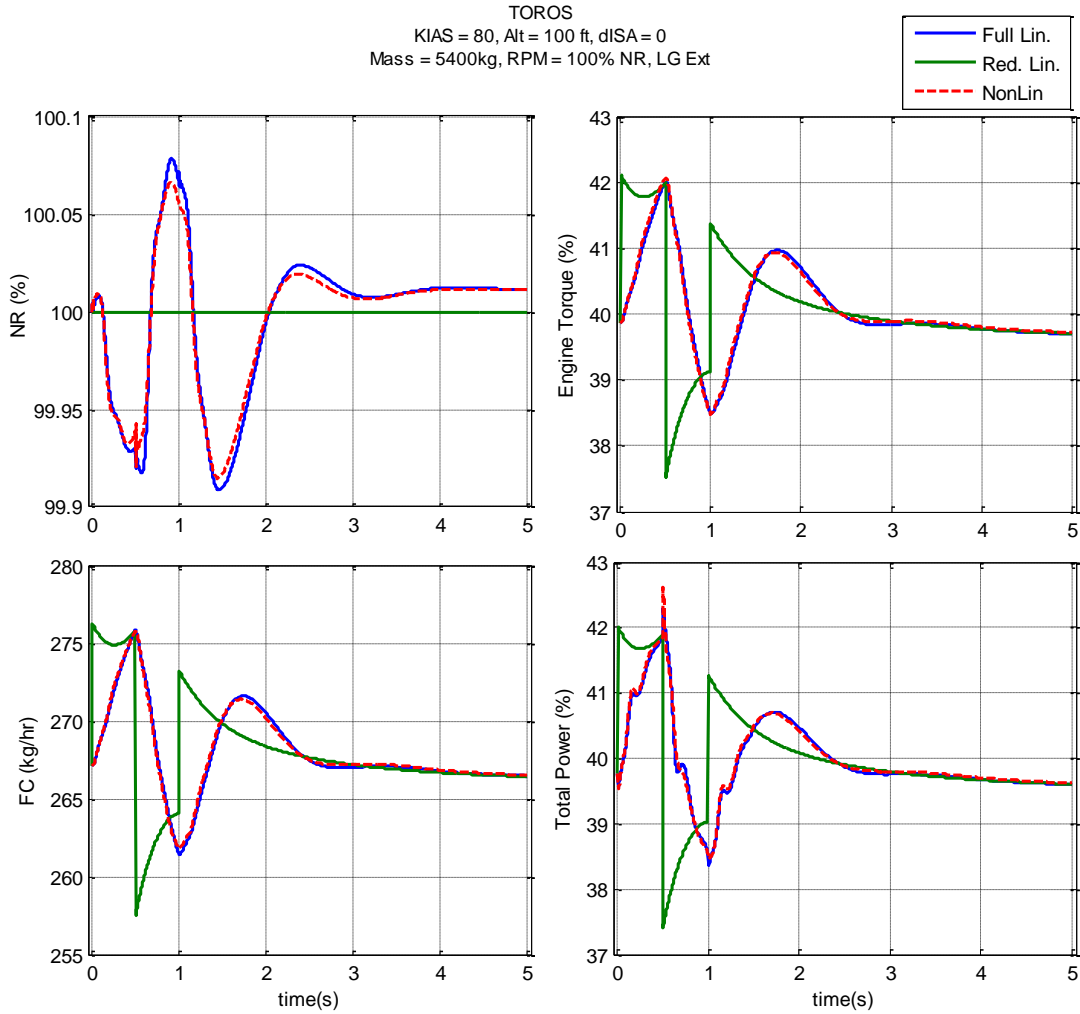


Figure 3-5 Variation of Main Rotor Speed, Engine States and Total Power

Due to the dynamics of engine model, giving doublet input in collective channel caused slight changes in main rotor speed and total power. Notice that, raising collective has increased required power from the engines which causes fuel consumption rate to increase. Lowering collective resulted in just the opposite behavior.

CHAPTER 4

AUTOROTATION CONTROLLER

4.1 Introduction

For quantifying handling qualities level of a rotorcraft, Cooper-Harper Handling Qualities Rating Scale (Figure 4-1) can be used. There are 3 handling qualities levels, HQ Level 1 being the best and HQ Level 3 being the worst, which are based on pilot workload and required task performance. Therefore, while designing the controller, in order to reduce pilot compensation as much as possible it is desired to reach Level 1 handling qualities rating for all channels (pitch, roll and yaw).

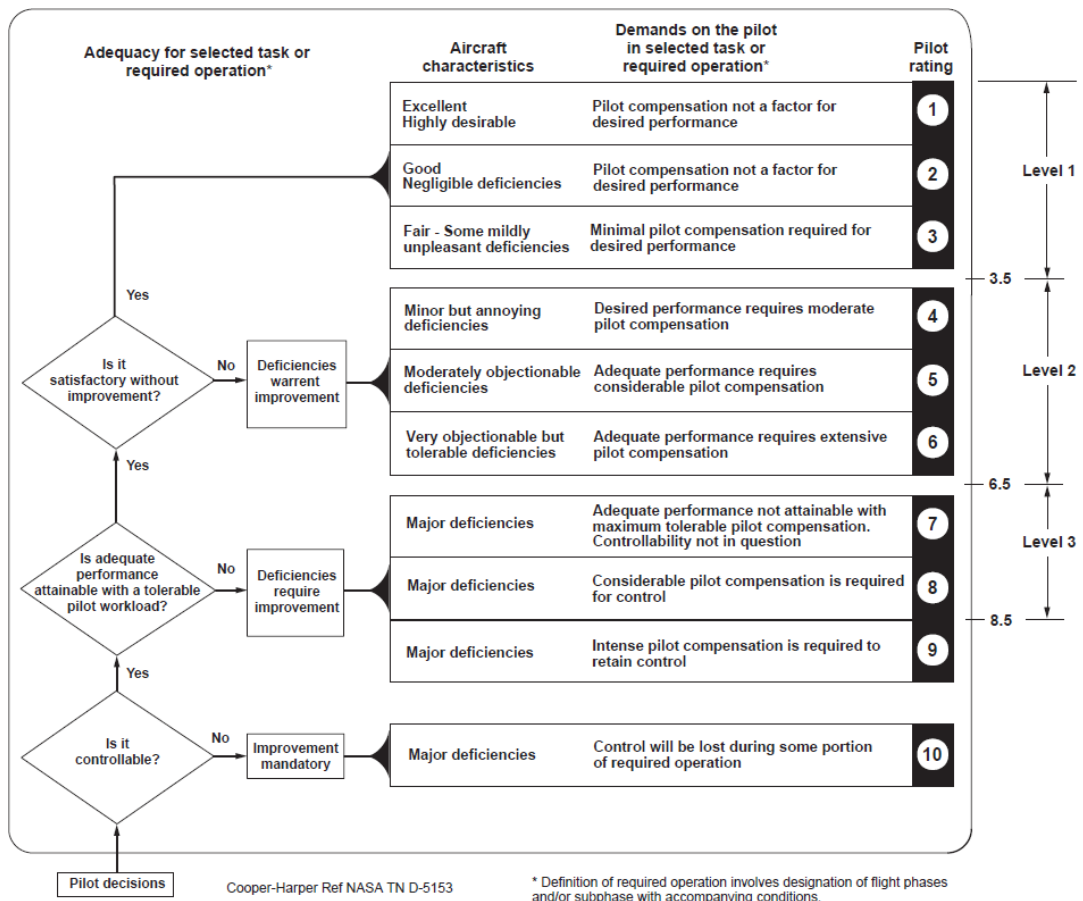


Figure 4-1 Definition of handling qualities Levels [33]

4.2 Flight Control Requirements

During development of flight control system, handling qualities requirements given in “Aeronautical Design Standard (ADS) 33E Performance Specifications” [33] are used as a guideline. As stated in [34], ADS-33E-PRF contains several requirements on short and long-term response characteristics as well as response type and usable cue environment expectations for all categories of rotorcraft. Requirements used in this study are given in the following sections. Notice that, while designing inner loops of the controller (disturbance rejection & attitude command attitude hold (ACAH)), different requirements are defined for hover/low speed and forward flight conditions. Hover and low speed requirements are applicable to operations up to 45 knots ground speed whereas forward flight requirements are applicable to operations greater than 45 knots ground speed.

4.2.1 Small-Amplitude Pitch (Roll) Attitude Changes

4.2.1.1 Short Term Response to Control Inputs (Bandwidth)

In [33], for quantifying handling quality level of a rotorcraft during short term response to control inputs, bandwidth (ω_{bw}) and phase delay (τ_p) parameters are defined which are obtained using frequency responses from longitudinal (lateral) control input channel to pitch (roll) attitude as defined in Figure 4-2.

In Figure 4-2, bandwidth is defined as lesser of $\omega_{bw_{gain}}$ and $\omega_{bw_{phase}}$ for rate response type systems whereas for the ACAH response type systems (attitude hold controller for this study) it is defined as $\omega_{bw_{phase}}$. Unlike usual gain and phase crossover frequencies, $\omega_{bw_{gain}}$ is defined as the frequency where bode magnitude plot crosses closed loop gain margin + 6dB point and $\omega_{bw_{phase}}$ is defined as the frequency that corresponds to 45° phase margin (i.e. frequency at $\Phi = -135^\circ$). For both rate and ACAH response types, phase delay is calculated as

$$\tau_p = \frac{\Delta\Phi 2\omega_{180}}{57.3(2\omega_{180})} \quad (4-1)$$

Where $\Delta\Phi_{2\omega_{180}}$ term corresponds to the phase margin at twice of phase crossover frequency ($2\omega_{180}$) and can simply be expressed as

$$\Phi_{@2\omega_{180}} + 180 \quad (4-2)$$

Phase delay:

$$\tau_p = \frac{\Delta\Phi_{2\omega_{180}}}{57.3 (2\omega_{180})}$$

Note: If phase is nonlinear between ω_{180} and $2\omega_{180}$, τ_p shall be determined from a linear least squares fit to phase curve between ω_{180} and $2\omega_{180}$

Caution:
For ACAH, if $\omega_{BW_{gain}} < \omega_{BW_{phase}}$ or if $\omega_{BW_{gain}}$ is indeterminate, the rotorcraft may be PIO prone for super-precision tasks or aggressive pilot technique.

Rate response-types:

ω_{BW} is lesser of $\omega_{BW_{gain}}$ and $\omega_{BW_{phase}}$

Attitude Command/Attitude Hold Response-Types (ACAH):

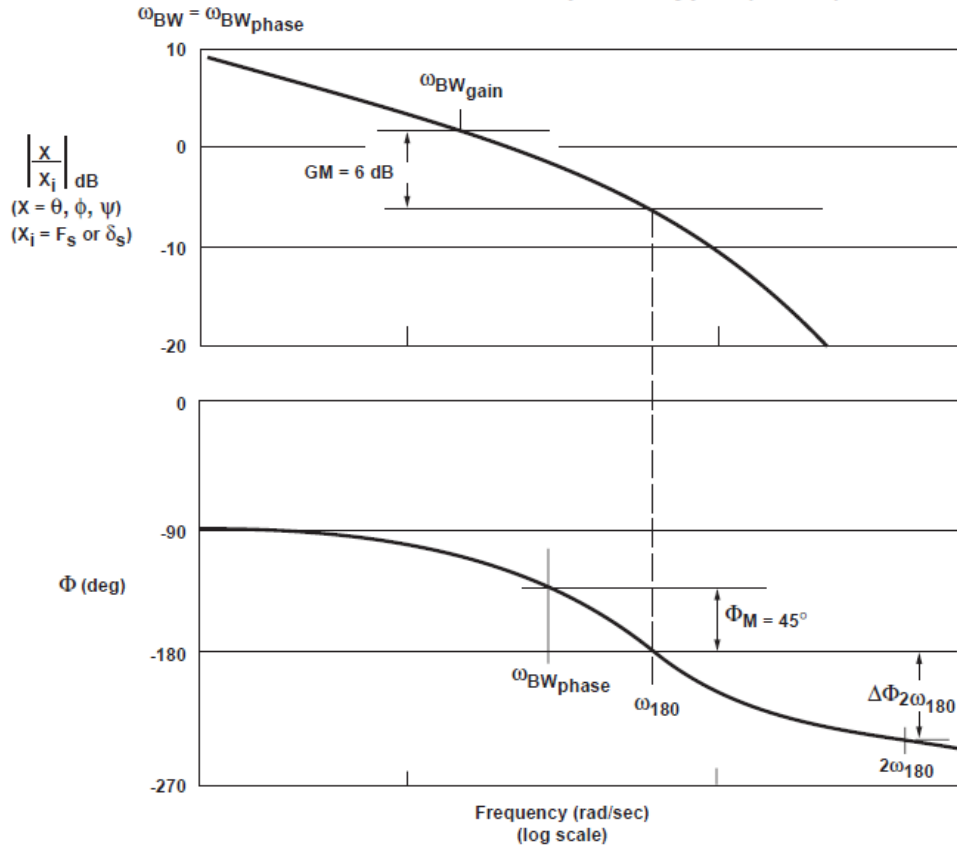


Figure 4-2 Definitions of bandwidth and phase delay [33]

After defining these ω_{bw} and τ_p parameters, handling quality levels of pitch (roll) attitude responses to longitudinal (lateral) control inputs can be assessed using the limits specified in Figure 4-3.

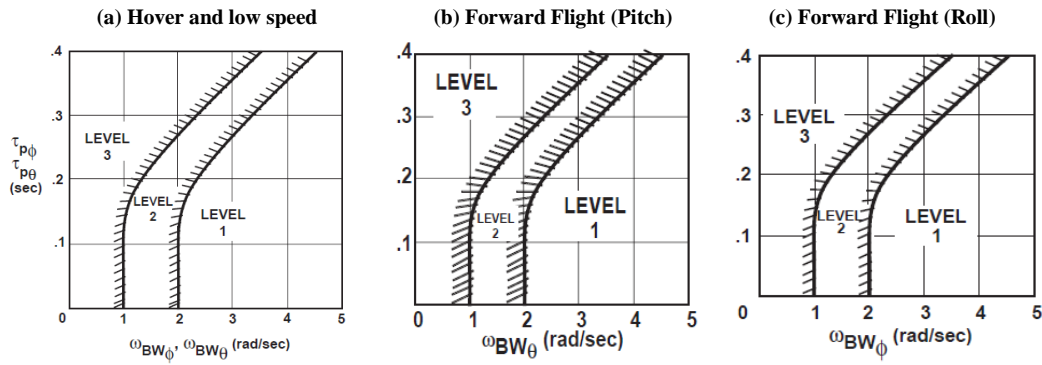


Figure 4-3 Requirements for small-amplitude pitch (roll) attitude changes [33]

4.2.1.2 Mid-Term Response to Control Inputs

According to [33], mid-term response characteristics are applicable to all frequencies below bandwidth frequency obtained in Section 4.2.1.1. For the inner loop LQR controller, required damping ratios on pitch (roll) oscillations are given in Figure 4-4. For attitude hold response type, an effective damping ratio of at least $\zeta = 0.35$ is required for HQ level 1 (shown with red dashed lines in Figure 4-4).

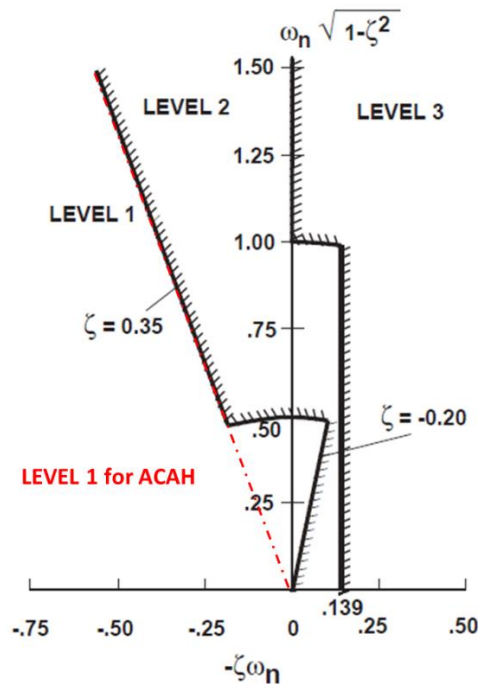


Figure 4-4 Limits on pitch (roll) oscillations – hover and low speed [33]

4.2.2 Small-Amplitude Yaw Attitude Changes

4.2.2.1 Short Term Response to Control Inputs (Bandwidth)

Similar to the pitch (roll) short term response characteristics, bandwidth (ω_{bw}) and phase delay (τ_p) parameters obtained from Figure 4-2 shall meet the limits specified in Figure 4-5.

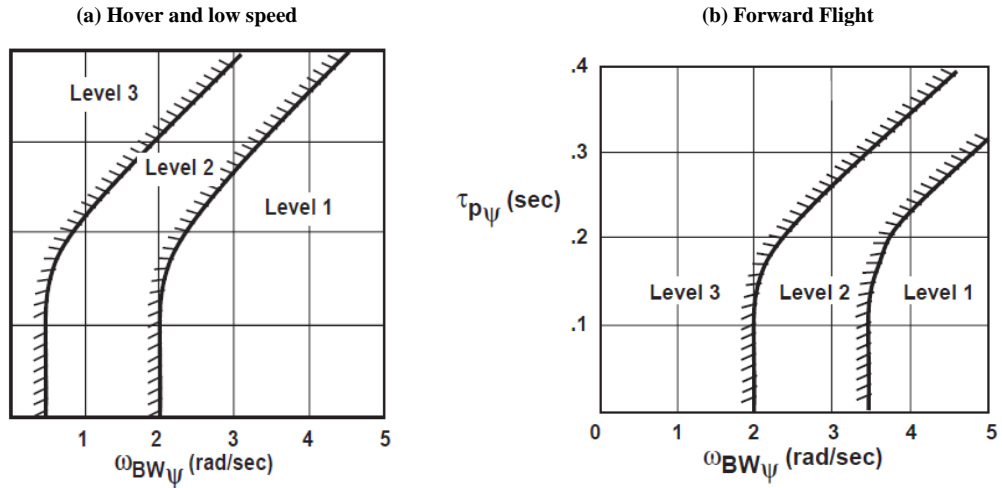


Figure 4-5 Requirements for small-amplitude heading changes [33]

4.2.2.2 Mid-Term Response to Control Inputs

Similar to the pitch (roll) response characteristics, mid-term response requirements are applied to all frequencies below the bandwidth frequency obtained from Section 4.2.2.1. Same effective damping ratio limits are used as in Section 4.2.1.2.

4.2.3 Character of Attitude and Heading Hold Response Types

Following a pulse input to the control actuator, pitch and roll attitudes as well as heading angle shall return to within 10 percent of peak or one degree, whichever is greater, in less than 10 seconds [33].

4.2.4 Transient Response of Attitude Hold Response Types

Helicopter shall return to reference attitude (pitch/roll) within one overshoot which shall not exceed 20% of the initial deviation [35].

4.3 Control Law Formulation

Structure of the controller used in this study consists of a standard inner-outer loop control architecture (see Figure 4-6). The inner loop, which is used for stabilization and disturbance rejection is constructed using a linear quadratic regulator (LQR) approach. This loop is surrounded with classical PI controllers for tracking helicopter attitudes and heading which takes pitch attitude reference from a forward velocity tracking controller. The outermost loop (i.e. autorotation controller) provides the desired forward velocity references to the inner loop as well as collective commands and maximum allowable attitude limits depending on the phase of autorotation.

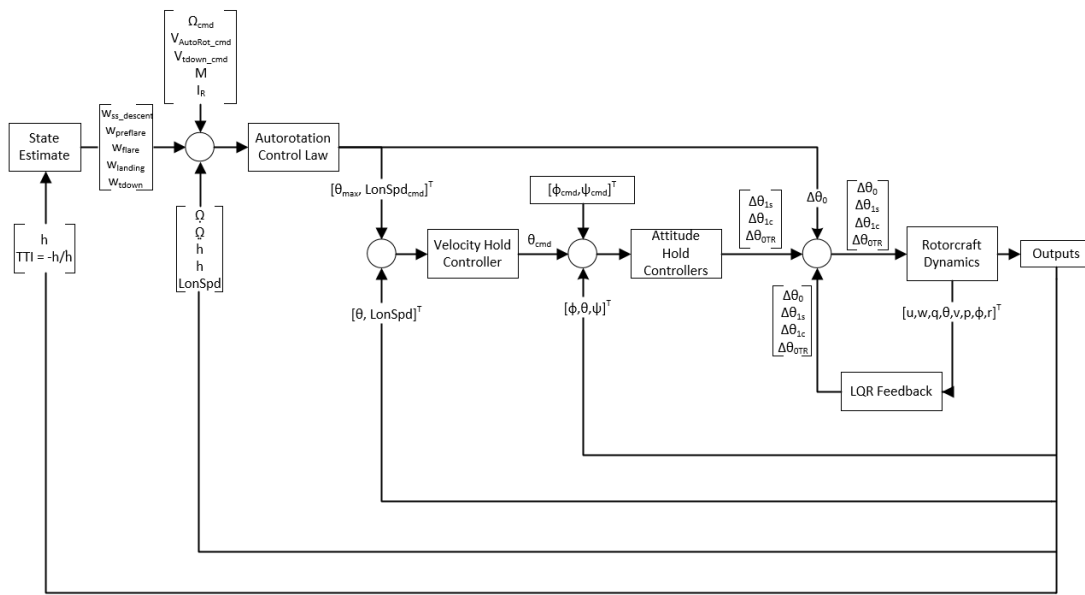


Figure 4-6 Control System Block Diagram

In order to reduce control effort, initial controller design is performed over the reduced order linear model. After gains are tuned according to the requirements given in Section 4.2, controller is implemented first to the full-linear model and then to the non-linear model.

4.3.1 Inner Loop Controller Design

Main purpose of the inner loop controller is to stabilize all unstable open-loop eigenvalues of the helicopter. In order to achieve this objective, linear quadratic regulator, which provides simultaneous feedback gains for all feedback states is used.

Moreover, using this method results in inherently good gain and phase margins while controlling a multi-input multi-output (MIMO) system [36].

4.3.1.1 Decoupling of Lateral and Longitudinal Dynamics

6-DoF helicopter model (8th order system) is still too complex to deal with analytically therefore, while developing LQR control laws for the inner loop system, longitudinal and lateral dynamics of the helicopter model are first decoupled. Although some information is lost during decoupling of longitudinal and lateral equations of motion, these losses are tried to be kept at a minimum level by comparing eigenvalues and frequency responses of the full, reduced (8x8) and low order approximated models (4x4) for certain input-output pairs.

While partitioning lateral and longitudinal dynamics from reduced linear model, model reduction techniques that are described in Section 3.2 are used.

4.3.1.1.1 Longitudinal equations of motion

Lateral states (v, p, ϕ, r) in the reduced order model are truncated to get the first approximated linear system

$$\dot{x}_{lon} = A_k^{lon(trun)} x_{lon} + B_k^{lon(trun)} u_{lon} \quad (4-3)$$

$$y_{lon} = C_k^{lon(trun)} x_{lon} + D_k^{lon(trun)} u_{lon} \quad (4-4)$$

To get second approximated linear model, lateral dynamics are residualized onto longitudinal dynamics by using matched DC method

$$\dot{x}_{lon} = A_k^{lon(MDC)} x_{lon} + B_k^{lon(MDC)} u_{lon} \quad (4-5)$$

$$y_{lon} = C_k^{lon(MDC)} x_{lon} + D_k^{lon(MDC)} u_{lon} \quad (4-6)$$

Where $x_{lon} = [u, w, q, \theta]^T$ and $u_{lon} = [\theta_0, \theta_{1s}]^T$. $A_k^{lon(trun)}(C_k^{lon(trun)})$ and $A_k^{lon(MDC)}(C_k^{lon(MDC)})$ are 4x4 matrices, $B_k^{lon(trun)}(D_k^{lon(trun)})$ and $B_k^{lon(MDC)}(D_k^{lon(MDC)})$ are 4x2 matrices, respectively.

Subscript k given in (4-3) through (4-6) indicate kth linear system. While designing the controller in this study, helicopter is linearized about 5 different forward flight trim conditions which are hover, 40 knots, 80 knots, 120 knots and 160 knots (which correspond to k = 1,2 ... 5 respectively.)

Among different linearized models, for illustration, 80 knots FF case (k = 3) is chosen and comparison of open loop eigenvalues (Figure 4-7) and frequency responses of full, reduced and two approximated linear models are provided for that flight condition (Figure 4-8 to Figure 4-10). Same methodology is used for all other airspeeds. For state and control matrices of the reduced order linear model of the selected case (80 knots), one can refer to Appendix C.

In Figure 4-7 and Figure 4-11, lateral and longitudinal modes of 6-DoF helicopter model which are described in Table 4-1 are also plotted.

Table 4-1 6-DoF Helicopter Modes

Longitudinal Modes	Lateral Modes
Phugoid (long period longitudinal mode, can be either stable or unstable)	Dutch Roll (long period lateral mode, can be either stable or unstable)
Pitch Subsidence (stable short period longitudinal mode)	Roll Subsidence (fastest stable short period lateral mode)
Heave Subsidence (stable short period longitudinal mode)	Spiral Subsidence (stable long period lateral mode)

More detailed information about longitudinal and lateral modes are provided in [31].

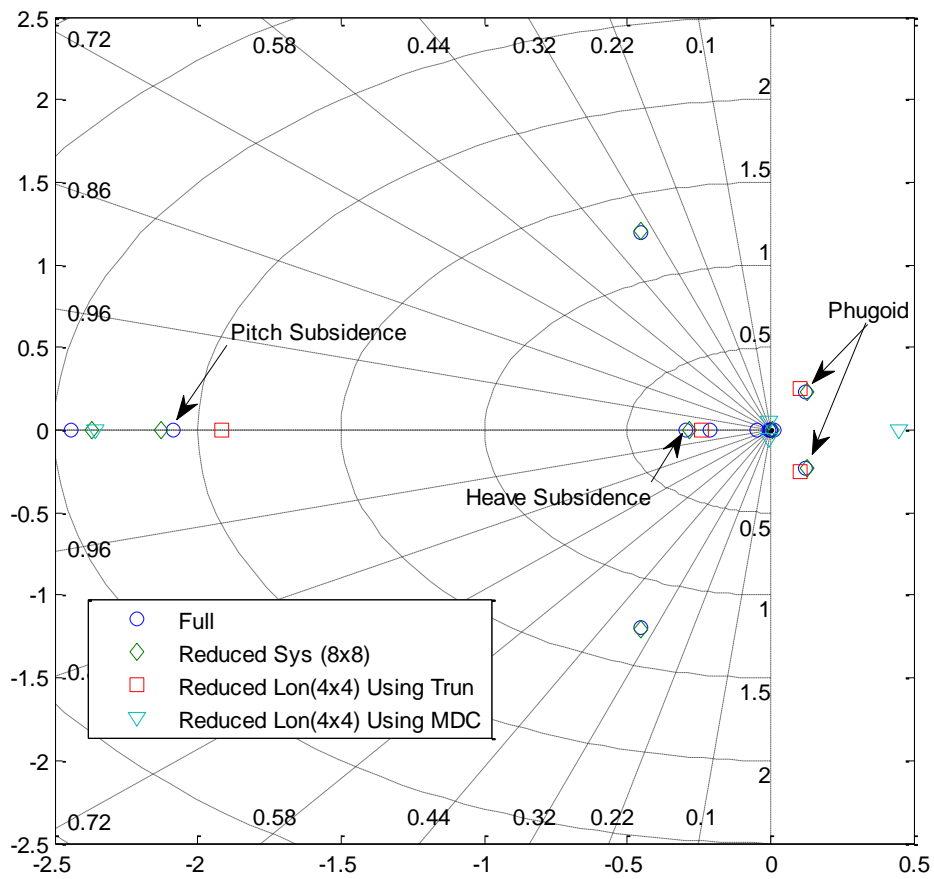


Figure 4-7 Open Loop Eigenvalues (Longitudinal)

Notice that linear system obtained using truncation method gives closer eigenvalue approximations to the full linear system. When lateral states are residualized onto longitudinal dynamics using MDC method, complex conjugate unstable phugoid mode is transformed into two real eigenvalues which may cause differences in dynamic responses of full linear and approximated model.

In the following figures frequency responses from collective to vertical velocity, from longitudinal cyclic to pitch rate and forward velocity are plotted for $k = 3$ (80 knots) case.

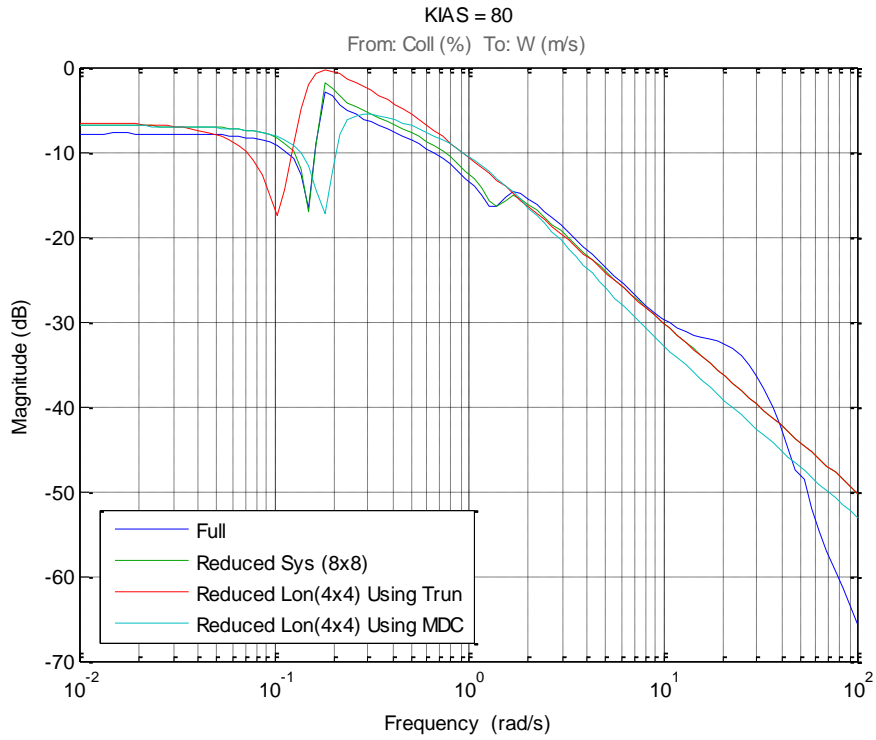


Figure 4-8 Collective to Vertical Velocity

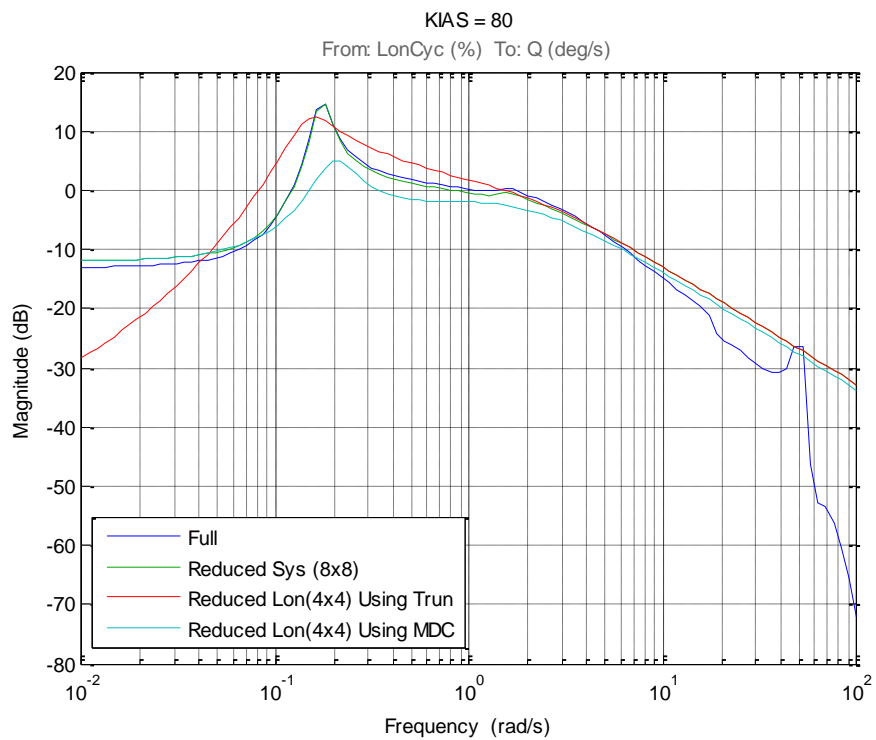


Figure 4-9 Longitudinal Cyclic to Pitch Rate

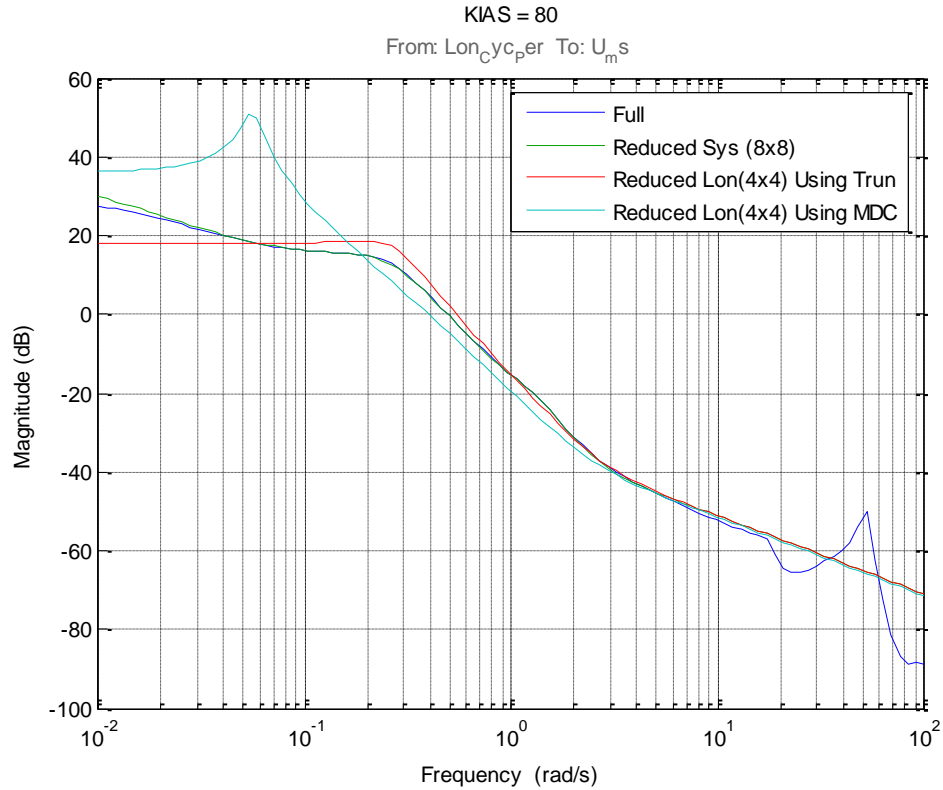


Figure 4-10 Longitudinal Cyclic to Forward Velocity

Notice that decoupling of longitudinal modes using truncation resulted in some losses in low frequency range but within desired frequency range (0.1 – 10 rad/s), 4th order approximate linear systems obtained using both methods give close results to the reduced and full linear systems.

From these results, it is concluded that, 4th order dynamical system obtained using truncation method gives closer results to the full linear system therefore while designing inner loop control laws it used to approximate longitudinal dynamics of the helicopter.

4.3.1.1.2 Lateral equations of motion:

Similar to the longitudinal equations of motion, two different lower order approximations of the reduced order model are obtained using model reduction techniques given in Section 3.2.

By truncating longitudinal states (u, w, q, θ) in the reduced order (8x8) model,

$$\dot{x}_{lat} = A_k^{lat(trun)} x_{lat} + B_k^{lat(trun)} u_{lat} \quad (4-7)$$

$$y_{lat} = C_k^{lat(trun)} x_{lat} + D_k^{lat(trun)} u_{lat} \quad (4-8)$$

Is obtained.

When lateral dynamics of the helicopter are approximated using matched DC method, following 4th order linear model is obtained

$$\dot{x}_{lat} = A_k^{lat(MDC)} x_{lat} + B_k^{lat(MDC)} u_{lat} \quad (4-9)$$

$$y_{lat} = C_k^{lat(MDC)} x_{lat} + D_k^{lat(MDC)} u_{lat} \quad (4-10)$$

Where $x_{lat} = [v, p, \phi, r]^T$ and $u_{lat} = [\theta_{1c}, \theta_{0TR}]^T$. $A_k^{lat(trun)}$ ($C_k^{lat(trun)}$) and $A_k^{lat(MDC)}$ ($C_k^{lat(MDC)}$) are 4x4 matrices, $B_k^{lat(trun)}$ ($D_k^{lat(trun)}$) and $B_k^{lat(MDC)}$ ($D_k^{lat(MDC)}$) are 4x2 matrices, respectively.

Comparison of open loop eigenvalues of full, reduced and two approximated linear models together with 6-DoF lateral models are given in Figure 4-11.

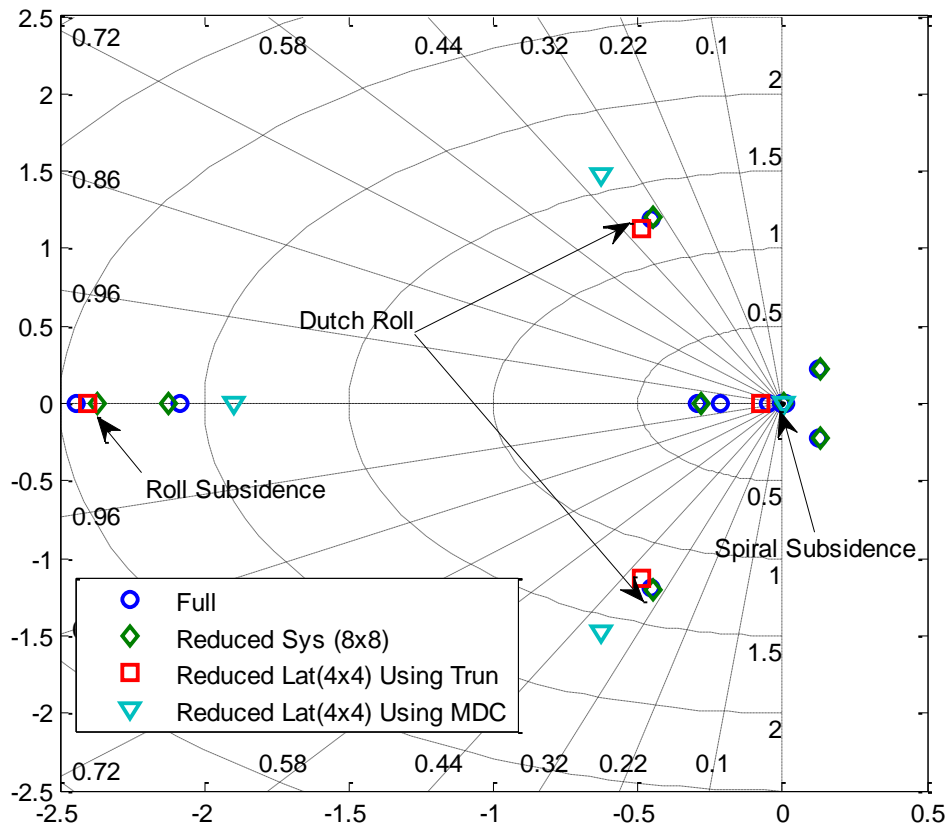


Figure 4-11 Open Loop Eigenvalues (Lateral)

Figure 4-11 shows that using truncation method resulted in closer eigenvalues with the reduced and full linear models and shows that lateral modes are better separated.

In order to compare lateral/directional modes of the full, reduced and two approximated linear models, frequency responses from lateral cyclic to roll rate and lateral velocity, together with frequency responses from pedal to yaw rate are plotted.

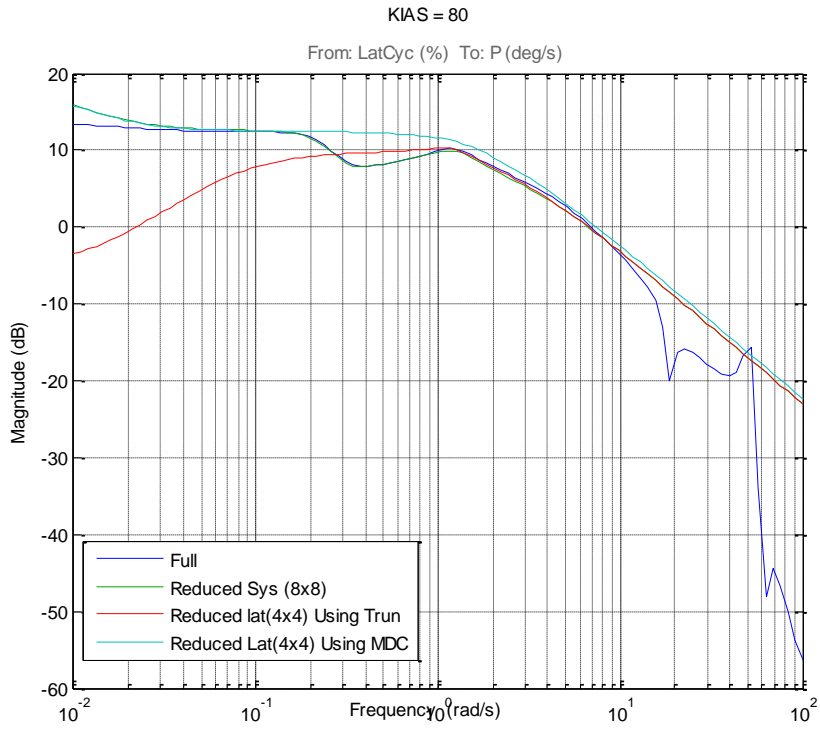


Figure 4-12 Lateral Cyclic to Roll Rate

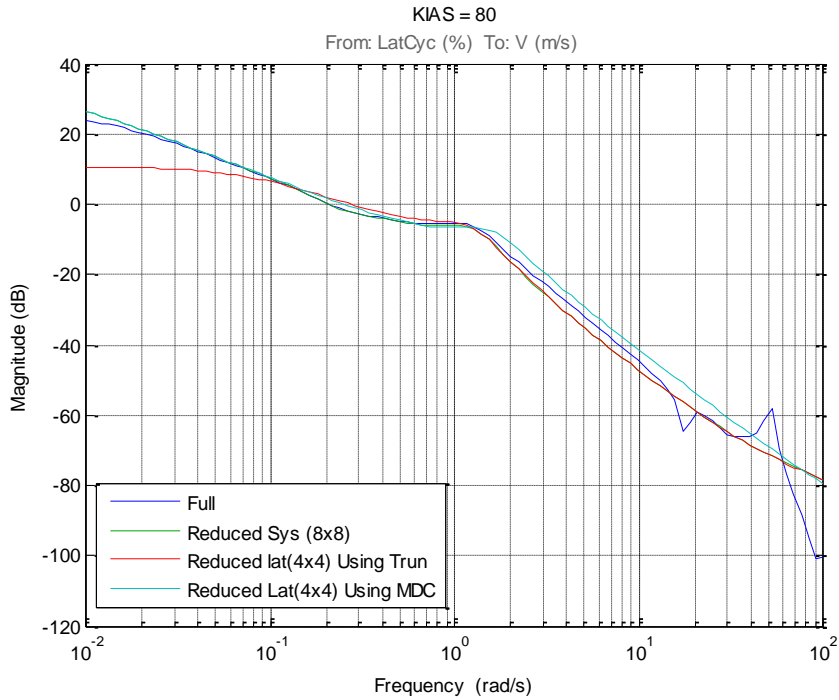


Figure 4-13 Lateral Cyclic to Body Lateral Velocity

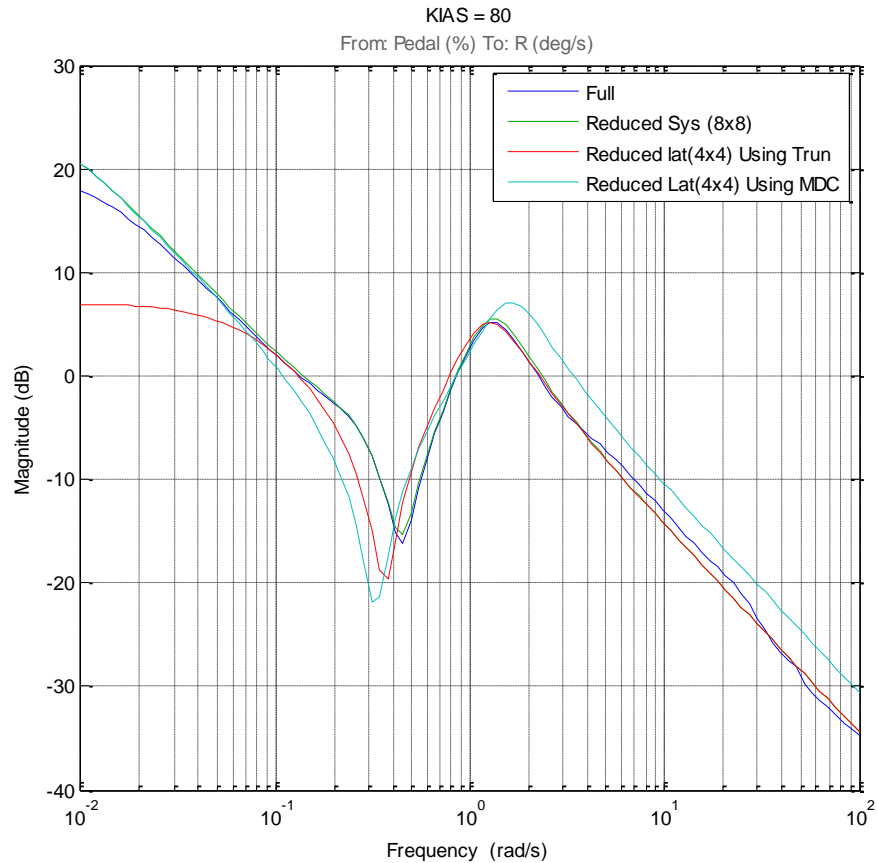


Figure 4-14 Pedal to Yaw Rate

Similar to the longitudinal equations of motion case, 4th order model obtained using truncation resulted in some losses in low frequency range but it tracks reduced and full linear system better within desired frequency range (0.1-10 rad/s).

Therefore, while designing inner loop control laws, 4th order system obtained using truncation method is used to approximate lateral dynamics of the helicopter.

4.3.1.2 Linear Quadratic Regulator Design

After 6-DoF aircraft model is decoupled into longitudinal and lateral modes, Linear Quadratic Regulator (i.e. an optimal control law) can be applied to stabilize the system.

As described before, LQR is a state feedback regulator which guarantees stability of a system by trying to drive any initial condition error to zero [36]. In order to minimize quadratic cost functions

$$J_{lon} = \frac{1}{2} \int_0^T (x_{lon}^T Q_{lon} x_{lon} + u_{lon}^T R_{lon} u_{lon}) dt \quad (4-11)$$

$$J_{lat} = \frac{1}{2} \int_0^T (x_{lat}^T Q_{lat} x_{lat} + u_{lat}^T R_{lat} u_{lat}) dt \quad (4-12)$$

state-feedback control laws

$$u_{lon} = -K_{lon} x_{lon} \quad (4-13)$$

$$u_{lat} = -K_{lat} x_{lat} \quad (4-14)$$

are applied where $Q_{lon(lat)} \geq 0$, $R_{lon(lat)} > 0$ are symmetric, positive (semi-) definite matrices.

For obtaining longitudinal and lateral optimal state feedback control gains

$$K_{lon} = -R_{lon}^{-1} B_{lon}^T P_{lon} \quad (4-15)$$

$$K_{lat} = -R_{lat}^{-1} B_{lat}^T P_{lat} \quad (4-16)$$

(assuming $T = \infty$) algebraic Ricatti equations given in (4-17) and (4-18) are solved for P_{lon} and P_{lat} .

$$A_{lon}^T P_{lon} + P_{lon} A_{lon} - P_{lon} B_{lon} R_{lon}^{-1} B_{lon}^T P_{lon} + Q_{lon} = 0 \quad (4-17)$$

$$A_{lat}^T P_{lat} + P_{lat} A_{lat} - P_{lat} B_{lat} R_{lat}^{-1} B_{lat}^T P_{lat} + Q_{lat} = 0 \quad (4-18)$$

With the requirements

- $Q_{lon(lat)}$ matrices being symmetric positive semi-definite
- $R_{lon(lat)}$ matrices being symmetric positive definite
- $(A_{lon(lat)}, B_{lon(lat)})$ pairs being stabilizable
- $(A_{lon(lat)}, Q_{lon(lat)}^{1/2})$ pairs being observable

While choosing weights of LQR that will result in desired performance, “Improved Linear Quadratic Regulator” steps described in [36] are used as a guideline. A flowchart of the steps is given in Figure 4-15. Using the steps given in Figure 4-15, separate LQR controllers are designed for lateral and longitudinal channels.

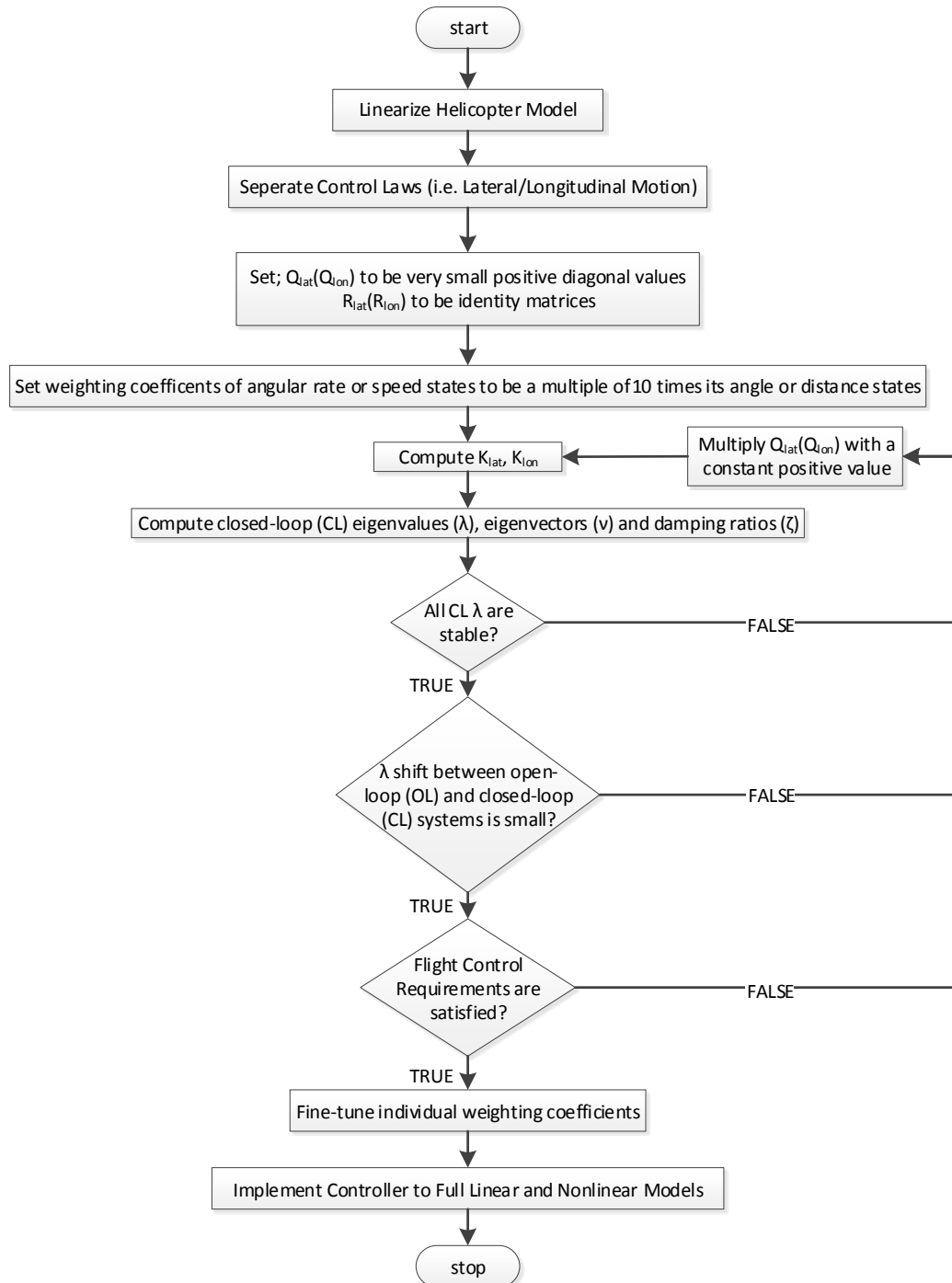


Figure 4-15 LQR controller design flowchart

4.3.1.3 Assessment of LQR Controller

After LQR controllers are designed using decoupled reduced order models, they are superposed as in (4-19) and implemented into the full linear model.

$$K_{LQR_k} = \begin{bmatrix} K_{lon_k} & 0 \\ 0 & K_{lat_k} \end{bmatrix} \quad (4-19)$$

Notice that both K_{lon_k} and K_{lat_k} are 2x4 matrices.

Since inner loop LQR controller is used to provide rate damping and stabilization, there is no integrator term (which can be used for input tracking). Moreover, inputs to the controller are in control inputs domain $\{\Delta\theta_0, \Delta\theta_{1s}, \Delta\theta_{1c}, \Delta\theta_{0TR}\}$ therefore, closed-loop system composed of LQR controller and plant cannot be treated as an ACAH or rate response type system. However, bandwidth (ω_{bw}) and phase delay (τ_p) parameters obtained from closed loop frequency response plots can still be evaluated. Notice that yaw attitude feedback is not included during LQR controller design therefore only longitudinal (pitch) and lateral (roll) channels are evaluated.

Around each trim point where helicopter equations of motion are linearized (hover, 40 knots, 80 knots, 120 knots and 160 knots) closed loop frequency responses from control inputs (θ_{1c}, θ_{1s}) to on axis attitude responses (ϕ, θ) are plotted to find bandwidth (ω_{bw}) and phase delay (τ_p) parameters (see 4.2.1.1). Small amplitude pitch and roll handling quality levels are then evaluated using limits given in Figure 4-3.

For hover and low speed flight (<45 knots), same bandwidth requirements are used for pitch and roll attitudes during degraded visual environment (UCE > 1) and divided attention operations.

Notice that inner loop controller is level 1 in pitch and roll axes for both hover and 40 knots cases (Figure 4-16).

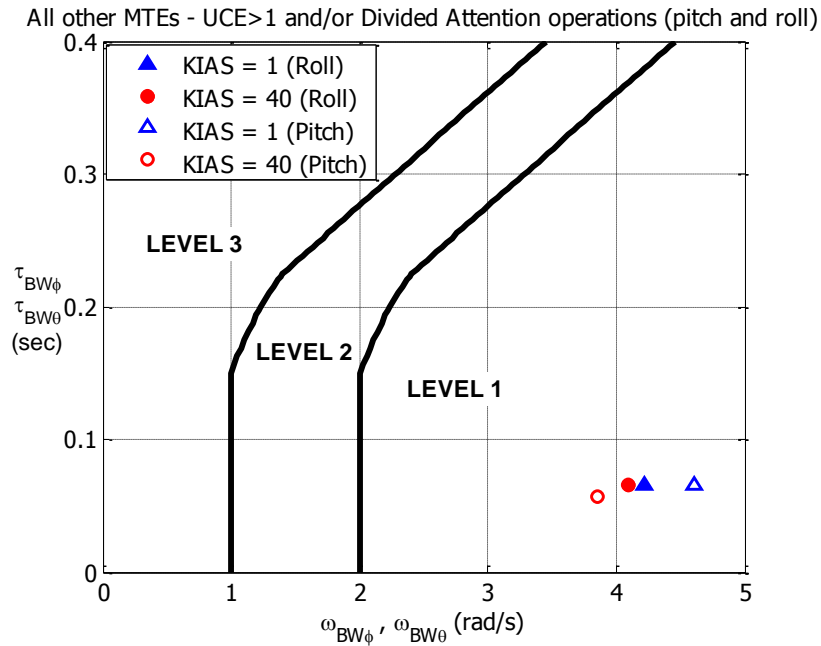


Figure 4-16 Pitch (Roll) bandwidth assessment – hover and low speed

Similar to the low-speed cases, for forward flight cases (>45 knots), both pitch and roll channels are level 1 in terms of small-amplitude pitch (roll) attitude changes (see Figure 4-17 and Figure 4-18) which means that pilot compensation is not a factor for desired performance.

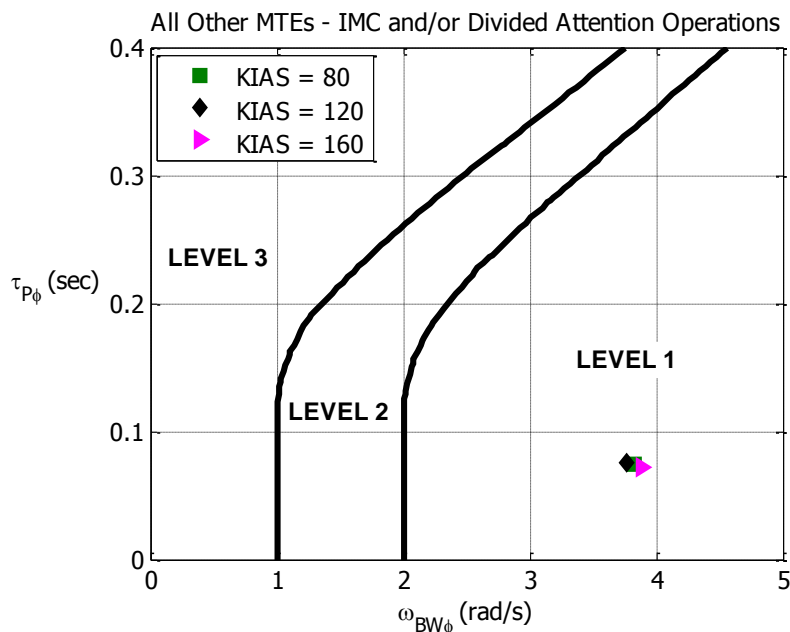


Figure 4-17 Roll bandwidth assessment – forward flight

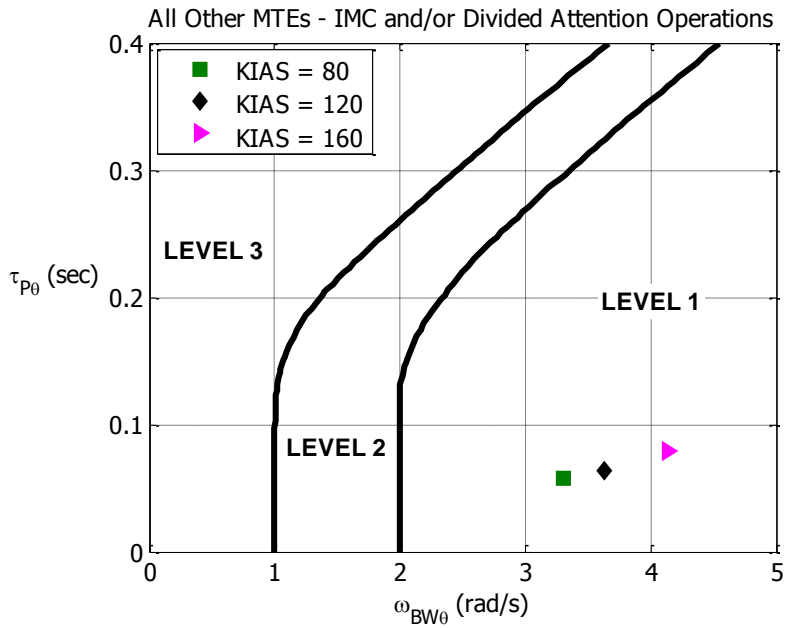


Figure 4-18 Pitch bandwidth assessment – forward flight

For checking closed loop eigenvalue locations and oscillation limits on each axis, requirements given in Figure 4-4 are used.

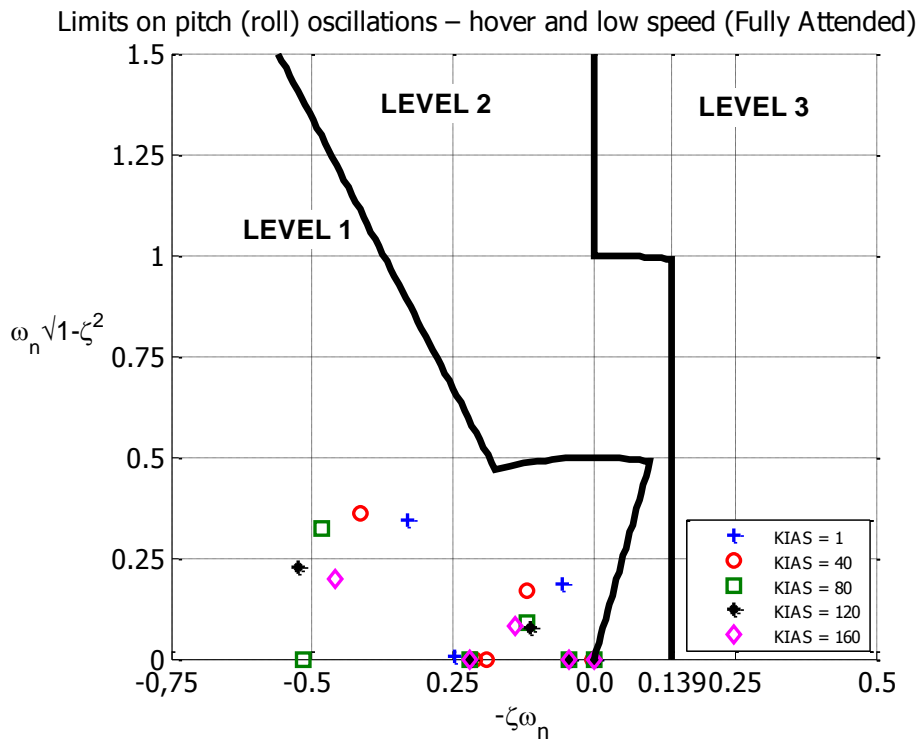


Figure 4-19 Pitch (roll) oscillations assessment

Notice that none of the eigenvalues given in Figure 4-19 have positive real part. Therefore, LQR controller makes the system stable at all airspeeds around which helicopter equations of motion are linearized. Moreover, all complex conjugate eigenvalues have enough damping ratios to satisfy handling quality level 1 requirements.

It can be concluded from the results that, regardless of the airspeed at which helicopter is linearized around, LQR controller satisfies handling quality level 1 requirements in both longitudinal and lateral channels.

4.3.2 Attitude Command Attitude Hold (ACAH) and Heading Hold (HH) Controllers Design

After inner loop stabilization is achieved, using classical control approach, attitude command attitude hold and heading hold controllers are designed for separate channels (ACAH for roll and pitch, HH for yaw). Other than flight control requirements given in Section 4.2, during controller design, for defining robustness of the system, gain, phase and stability margins are used. In [37], typical intervals of these margins are given as; $\Phi_m = 30^\circ - 60^\circ$ for phase margin, $g_m = 2 - 5$ for gain margin and $s_m = 0.5 - 0.8$ for stability margin. Similarly, in [29], $g_m > 6 \text{ dB}$ is suggested for good performance whereas desired phase margin range is again $\Phi_m = 30^\circ - 60^\circ$. While adjusting controller gains, MATLAB Simulink[®] PID controller block is used to achieve desired performance and level 1 handling quality.

4.3.2.1 Pitch Channel ACAH Controller Design

For tracking pitch attitude of the helicopter, a proportional-integral type controller, which generates longitudinal cyclic commands to the inner loop controller, is used. Reference pitch attitudes of the controller are generated from the outer loop longitudinal speed controller. Structure of the pitch channel attitude command attitude hold controller is given in Figure 4-20.

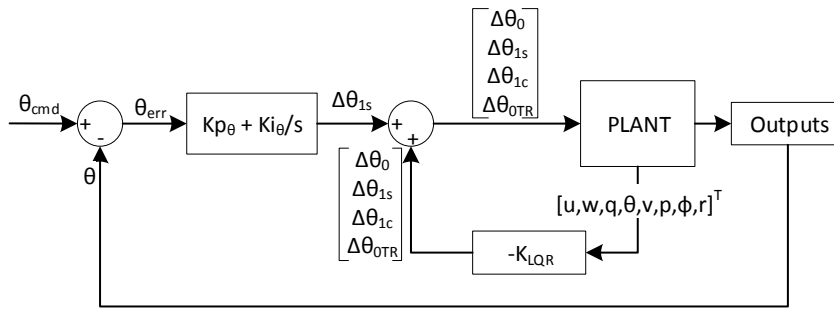


Figure 4-20 Pitch Attitude Command Attitude Hold Controller Structure

Similar to the inner loop LQR controller, different gains are determined for each linear model. Figure 4-21 shows responses of the ACAH controllers to reference pitch attitude step commands. It can be seen that, rise time is less than 1 second, settling time is about 5 seconds and maximum overshoot is less than 20% which indicates that the requirements given in Section 4.2.4 are satisfied.

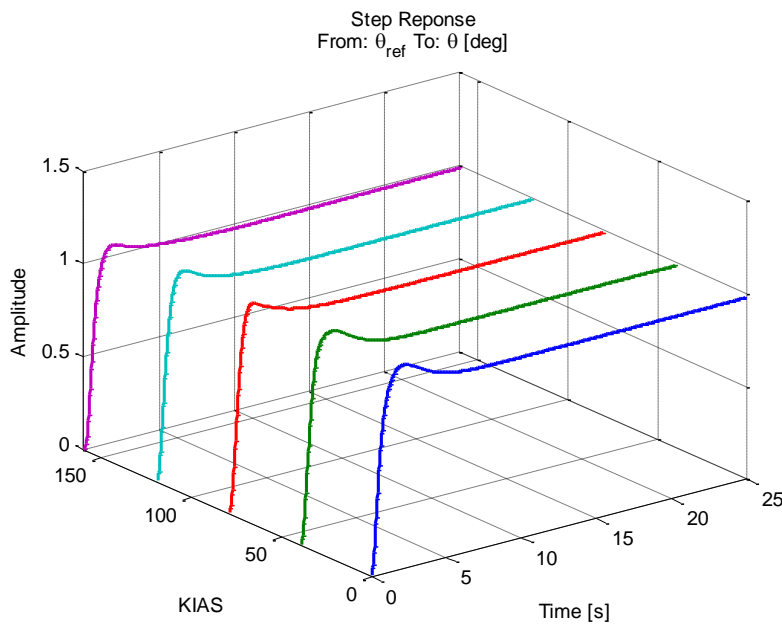


Figure 4-21 ACAH Responses to Reference Pitch Attitudes

In order to check flight control requirements defined in section 4.2.3, pitch attitude impulse responses are plotted in Figure 4-22. Results show that all controllers return to 10 percent of their peak amplitudes in less than 4 seconds and the requirements are satisfied.

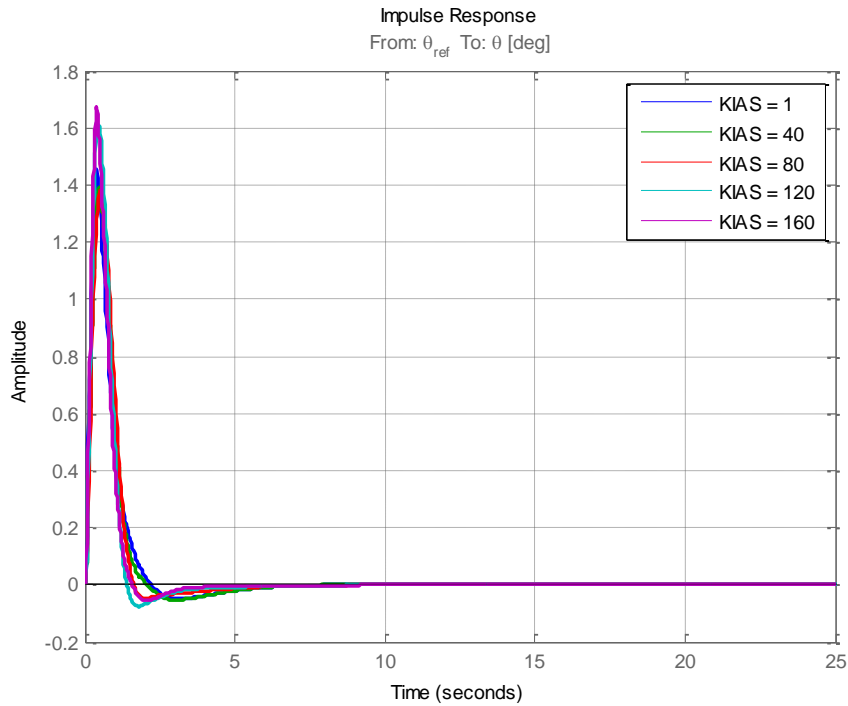


Figure 4-22 ACAH Responses to Pitch Attitude Pulse Inputs

Apart from time domain responses, stability and robustness properties in frequency domain need to be checked using the loop transfer function $L(s) = P(s)C(s)$.

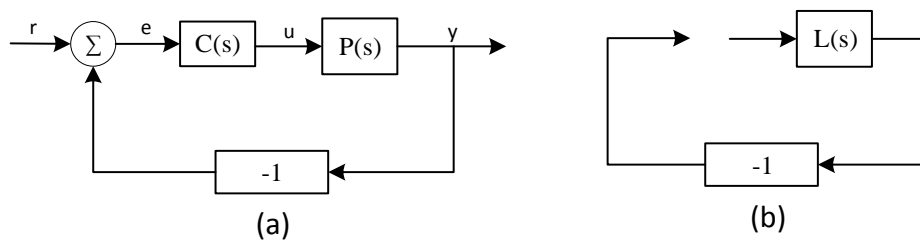


Figure 4-23 Loop Transfer Function

Bode and Nyquist plots contain the same information therefore any of these plots can be used for determining gain and phase margins of the system. However, Nyquist plots also provide information about the stability margin of the loop gain which cannot be obtained using bode plots (see Figure 4-24). This margin is important for determining disturbance attenuation of the system. Therefore, for frequency domain analyses, Nyquist plots are used in this study.

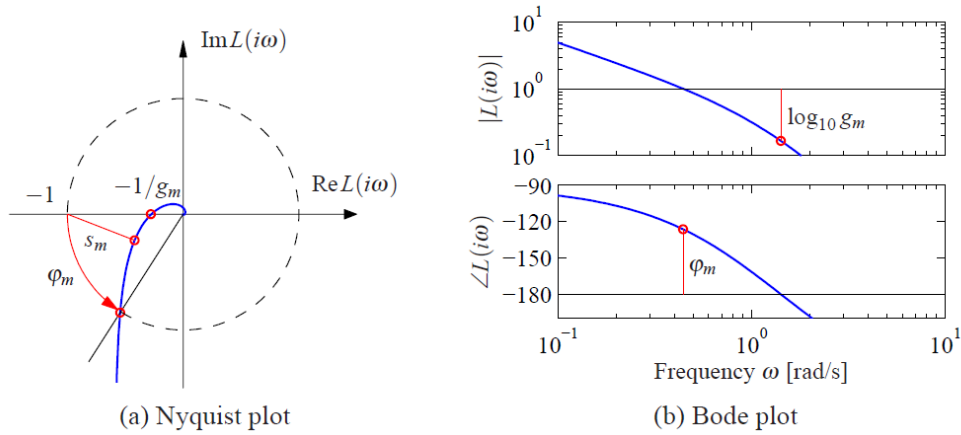


Figure 4-24 Stability margins [37]

In Figure 4-25, Nyquist plots of five loop gains, which are obtained using full-linear models of five different airspeed conditions, are given. Gain, phase and stability margins together with crossover frequencies obtained from these plots are provided in Table 4-2.

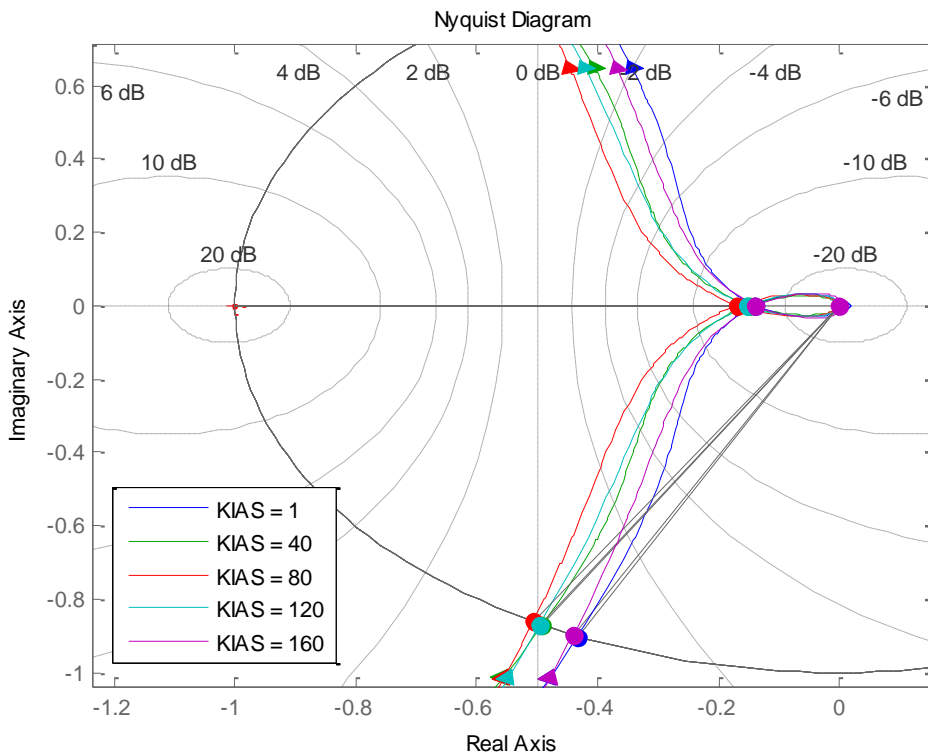


Figure 4-25 Nyquist Plots Pitch Channel ACAH

Table 4-2 Pitch Channel ACAH Stability Margins

Airspeed (knots)	g_m (dB)	ω_{pc} (rad/s)	Φ_m (deg)	ω_{gc} (rad/s)	s_m	ω_{ms} (rad/s)
Hover	17.2	7.95	64.3	1.51	0.78	4.68
40	16.6	6.86	60.6	1.54	0.73	3.87
80	15.5	6.15	59.6	1.6	0.70	3.61
120	16.3	6.88	60.4	1.58	0.73	3.87
160	17.2	7.74	63.9	1.55	0.77	4.12

It can be concluded from Table 4-2 that, the closed loop system has enough margin of stability and robustness.

Similar to the inner loop controller case, in order to evaluate handling quality level of the ACAH controller in longitudinal channel, bandwidth and phase-delay parameters are obtained from Figure 4-2 using the closed loop frequency response from θ_{ref} to θ .

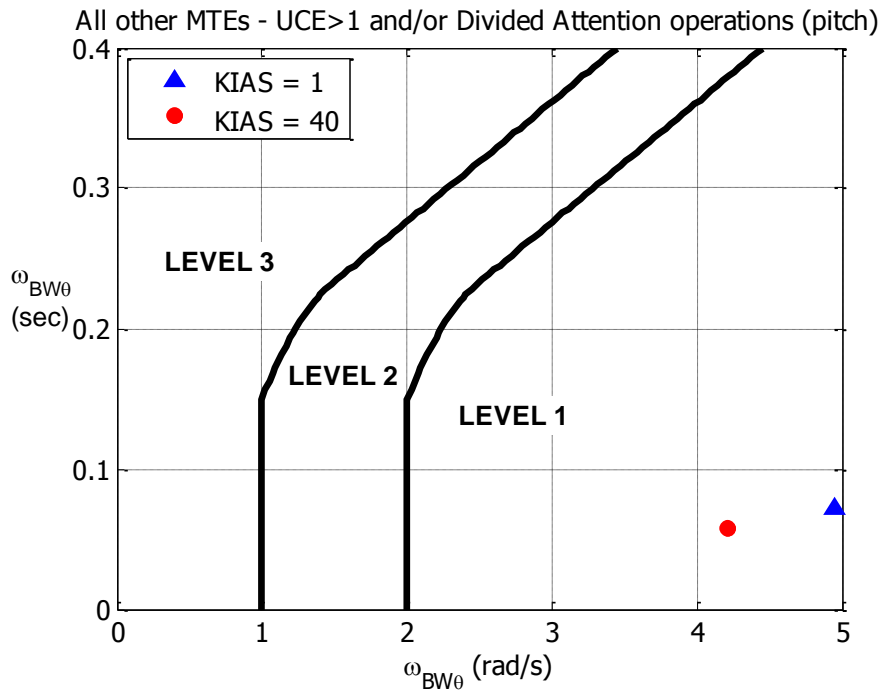


Figure 4-26 Pitch bandwidth assessment – hover and low speed

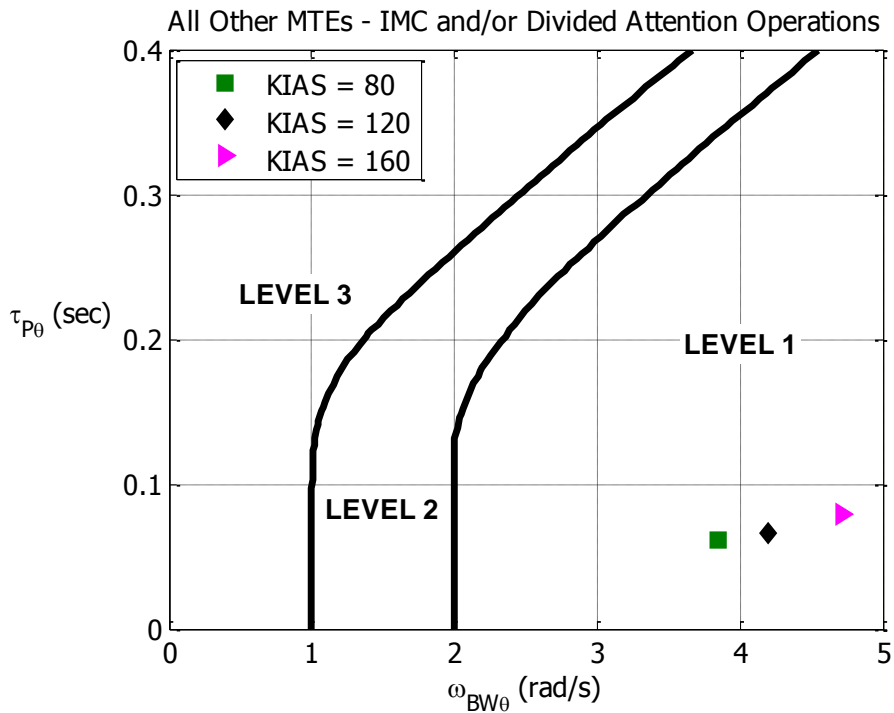


Figure 4-27 Pitch bandwidth assessment – forward flight

Notice that for all airspeeds that the controller is designed for, level 1 handling quality specifications are met for the short-term responses in longitudinal channel.

4.3.2.2 Roll Channel ACAH Controller Design

For tracking roll attitude of the helicopter, a proportional-integral type controller is used which generates lateral cyclic commands to the inner loop controller. Structure of the roll channel attitude command attitude hold controller is given in Figure 4-28.

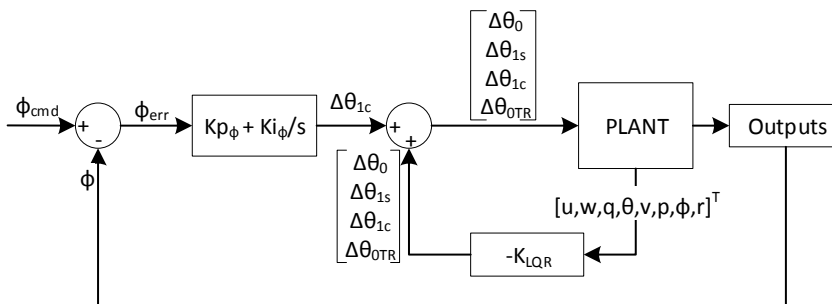


Figure 4-28 Roll Attitude Command Attitude Hold Controller Structure

Similar to the pitch ACAH controller, different gains are determined for each linear model. Figure 4-29 shows responses of the ACAH controllers to reference roll attitude step commands. It can be seen that, rise time is less than 1.5 seconds, settling time is about 10 seconds and maximum overshoot is less than 20% which indicates that the requirements given in Section 4.2.4 are satisfied.

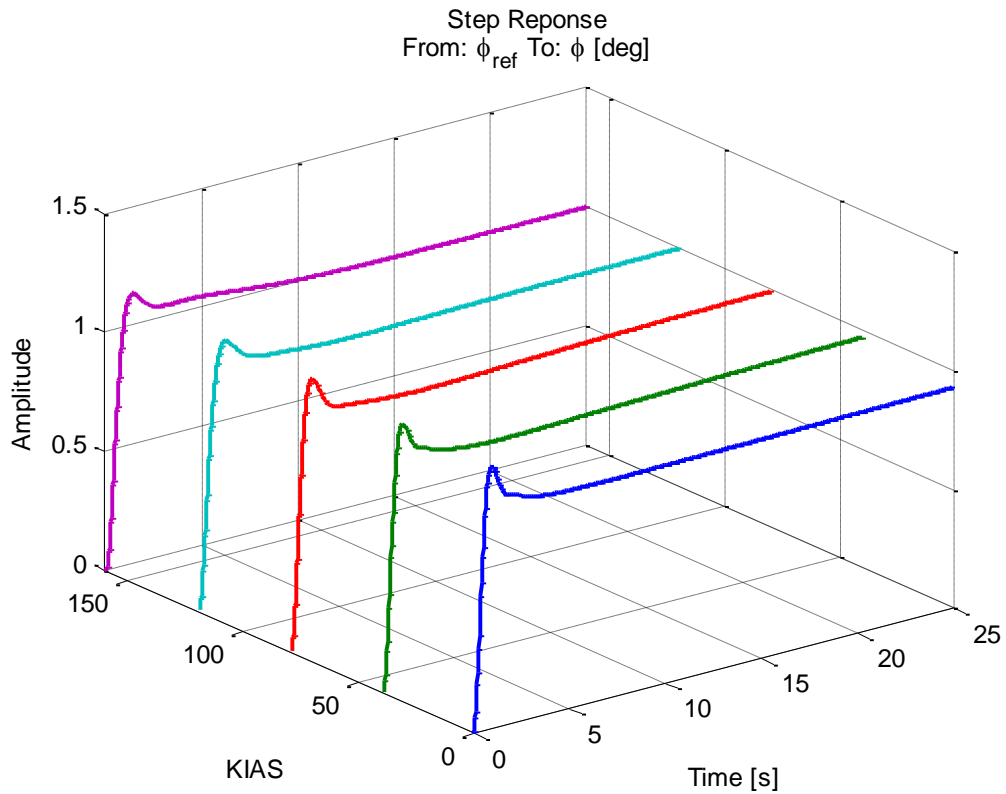


Figure 4-29 ACAH Responses to Reference Roll Attitudes

In order to check flight control requirements defined in section 4.2.3, roll attitude impulse responses are plotted in Figure 4-30. Notice that all controllers return to 10 percent of their peak amplitudes in less than 3 seconds and the requirements are satisfied.

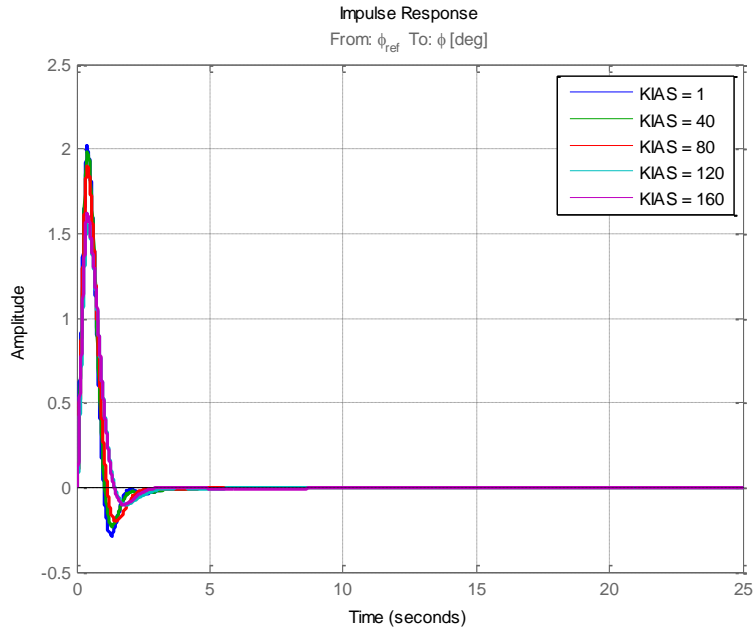


Figure 4-30 ACAH Responses to Roll Attitude Pulse Inputs

Apart from time domain responses, using the loop transfer function, stability and robustness properties in frequency domain are checked.

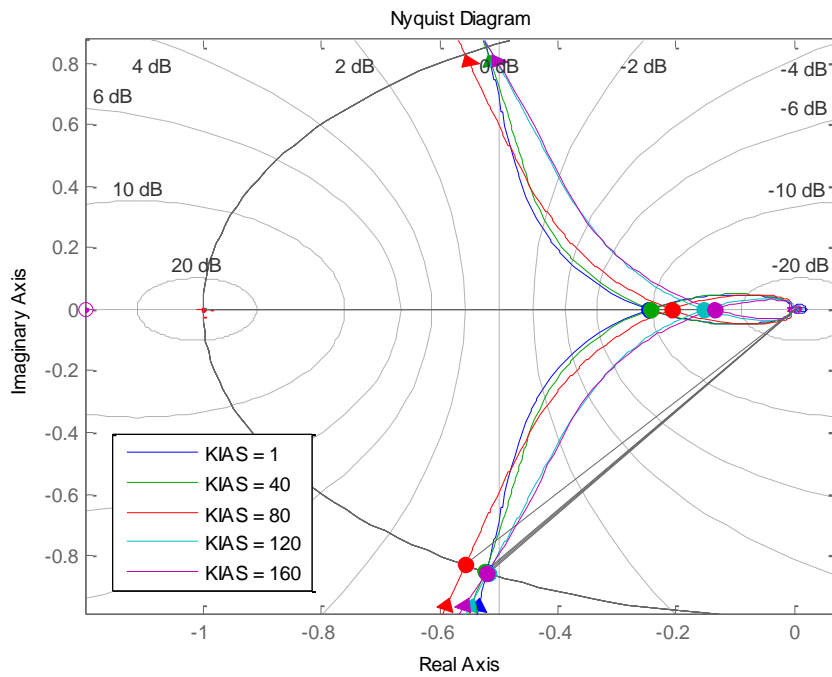


Figure 4-31 Nyquist Plots Roll Channel ACAH

In Figure 4-31, Nyquist plots of five loop gains, which are obtained using full-linear models of five different airspeed conditions, are given. Gain, phase and stability margins together with crossover frequencies obtained from these plots are provided in Table 4-3.

Table 4-3 Roll Channel ACAH Stability Margins

Airspeed (knots)	g_m (dB)	ω_{pc} (rad/s)	Φ_m (deg)	ω_{gc} (rad/s)	s_m	ω_{ms} (rad/s)
Hover	12.2	6.84	58.7	2.42	0.63	4.68
40	12.3	6.86	58.5	2.3	0.64	4.66
80	13.6	7.17	56.2	2.24	0.66	4.28
120	16.3	7.43	58.8	1.84	0.71	3.81
160	17.3	7.97	58.7	1.86	0.71	3.81

It can be concluded from Table 4-3 that, the closed loop system has enough margin of stability and robustness.

Similar to the pitch channel ACAH design case, in order to evaluate handling quality level of the lateral channel ACAH controller, bandwidth and phase-delay parameters are obtained from Figure 4-2 using the closed loop frequency response from ϕ_{ref} to ϕ .

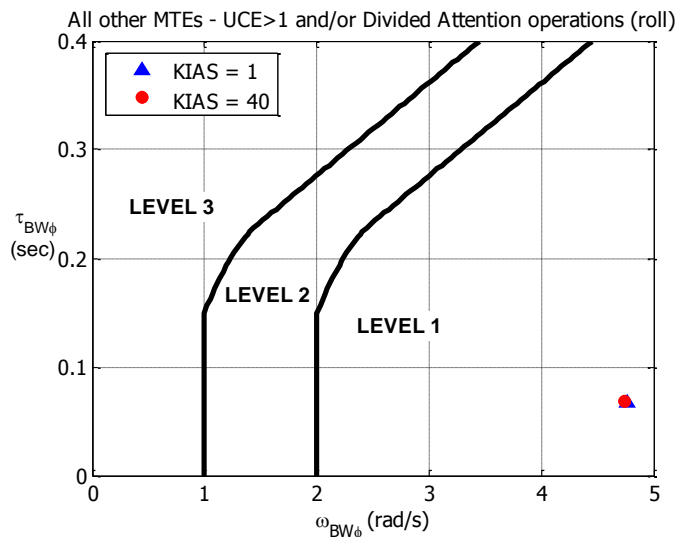


Figure 4-32 Roll bandwidth assessment – hover and low speed

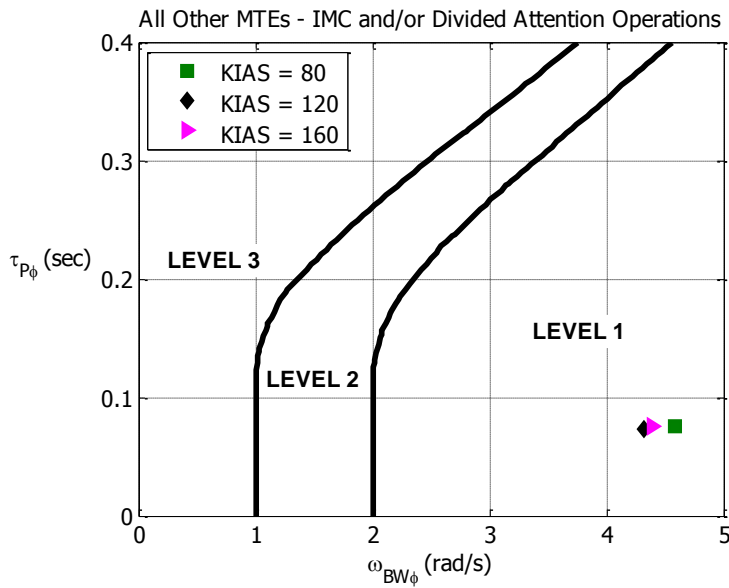


Figure 4-33 Roll bandwidth assessment – forward flight

Figure 4-32 and Figure 4-33 shows that for all airspeeds that the controller is designed for, handling quality level 1 specifications are met for the lateral channel.

4.3.2.3 Yaw Channel Heading Hold Controller Design

For tracking heading of the helicopter, a proportional-integral type controller is used which generates pedal commands to the inner loop controller. Notice that, for high airspeeds (>40 knots) instead of tracking yaw attitude, sideslip/ N_y controllers can be used as an alternative. Structure of the yaw channel heading hold controller is given in Figure 4-34.

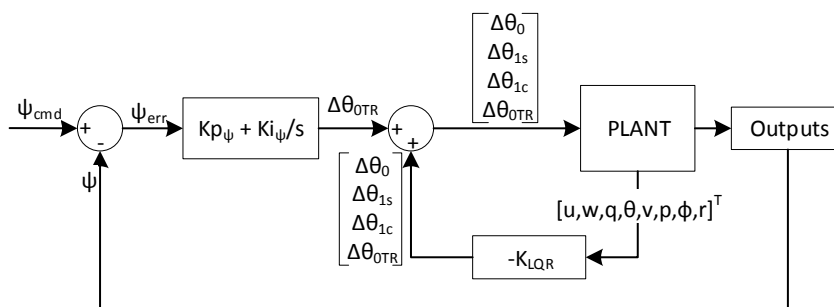


Figure 4-34 Heading Hold Controller Structure

Similar to the pitch/roll ACAH controllers, different gains are determined for each linear model. Figure 4-35 shows responses of the HH controllers to reference yaw attitude step commands. It can be seen that, rise time is less than 2 seconds for all cases, settling time is about 13 seconds and maximum overshoot is less than 20% which indicates that the requirements given in Section 4.2.4 are satisfied.

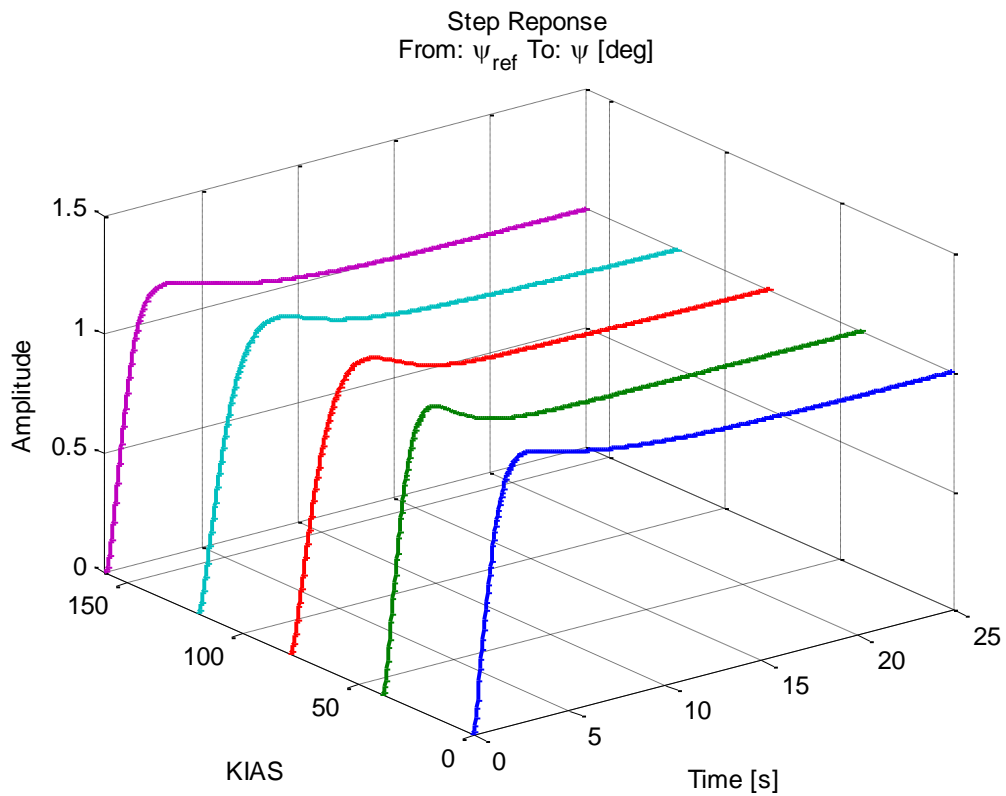


Figure 4-35 HH Responses to Reference Yaw Attitudes

In order to check flight control requirements defined in section 4.2.3, yaw attitude impulse responses are plotted in Figure 4-36. Notice that all controllers return to 10 percent of their peak amplitudes in less than 4 seconds and the requirements are satisfied.

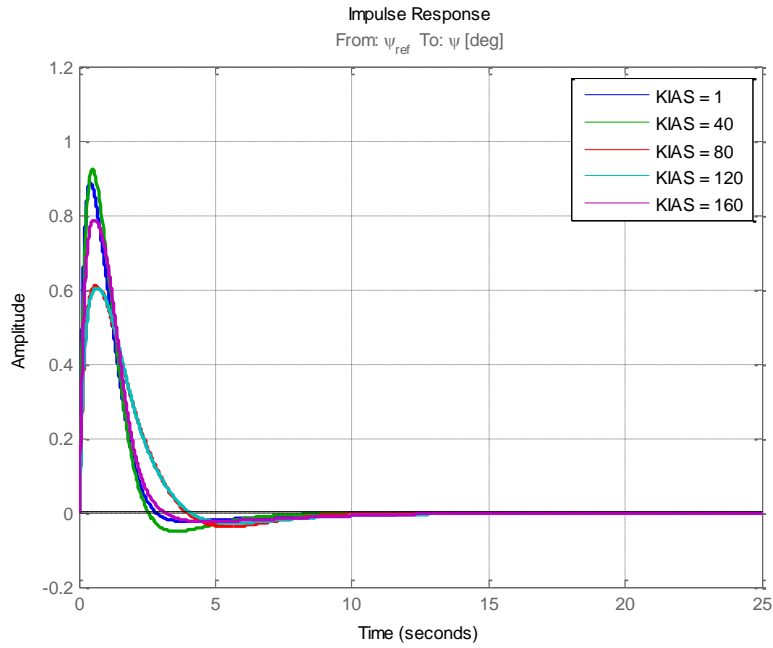


Figure 4-36 HH Response to Yaw Attitude Pulse Input

Apart from time domain responses, using the loop transfer function, stability and robustness properties in frequency domain are checked.

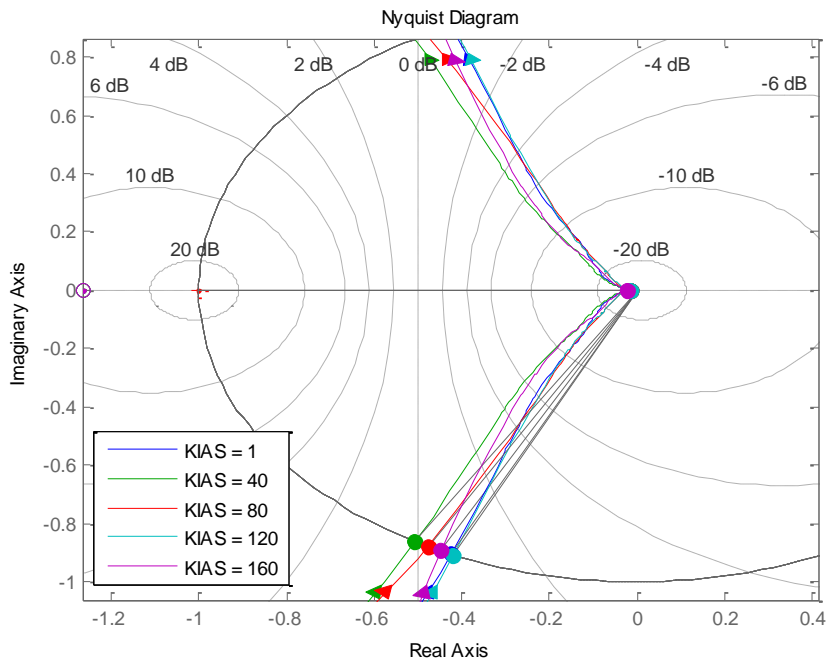


Figure 4-37 Nyquist Plots Yaw Channel HH

In Figure 4-37, Nyquist plots of five loop gains, which are obtained using full-linear models of five different airspeed conditions, are given. Gain, phase and stability margins together with crossover frequencies obtained from these plots are provided in Table 4-4.

Table 4-4 Yaw Channel HH Stability Margins

Airspeed (knots)	g_m (dB)	ω_{pc} (rad/s)	Φ_m (deg)	ω_{gc} (rad/s)	s_m	ω_{ms} (rad/s)
Hover	36.8	20.5	64.9	1.12	0.85	2.45
40	36	17.9	59.5	1.18	0.81	2.25
80	37	15.1	61.5	0.755	0.86	1.63
120	36.1	14.6	65.3	0.768	0.85	1.61
160	32.6	13.9	63.4	1.06	0.82	2.16

It can be concluded from Table 4-4 that, the closed loop system has enough margin of stability and robustness.

Similar to the pitch/roll channel ACAH design cases, in order to evaluate handling quality level of the yaw channel HH controller, bandwidth and phase-delay parameters are obtained from Figure 4-2 using the closed loop frequency response from ψ_{ref} to ψ .

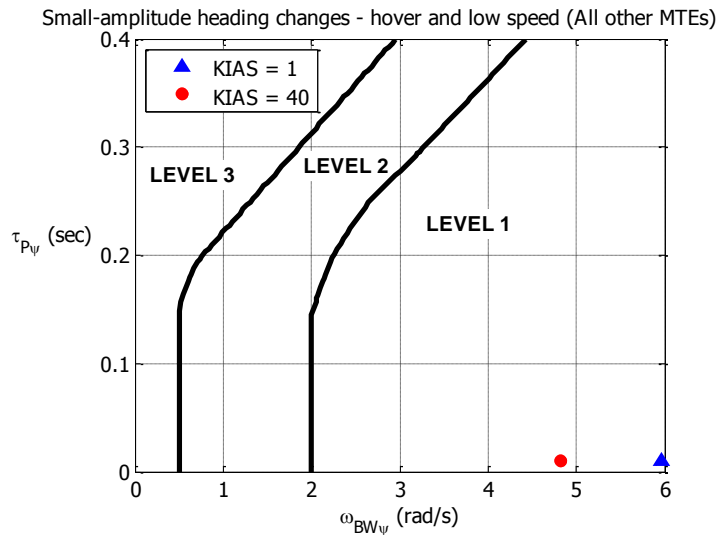


Figure 4-38 Yaw bandwidth assessment – hover and low speed

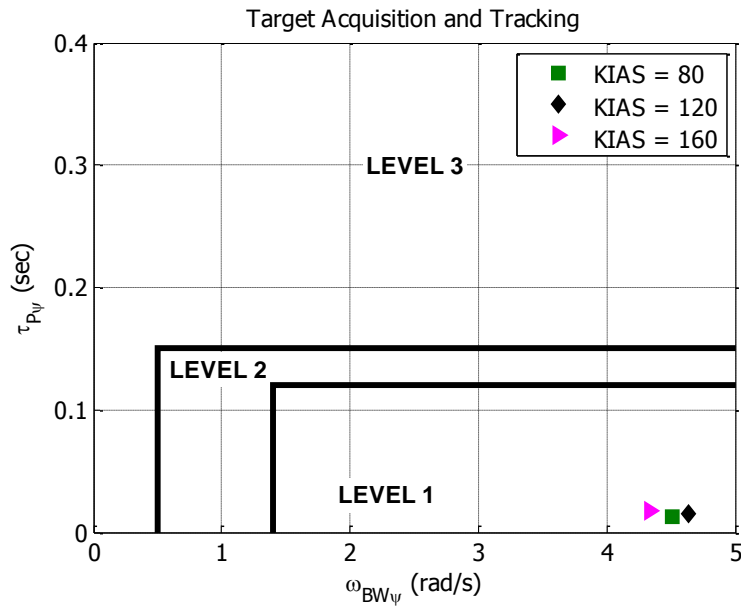


Figure 4-39 Yaw bandwidth assessment – forward flight

Figure 4-38 and Figure 4-39 show that for all airspeeds that the controller is designed for, handling quality level 1 specifications are met for the yaw channel.

4.3.2.4 Assessment of ACAH + HH Controllers Mid-term Response Characteristics

Flight control requirements given in Sections 4.2.1.2 and 4.2.2.2 indicate that closed loop poles must have a damping ratio of at least $\zeta = 0.35$ for HQ level 1.

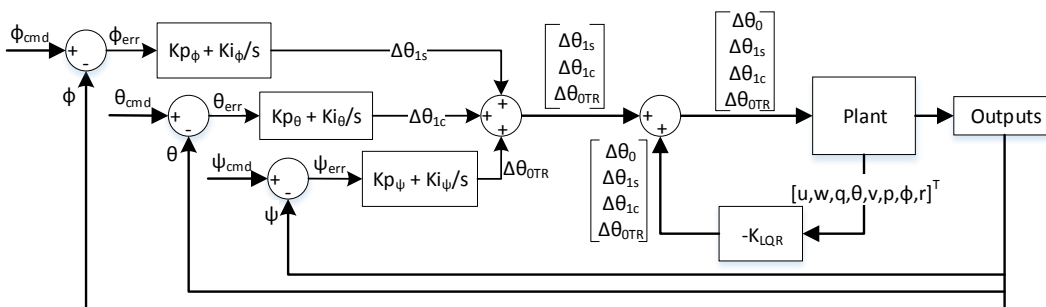


Figure 4-40 ACAH + HH Controllers Structure

In order to check this specification, linear model which consists of plant + LQR + ACAH & HH controllers is used (Figure 4-40). After obtaining closed loop linear model, eigenvalues of the system are investigated.

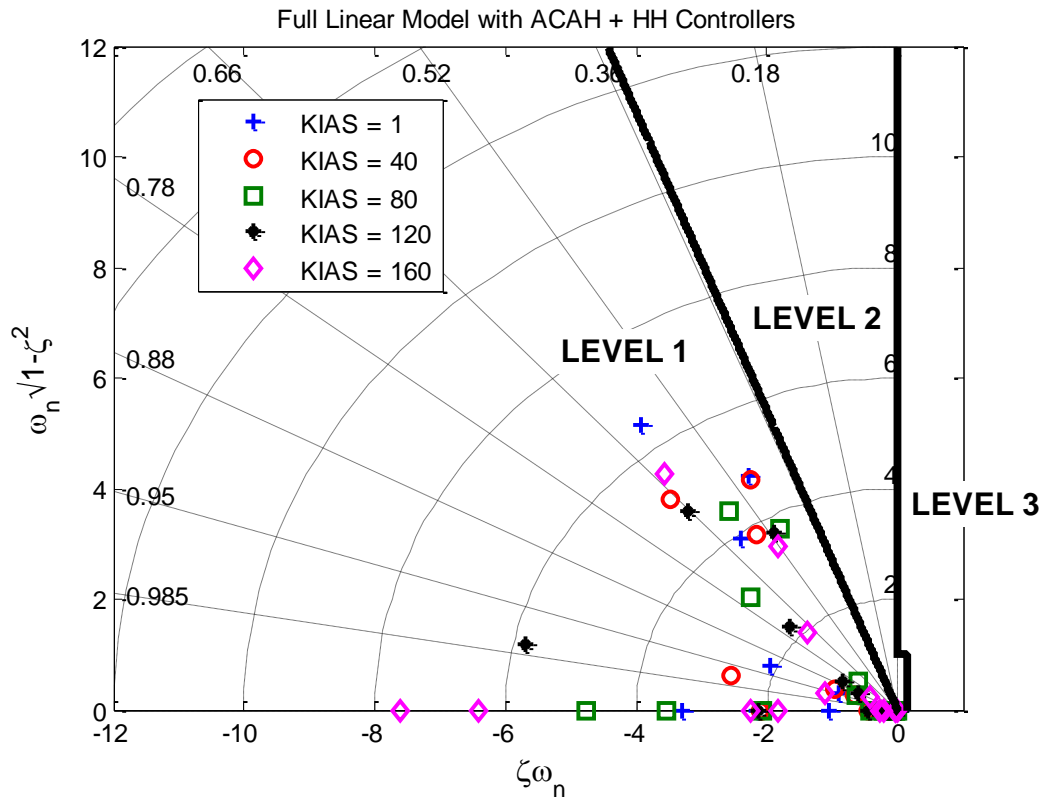


Figure 4-41 ACAH + HH controllers oscillations assessment

Notice that oscillation limits for level 1 handling quality rating are satisfied. Moreover, all eigenvalues given in Figure 4-41 have negative real part. Therefore, helicopter is stable at all airspeeds around which equations of motion are linearized.

4.3.3 Longitudinal Speed Controller Design

For tracking longitudinal speed of the helicopter, a proportional-integral type controller, which generates θ_{ref} commands to the inner loop pitch channel ACAH controller, is used. Reference longitudinal speeds to the controller are generated from the outer loop autorotation controller. Structure of the longitudinal speed hold controller is given in Figure 4-42.

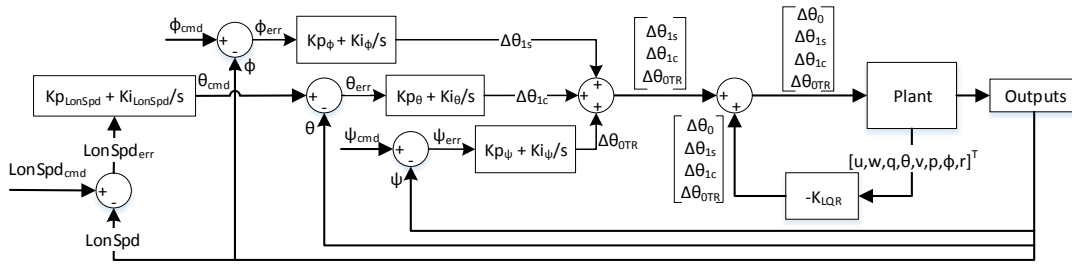


Figure 4-42 Longitudinal Speed Hold Controller Structure

Similar to the ACAH and HH controllers, for each linear model different gains are determined. Figure 4-43 shows responses of the longitudinal speed controllers to reference longitudinal speed step commands. It can be seen that, rise time is less than 3 seconds, settling time is about 10 seconds and maximum overshoot is less than 20% which indicates that the requirements given in Section 4.2.4 are satisfied.

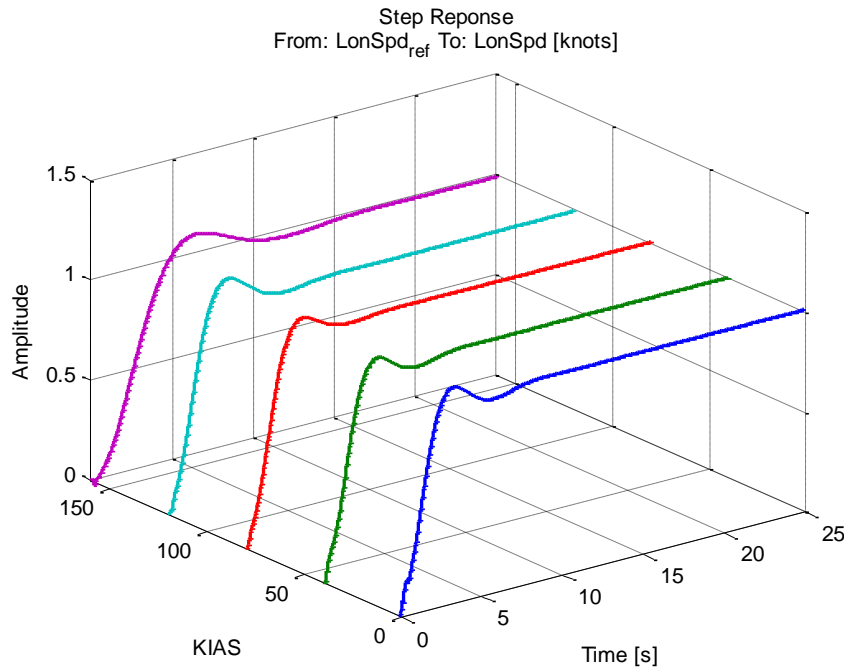


Figure 4-43 ACAH Responses to Reference Longitudinal Ground Speeds

In Figure 4-44, Nyquist plots of five loop gains, which are obtained using full-linear models of five different airspeed conditions, are given. Gain, phase and stability margins together with crossover frequencies obtained from these plots are provided in Table 4-5.

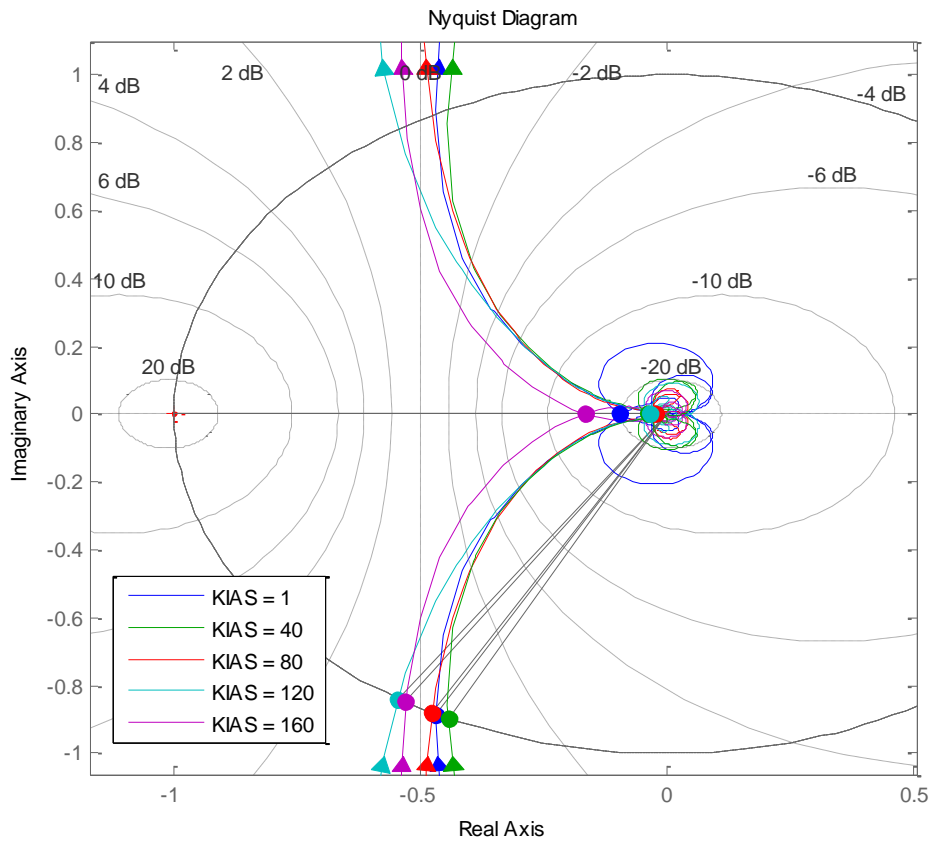


Figure 4-44 Nyquist Plots Longitudinal Speed Controller

It can be concluded from Table 4-5 that, the closed loop system has enough margin of stability and robustness.

Table 4-5 Longitudinal Speed Controller Stability Margins

Airspeed (knots)	g_m (dB)	ω_{pc} (rad/s)	Φ_m (deg)	ω_{gc} (rad/s)	s_m	ω_{ms} (rad/s)
Hover	20.6	45.6	62.1	0.836	0.72	1.36
40	28.3	44	63.7	0.831	0.72	1.42
80	33.8	15.9	61.6	0.786	0.73	1.36
120	29.5	44.1	57	0.766	0.71	1.28
160	17.6	1.45	57.6	0.41	0.66	0.66

4.3.4 Gain Scheduling

Helicopters are nonlinear systems and depending on their operating condition, their dynamics may change. Linearized models, which are used to develop control laws, represent the behavior of nonlinear helicopter around the specified trim conditions only. Therefore, after designing satisfactory linear controllers, transitions between controller gains can be made to cover a wide range of operating conditions.

For gain scheduling, one or more independent variables (airspeed, altitude, helicopter cg, weight etc.) can be used for helicopter. In this study, longitudinal ground speed which alters helicopter dynamics significantly is used as the only gain scheduling variable. As described in previous sections, controllers are developed using linear models around 5 different airspeeds which are hover, 40 knots, 80 knots, 120 knots and 160 knots. Using MATLAB Simulink[®] 1-D lookup tables, PI and LQR controller gains are linearly interpolated as shown in Figure 4-45, based on operating ground speed.

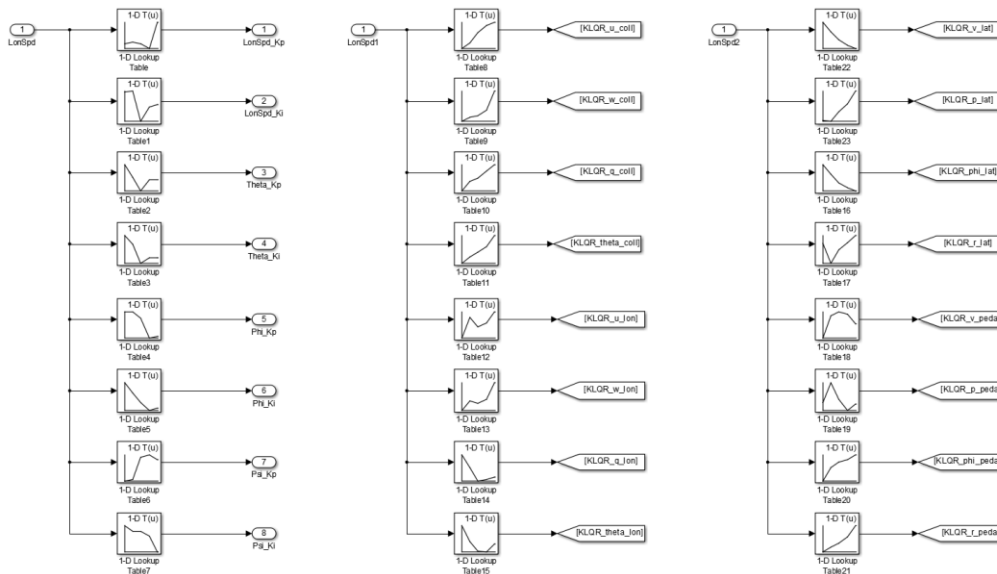


Figure 4-45 1-D Lookup Tables Used for Gain Scheduling

Notice that each element of LQR gain matrices are treated separately. Therefore, for lateral and longitudinal LQR controllers 16 different lookup tables are used. Gain matrices for the LQR control law together with PI controller gains are provided in Appendix D.

4.3.5 Autorotation Controller Design

For designing the outermost loop, similar approach to Sunberg et al. work [21], [22] is used. Autorotation maneuver is divided into 5 different phases, which are steady-state descent, preflare, flare, landing and touchdown (see Figure 4-46) based on height above ground and estimated time to impact assuming constant descent rate. Different control laws are used for different autorotation phases. Each controller provides forward velocity references and maximum allowable pitch attitude limits to the inner loop controller as well as collective commands.

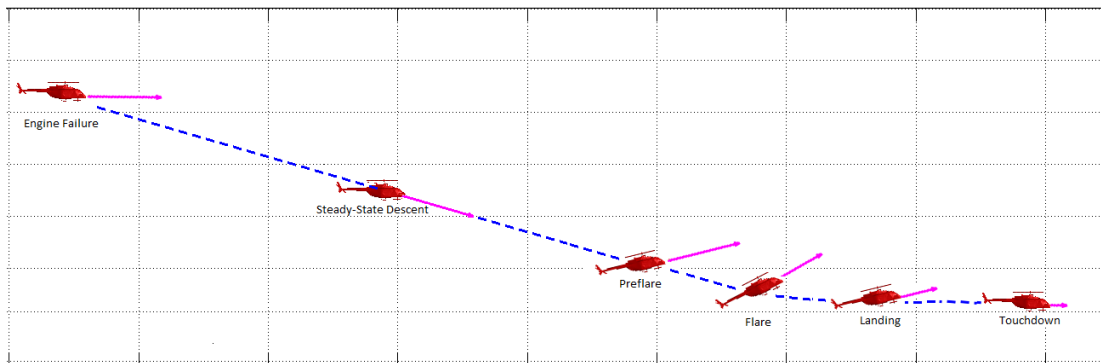


Figure 4-46 Phases of Autorotation Landing Flight

Depending on fuzzily defined autorotation phases (Figure 4-47), controller outputs are blended using trapezoidal membership functions (see Appendix E). By using this kind of approach, abrupt control switching is prevented and transition between phases occur over a period of time.

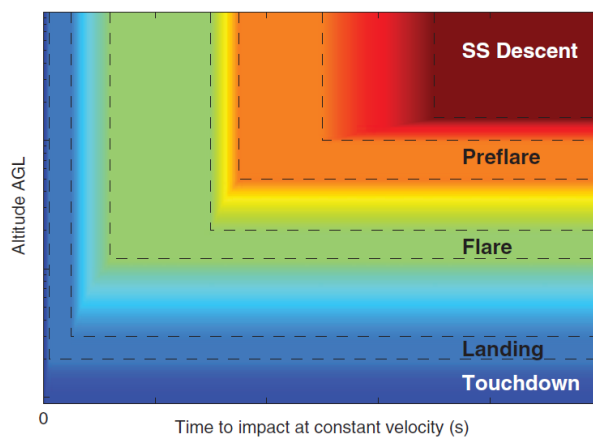


Figure 4-47 Autorotation Controller Phase Diagram [22]

While transitioning between different autorotation phases, backward transitions are not allowed (flare to preflare, landing to flare etc.) even though time to impact or height above ground parameters increase. Also, an autorotation phase is initiated when either of height above ground or estimated time to impact assuming constant descent rate parameters are met.

For calculating weight of these controllers depending on the phase of autorotation, state-flow charts are used. A sample state-flow illustration between preflare and flare phases is shown in Figure 4-48. Each yellow box given in this figure represent different autorotation state. Total number of states are 9, 5 of which represent pure autorotation phases (ss-descent, flare etc.) and 4 of which represent transition between these phases (ex: ss-descent to preflare transition etc.).

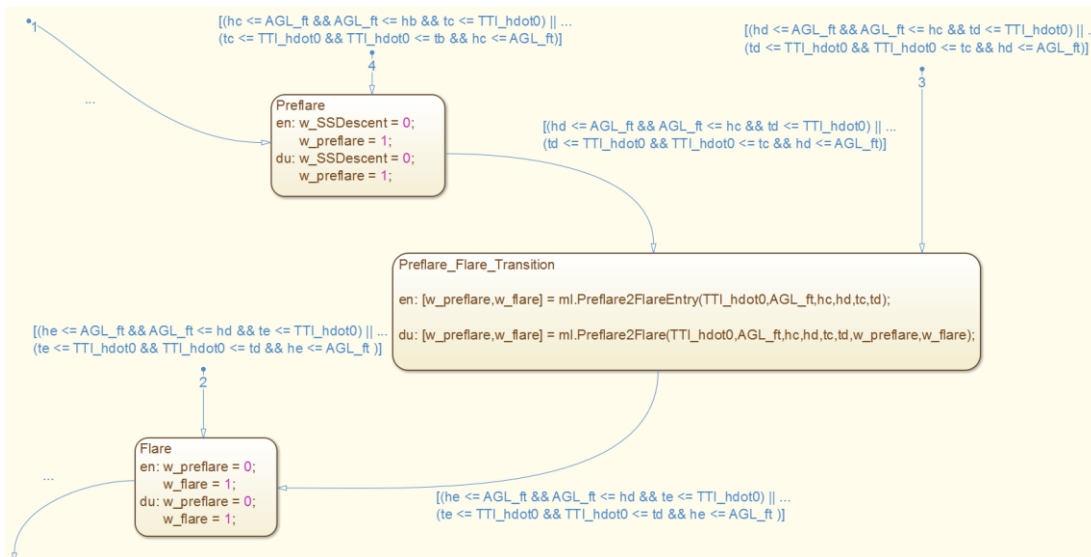


Figure 4-48 State flow of Autorotation Controller Phase Transitions

After engine failure, depending on values of height above ground (h) and time to impact assuming constant descent rate ($TTI_{h=0}$), one state becomes active and calls its function. Weights of autorotation controllers are then calculated using trapezoidal membership functions. Once transition condition to the next state is satisfied (either h or $TTI_{h=0}$), subsequent state becomes active. These phase transitions continue until last phase (i.e. touchdown) is achieved. Notice that only forward transitions are allowed (check arrow directions) as described before.

4.3.5.1 Steady-State Descent Phase

Steady-State descent is the first phase of autorotation in which smooth and rapid reduction of collective pitch angle is required in order to maintain rotational energy of the main rotor. During descent, airspeed of the helicopter is also adjusted depending on the location of landing site. The speed of minimum rate of descent and best angle of glide (range) are of particular importance, as they are useful for saving time or increasing landing distance. In most of the rotorcraft flight manuals, an autorotational speed slightly higher than minimum rate of descent speed which has effective flare capability and yet allows controllable and relatively slow touchdown condition is suggested [38].

In this study real-time path planning is not considered therefore helicopter is forced to a constant airspeed during steady state descent phase, which is u_{SS} . After engine failure, in order to maintain rotor speed within allowable ranges, a PID controller is used. Structure of the controller is given in Figure 4-49. Since engine failure can occur at various airspeeds, the rate of airspeed change (towards u_{SS}) depends on maximum allowable pitch limit, $\theta_{SS,max}$. During steady state descent phase, $\theta_{SS,max}$ is limited by the inner loop speed tracking controller which is determined by considering field of view of test pilots.

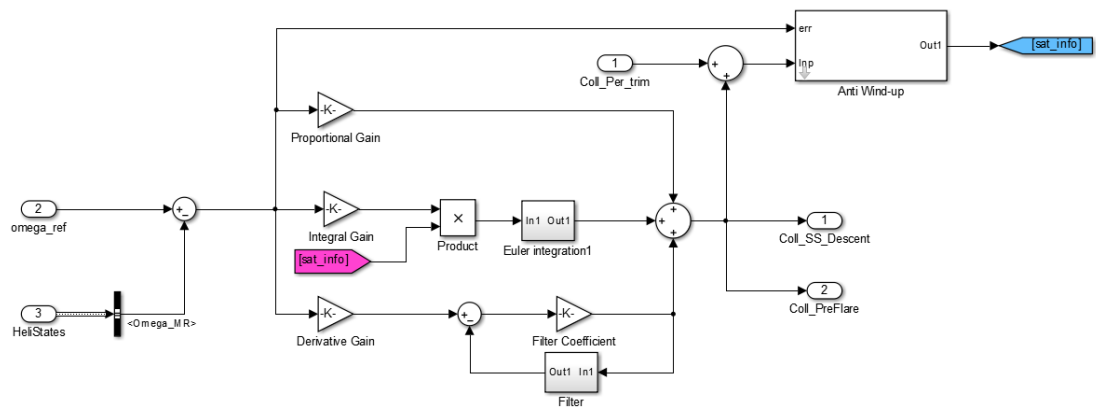


Figure 4-49 Steady State Controller Structure

Anti-wind up block is used to prevent integration wind-up when collective control is saturated. Structure of this block is provided in Figure 4-50.

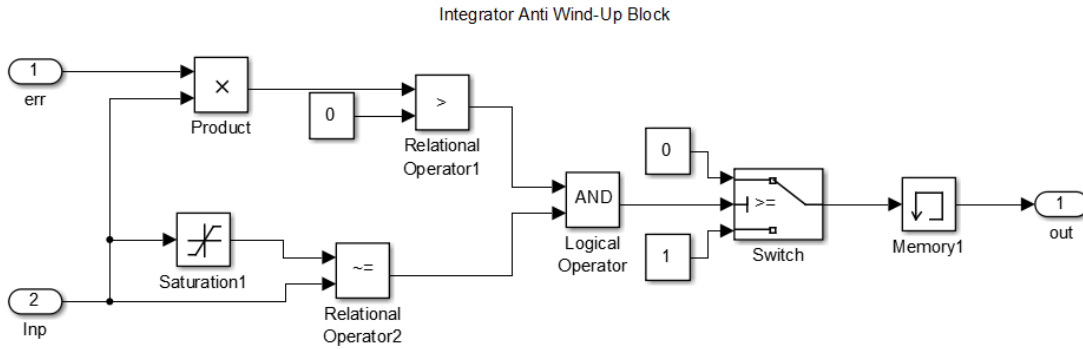


Figure 4-50 Integrator Anti Wind-Up Block

4.3.5.2 Preflare Phase

As can be seen in Figure 4-49, collective commands generated during preflare phase is exactly the same as steady-state descent phase. Moreover, desired airspeed is again u_{ss} . Only difference between preflare phase and steady-state descent phase is the maximum allowable helicopter orientation. In order to achieve a successful and effective flare maneuver, aircraft orientation $\theta_{pf,max}$ is limited just before flare phase.

4.3.5.3 Flare Phase

Flare can be regarded the most difficult stage of autorotation [39] and finding an optimal flare trajectory is very challenging [16]. Considering limited available energy in the rotor, correct timing is critical to utilize this stored energy effectively to arrest descent rate and reduce forward speed before touchdown.

As mentioned in Section 1.1, there are various studies in literature where a state trajectory is sought. In many of these studies, flare phase is discretized into small time intervals and optimal control inputs within a constrained solution space is calculated. There are also some applications in which neural network algorithms are used to generate target flare trajectories based on idealized version of flight test results. Most of the optimization algorithms used for these kinds of studies require significant computational power and they are time inefficient. Drawback of reinforcement learning algorithms is that they require quite a lot of flight data which might be

unavailable. In this study, an approach similar to Sunberg et al. work [22], which has potential to be applied on practical systems, is used.

In order to generate vertical trajectory during flare, “time to impact (TTI) domain” consisting of following four variables is generated.

- $TTI_{\dot{h}=0}$: This parameter is used to estimate time to impact assuming zero vertical acceleration. It is used for autorotation phase transitions. It can be calculated as the ratio of height above ground and constant descent rate $\left(-\frac{h}{\dot{h}}\right)$.
- TTI_L : This parameter is the desired TTI during landing phase. It is used in collective control law of landing phase.
- $TTLE$: This parameter is the desired time before entering landing phase. It is based on available kinetic energy of the system. It is used to calculate desired TTI during flare phase.
- TTI_F : This parameter is the desired TTI during flare phase which is a summation of $TTLE$ and TTI_L parameters. It is used in collective control law of flare phase.

Notice that all parameters except TTI_L (which is constant), are calculated and updated in each time-step of simulation based on feedback states.

As stated before, $TTLE$ is the difference between desired time to impact during flare and landing phases. If available kinetic energy of the system is adequate, helicopter can spend much time during flare phase (i.e. $TTLE$ can be large) and gradual maneuvers can be performed. On the other hand, if total kinetic energy is less than expected, helicopter must flare rapidly and should pass to the landing phase earlier (i.e. $TTLE$ is less).

Available kinetic energy during flare is defined in (4-20) as the summation of rotational energy of the main rotor and energy due to longitudinal speed of the helicopter.

$$KE_{available} = \frac{1}{2}Mu^2 + \frac{1}{2}I_R\Omega^2 \quad (4-20)$$

After obtaining available energy, it can be related to the desired flare entry and exit kinetic energy values as

$$\alpha = \frac{KE_{available} - KE_{flare_{exit}}}{KE_{flare_{entry}} - KE_{flare_{exit}}} \quad (4-21)$$

Where $KE_{flare_{entry}}$ and $KE_{flare_{exit}}$ are simply

$$KE_{flare_{entry}} = \frac{1}{2}Mu_{ss}^2 + \frac{1}{2}I_R\Omega_{des}^2 \quad (4-22)$$

$$KE_{flare_{exit}} = \frac{1}{2}Mu_{tdown}^2 + \frac{1}{2}I_R\Omega_{des}^2 \quad (4-23)$$

Ω_{des} given in (4-22) and (4-23) is the desired main rotor speed during autorotation which is between 90% - 110% NR.

Desired time before entering landing phase can then be calculated as

$$TTLE = TTLE_{max} \times \min(1, \max(0, \alpha)) \quad (4-24)$$

Where $TTLE_{max}$ term is the maximum landing phase entry duration and it is limited by

$$TTLE_{max} = TTI_{F_{max}} - TTI_L \quad (4-25)$$

Notice that in (4-24), $TTLE$ is limited between 0 and $TTLE_{max}$ which indicates that if available kinetic energy is less than desired kinetic energy at flare exit, helicopter enters to landing phase immediately. After computing $TTLE$ parameter, it is summed with TTI_L to get TTI_F which is used to generate vertical trajectory during flare.

While generating flare trajectory, using TTI_F parameter and current helicopter states (height above ground level, h and vertical speed, \dot{h}), desired vertical acceleration $\ddot{h}(t)$

is calculated. This calculation is repeated at each time step, which will result in a time-varying vertical acceleration profile. For a given simulation time t , it is expected for the helicopter to touch the ground after TTI_F seconds. Therefore, assuming constant vertical acceleration following equation can be written

$$h(t + TTI_F) = 0 = h(t) + \dot{h}(t)TTI_F + \frac{1}{2}\ddot{h}(t)TTI_F^2 \quad (4-26)$$

Which gives desired \ddot{h} at time t as

$$\ddot{h}(t)_{des} = -\frac{2h(t)}{TTI_F^2} - \frac{2\dot{h}(t)}{TTI_F} \quad (4-27)$$

Notice that, (4-26) is a second order polynomial and it may have another root before $t + TTI_F$ time (see Figure 4-51) which indicates that helicopter will hit the ground earlier than expected.

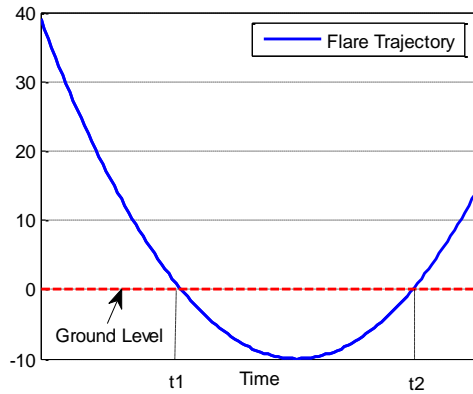


Figure 4-51 Flare trajectory assuming constant vertical acceleration

In order to guarantee that first ground intersection occurs at time equals $t + TTI_F$, derivative of $h(t)$ must be ≤ 0 at $t + TTI_F$ (i.e. t_1). Taking derivative of (4-26) at time $t + TTI_F$ gives

$$\dot{h}(t + TTI_F) = \dot{h}(t) + \ddot{h}(t)TTI_F \leq 0 \rightarrow TTI_F \leq -\frac{\dot{h}(t)}{\ddot{h}(t)} \quad (4-28)$$

Putting this relation into (4-26) will give the condition which guarantees that first ground intersection will occur at $t + TTI_F$

$$TTI_F \leq \frac{-2h(t)}{\dot{h}(t)} \quad (4-29)$$

When (4-29) is satisfied, using vertical acceleration feedback, collective commands are generated by the controller for tracking desired vertical acceleration, $\ddot{h}(t)_{des}$.

If this relation is violated, rapid collective pitch increase is given by the controller. Summing up all these points, collective control law during flare phase can be given as

$$\dot{\theta}_0 = \begin{cases} K_{col} \left(-\frac{2(h + \dot{h}TTI_F)}{TTI_F^2} - \ddot{h} \right) & \text{for } -\frac{2h}{\dot{h}} \geq TTI_F \\ \dot{\theta}_{0F,max} & \text{for } -\frac{2h}{\dot{h}} < TTI_F \end{cases} \quad (4-30)$$

Where K_{col} is a controller tuning parameter and $\dot{\theta}_{0F,max}$ is the rapid collective pitch increase input. It is used when $-\frac{2h}{\dot{h}} < TTI_F$ which indicates that time to impact is less than its desired value. During flare phase, similar to the steady-state descent phase, maximum pitch attitude is limited only by the velocity tracking controller.

4.3.5.4 Landing Phase

After flare phase, just before touchdown, pitch attitude must be reduced in order to avoid tail-boom strike on ground surface. Therefore, maximum pitch attitude during landing phase is limited by $\theta_{land,max}$. As airflow through the rotor disk will decrease when helicopter pitch attitude is leveled, descent rate will increase. In order to compensate this and cushion landing, collective input is applied using the relation given in (4-31).

$$\dot{\theta}_0 = \begin{cases} K_{col} \left(-\frac{2(h + \dot{h}TTI_L)}{TTI_L^2} - \ddot{h} \right) & \text{for } -\frac{2h}{\dot{h}} \geq TTI_L \\ \dot{\theta}_{0L,max} & \text{for } -\frac{2h}{\dot{h}} < TTI_L \end{cases} \quad (4-31)$$

Similar to the control law in flare phase, rapid collective increase ($\dot{\theta}_{0L,max}$) is applied when helicopter is assumed to impact the ground sooner than expected. Target airspeed during landing phase is the same as flare phase which is u_{tdown} .

4.3.5.5 Touchdown Phase

Touchdown phase is the last phase of autorotation in stop the helicopter on ground is the main purpose while keeping helicopter orientation level. In this phase collective is lowered at a constant rate until minimum pitch on ground is reached. Desired airspeed and maximum allowable pitch limit are u_{tdown} and $\theta_{tdown,max}$ respectively.

CHAPTER 5

SIMULATION RESULTS

This chapter includes simulation results of the non-linear helicopter model to which the designed controller is integrated. Starting from various trim points, power-off landings are simulated in order to evaluate control law performance under different flight conditions. For measuring touchdown performance, critical touchdown parameters are compared with the metrics given in Table 5-1.

Table 5-1 Conditions for Successful and Marginal Landings

Parameter	Condition for Successful Landing	Condition for Marginal Landing
Pitch Angle, θ	$< 12^0$	$< 20^0$
Longitudinal Ground Speed	< 35 knots	< 60 knots
Vertical Speed	< 8.5 ft/s	< 15 ft/s

In the first simulation, helicopter is initially trimmed at 300 ft. above ground level with 120 knots forward flight condition. After 2 seconds from the start, both engines are shut down and a sample power-off landing is simulated. Figure 5-1 shows inputs of the controller together with helicopter pitch and roll attitudes.

Notice that after losing both engines, collective is lowered immediately in order to prevent rotor speed decay and let helicopter descent. At the same time, aft cyclic is given by the controller in order to slow down from 120 knots and hold longitudinal speed of the helicopter at the desired value (which is 75 knots for this case). Maximum pitch attitude that is reached during flare phase is 30 degrees and pitch attitude during touchdown is 4.5 degrees. Roll attitude during touchdown is -3.6 degrees.

TOROS
 Initial Speed = 120 knots, Initial Altitude = 300 ft
 Mass = 5400kg
 LG Ext

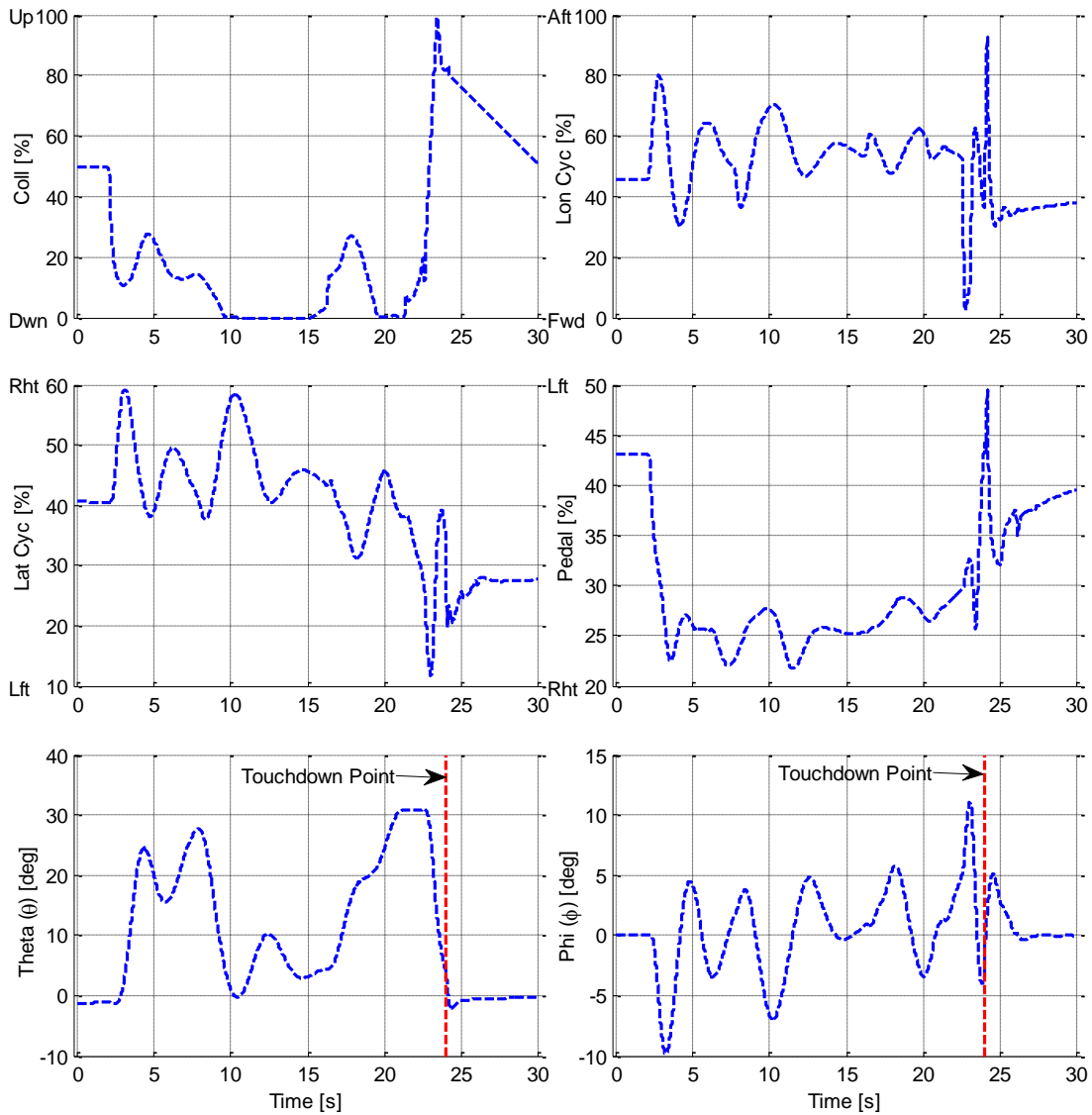


Figure 5-1 Control Inputs and Helicopter Attitude during Power-off Landing

From Figure 5-2 it can be seen that engine power is lost after 2 seconds from the start and because of high anti-torque produced by the tail rotor, heading angle yaws towards left. There is an increase in ground altitude which is caused by the deceleration of aircraft from 120 knots to 75 knots. Helicopter reaches a maximum descent rate of 44 ft/s during steady state autorotation stage. After entering flare phase ($t \cong 17$ sec), both descent rate and longitudinal ground speed start to decrease and at time = 24 seconds,

helicopter landing gear touches the ground. During touchdown, longitudinal ground speed is 28 knots and descent rate is 5.4 ft/s which are within successful landing limits. Results given in Figure 5-2 also show that rotor speed is managed quite well after the power loss.

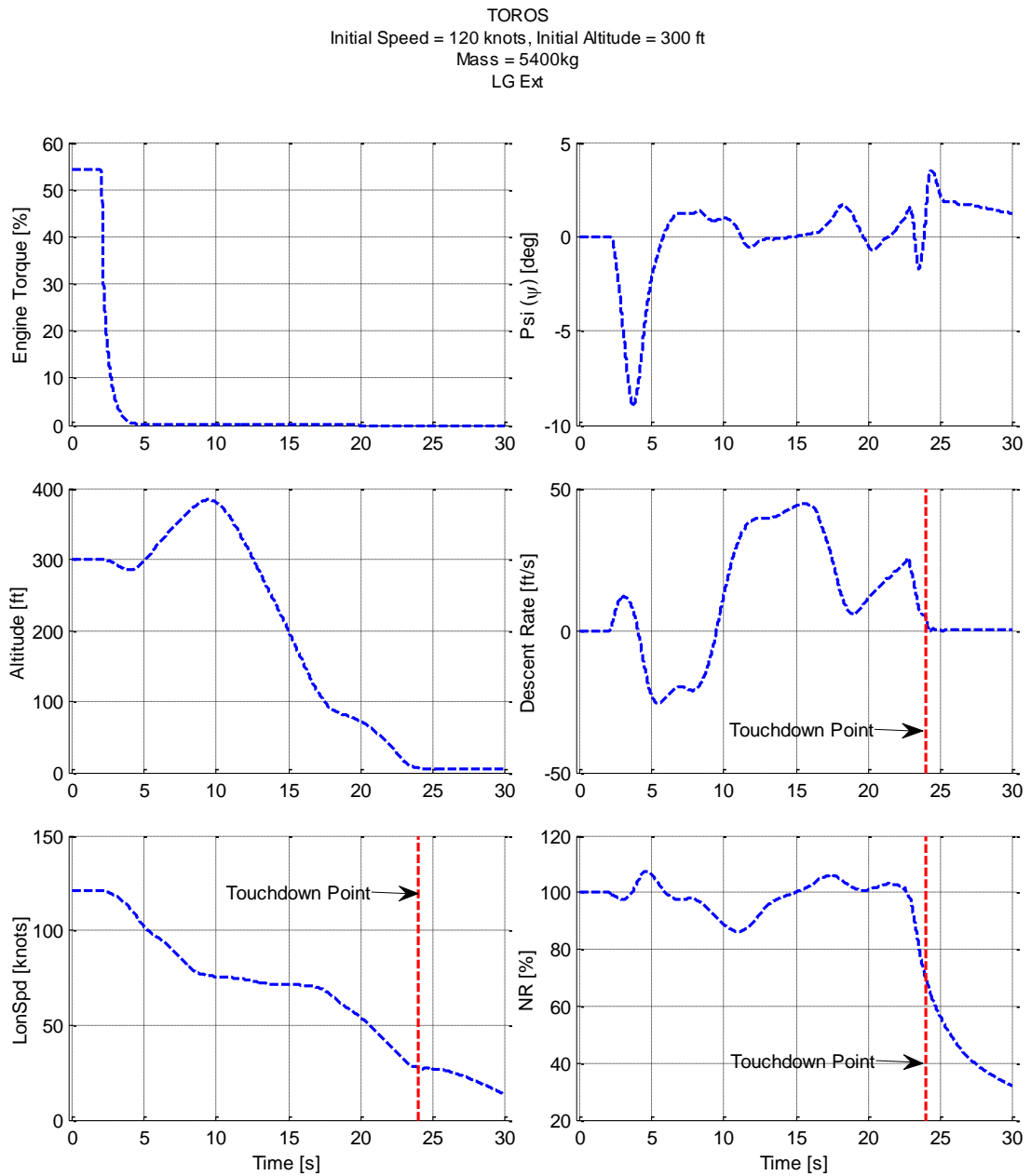


Figure 5-2 Other Autorotation Related Parameters

5.1 Effect of Wind during Autorotation

During autorotation head-wind is preferable since it increases the airflow through the rotor (therefore available energy). In order to see the effect of wind during autorotation, power-off landing simulations are performed with 10 knots head and tail wind conditions. In addition, severe turbulence is applied to the system to assess the performance of the controller under different environment conditions. All simulations are initiated from 75 knots forward flight condition with 300 ft. height above ground.

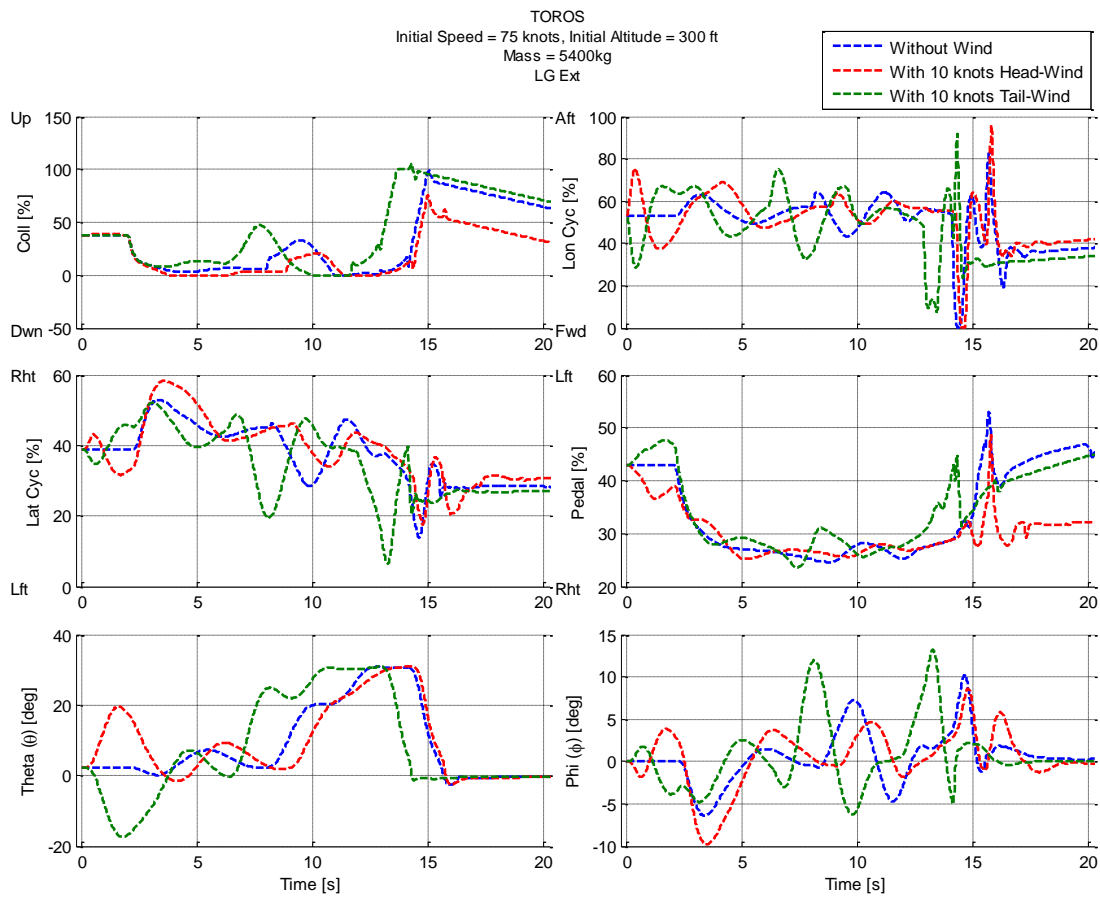


Figure 5-3 Effect of Wind during Power-off Landing - 1

Head and tail winds are applied to the helicopter just after simulation starts. As can be seen from the pitch attitude graph, in order to hold the airspeed at target autorotation speed (75 knots). When there is tail wind, when airspeed is held constant, ground speed of the helicopter increases (i.e. nose down pitch attitude) and when there is head wind

opposite behavior is present. Notice that in Figure 5-4, longitudinal ground speeds during steady state autorotation is different.

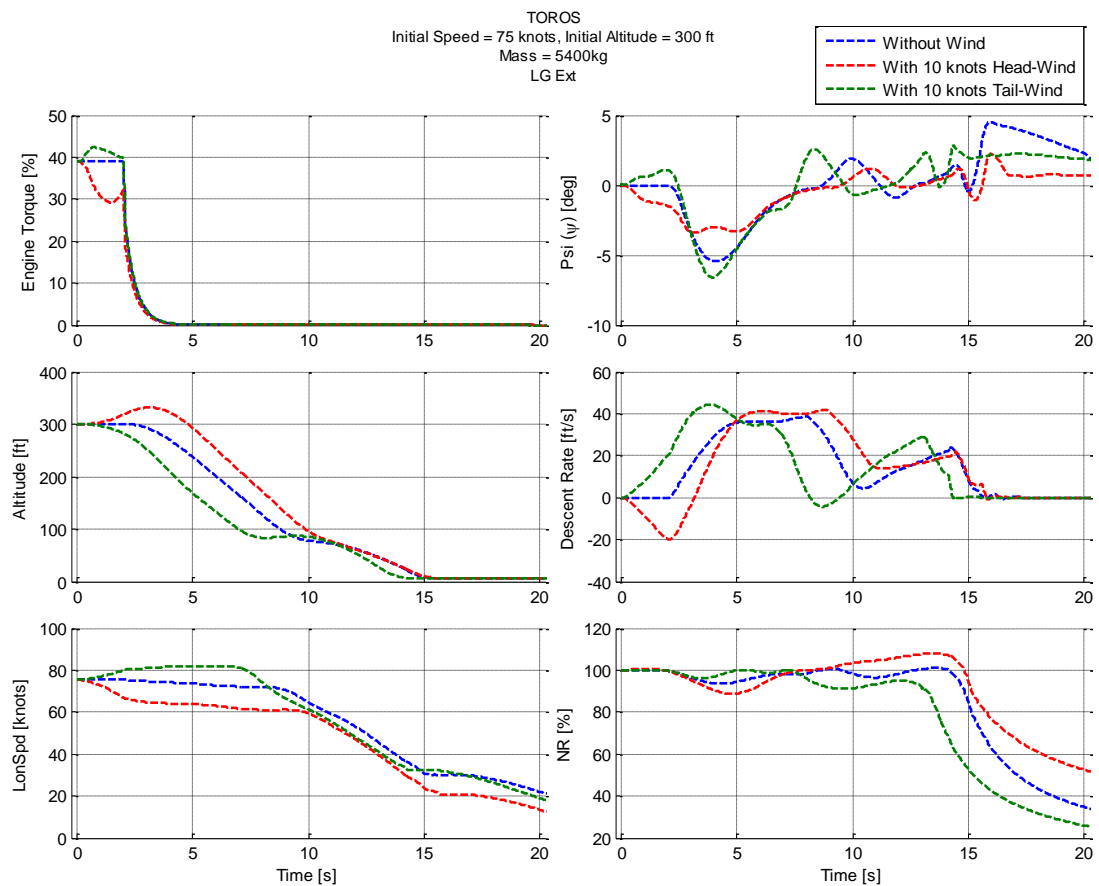


Figure 5-4 Effect of Wind during Power-off Landing – 2

As can be seen from main rotor speed plot, there is less energy in the rotor when the wind is coming from tail direction and it is consumed at a higher rate when compared with other two cases. Moreover, as less energy is available for this case, landing phase is initiated earlier which causes longitudinal ground speed and vertical touchdown speed to be higher for this case. On the other hand, when there is 10 knots of head-wind, ground speed during touchdown is reduced from 30 to 22 knots. Moreover, nearly 80% of rotor kinetic energy is available for this case, during touchdown.

To check controller performance under disturbance, severe turbulence is applied to the system (see Figure 5-5 and Figure 5-6).

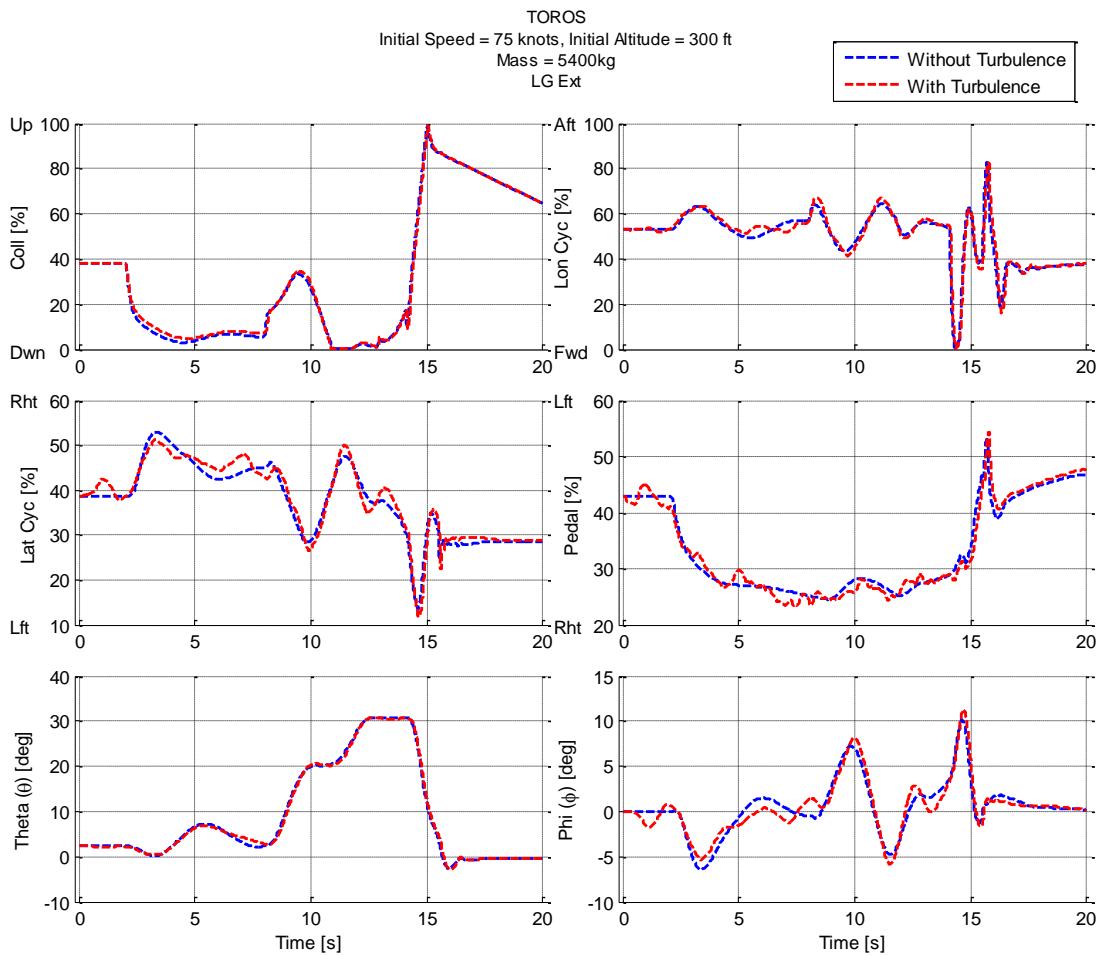


Figure 5-5 Effect of Severe Turbulence during Power-off Landing – 1

Nonlinear simulation results show that even severe turbulence does not have a major impact on controller performance during power-off landing. This might be the effect of inner loop LQR controller which damps these types of disturbances quite fast.

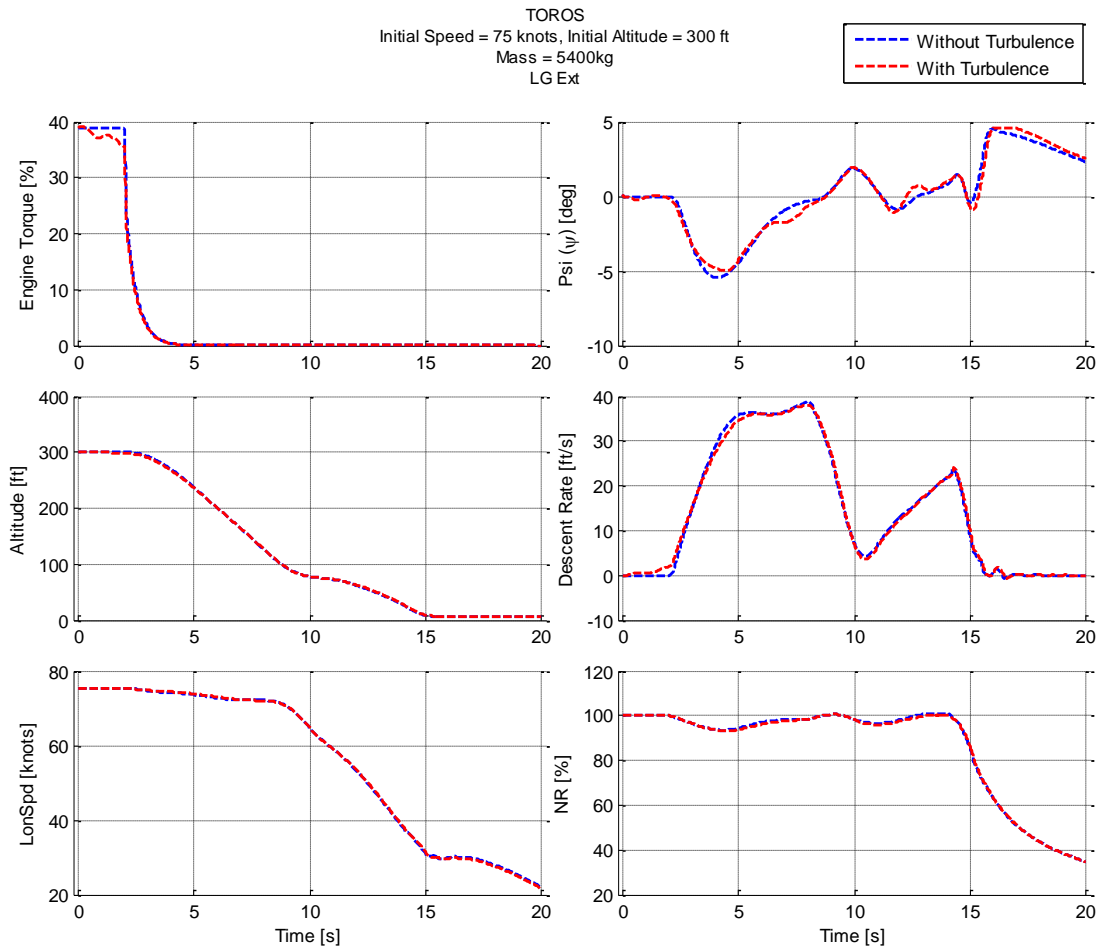


Figure 5-6 Effect of Severe Turbulence during Power-off Landing – 2

There are slight differences in heading angles and vertical descent rate, however both cases with or without turbulence give similar results.

5.2 Effect of Pilot Reaction Time during Autorotation Entry

In the following simulations, the effect of pilot delay after engine loss is investigated. 3 different simulations are performed in which collective controller generates commands immediately after, 1 second after and 2 seconds after engine loss.

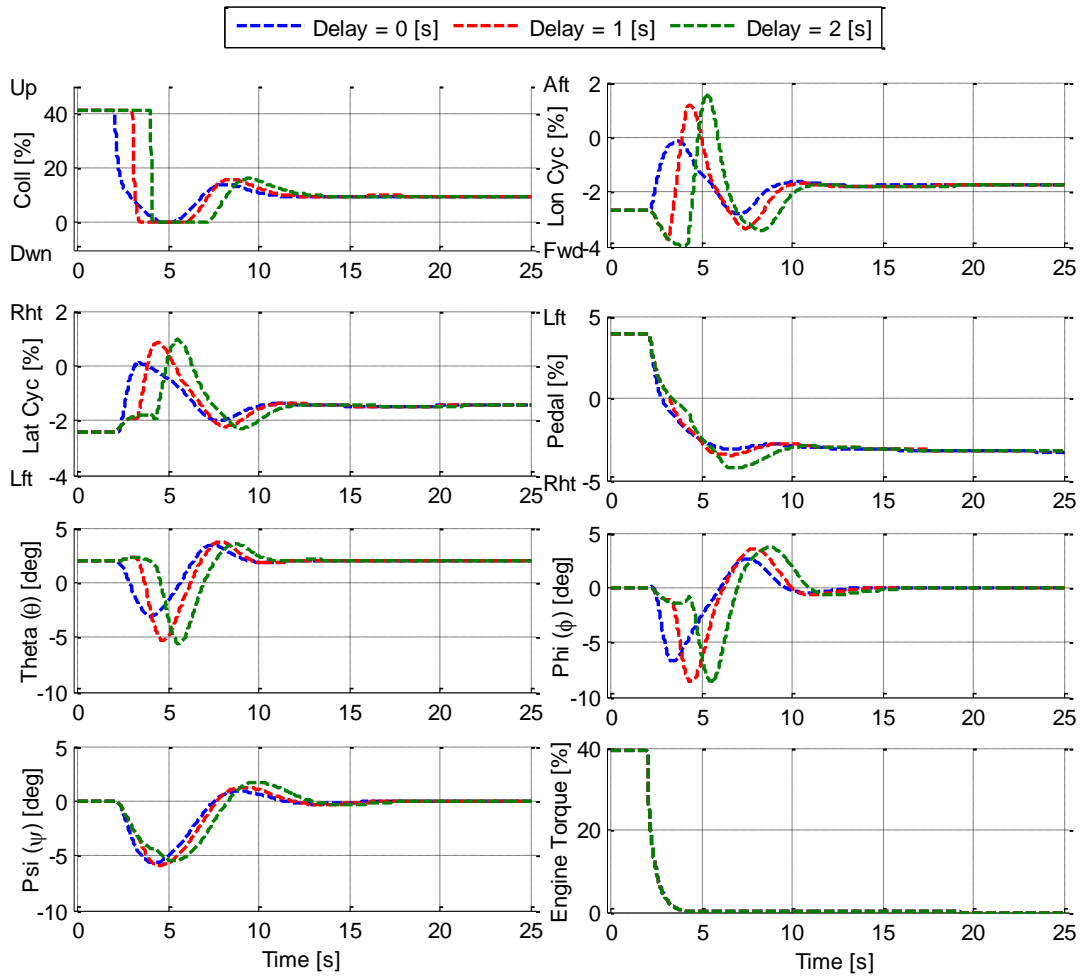


Figure 5-7 Effect of pilot delay during autorotation entry

As can be seen from Figure 5-7, engine torque is lost after 2 seconds and after pilot (or controller) reaction time, collective is lowered immediately in order to prevent rotor speed from exceeding its lower limit. After power loss, right pedal is applied in order to balance the thrust of the vertical tail.

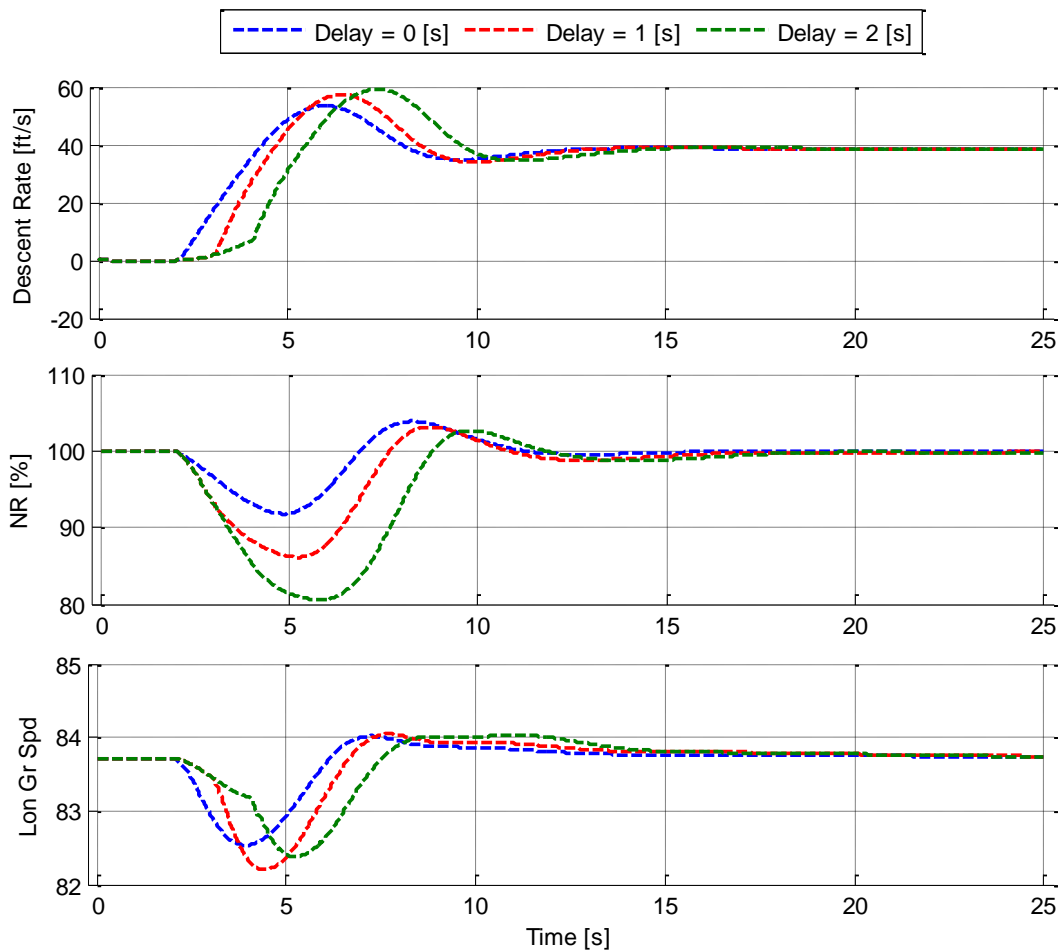


Figure 5-8 Effect of pilot delay during autorotation entry

Figure 5-8 shows that, after power loss, helicopter immediately enters steady state autorotation phase during which descent rate is around 38.5 ft/s (2310 ft/min). During autorotation, power required by the tail rotor is supplied from the main rotor. Total power, on the other hand, is zero. Notice that, when there is no delay, rotor speed reaches a minimum value of 92% during recovery whereas this value reduces to 81% NR when there is 2 second pilot-delay. Figure 5-8 also shows that the controller successfully holds longitudinal speed of the helicopter after power loss.

5.3 Effect of Entry Speed

After trimming the helicopter at 500 ft. AGL using three different airspeeds (30 knots, 75 knots and 130 knots), power-off landing simulations are performed. For 30 knots case, for increasing airspeed, helicopter pitches down as expected. However this also causes descent rate to increase therefore entry to landing state is initiated earlier when it is compared with other two conditions.

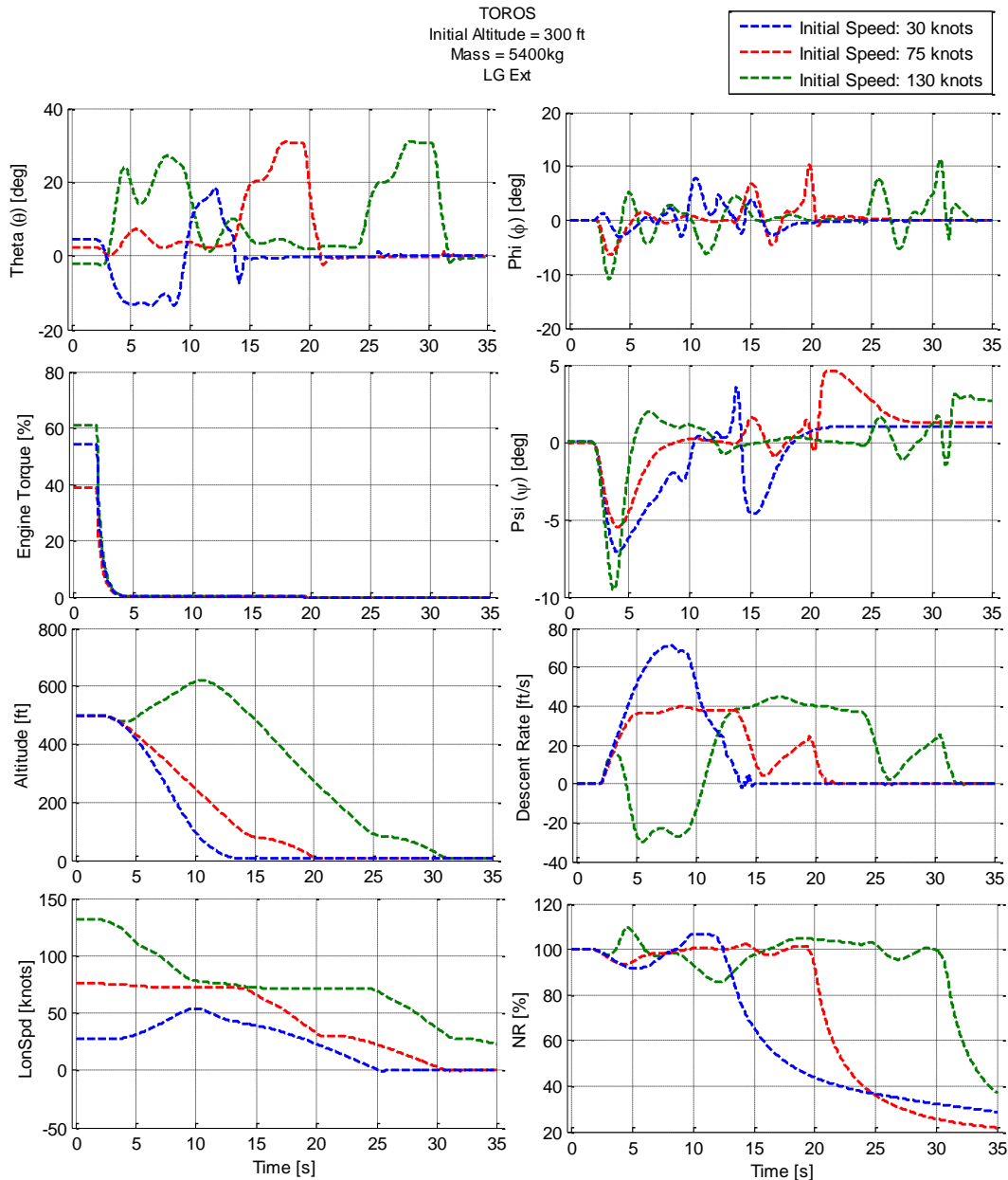


Figure 5-9 Effect of Initial Speed during Power-off Landing

Engine torque plot shows that, total engine power is lost after 2 seconds from the start and helicopter starts to descent after that point in order to keep main rotor speed within desired range. Amount of heading change is less when initial speed is 75 knots because less power (i.e. engine torque) is required for that speed when compared with the 30 and 130 knots cases. When engine loss occurs at 130 knots, velocity tracking controller commands 75 knots as the airspeed reference and therefore pitch attitude increases. This attitude change causes more flow to pass through the rotor disc which increases rotor speed and also altitude. For 30, 75 and 130 knots initial speed conditions, longitudinal ground speeds are recorded as 43, 30 and 25 knots respectively. Although longitudinal ground speed for 30 knots initial speed case is less than condition for marginal landing speed (60 knots) it is slightly higher than the desired forward speed (<35 knots). Possible reason for that is, this initial condition being close or inside of the height-velocity diagram (see Appendix B), where achieving successful landings is either very difficult or impossible. When vertical touchdown speeds of 3 different simulations results are compared, it can be seen that they are very close to each other (5, 3.3 and 5.5 ft/s respectively) and they stay within desired limits (< 8.5 ft/s).

5.4 Pilot in the Loop Simulation Comparison

Among limited number of pilot in the loop simulation tests performed in the system integration lab, a sample power-off landing result, which obeys successful landing conditions defined in Table 5-1 is selected and it is compared with the results achieved by the controller. Both simulations are started from steady-state descent phase with 75 knots of indicated airspeed. As can be seen from the results (see Figure 5-10), 10 knots of head-wind is present during simulations and both cases start with 65 knots of ground speed.

From Figure 5-10 it can be seen that the autorotation controller generates realistic inputs and the behavior of the aircraft is quite similar when compared with the pilot in the loop simulation results. Results show that, descent rate and pitch attitude during touchdown is lower for the autorotation controller case (5.3 ft/s instead of 8.4 ft/s and 4.8 deg instead of 8.7 degrees). Also more energy is preserved in the main rotor for the autorotation controller case, which indicates that available energy is managed more

effectively. There is a slight difference in the longitudinal ground speed of the helicopter (7.7 instead of 3.7 knots) during simulations and it seems that the test pilot managed to land 4 knots slower than the autorotation controller. This can be a reason of increasing pitch attitude earlier and having a higher touchdown pitch attitude. Nevertheless, both cases successfully satisfy the conditions given in Table 5-1. The advantage of using the proposed autorotation controller is that, it gives consistent results and same maneuver can be performed multiple times from various initial conditions which is not possible with pilot in the loop simulations

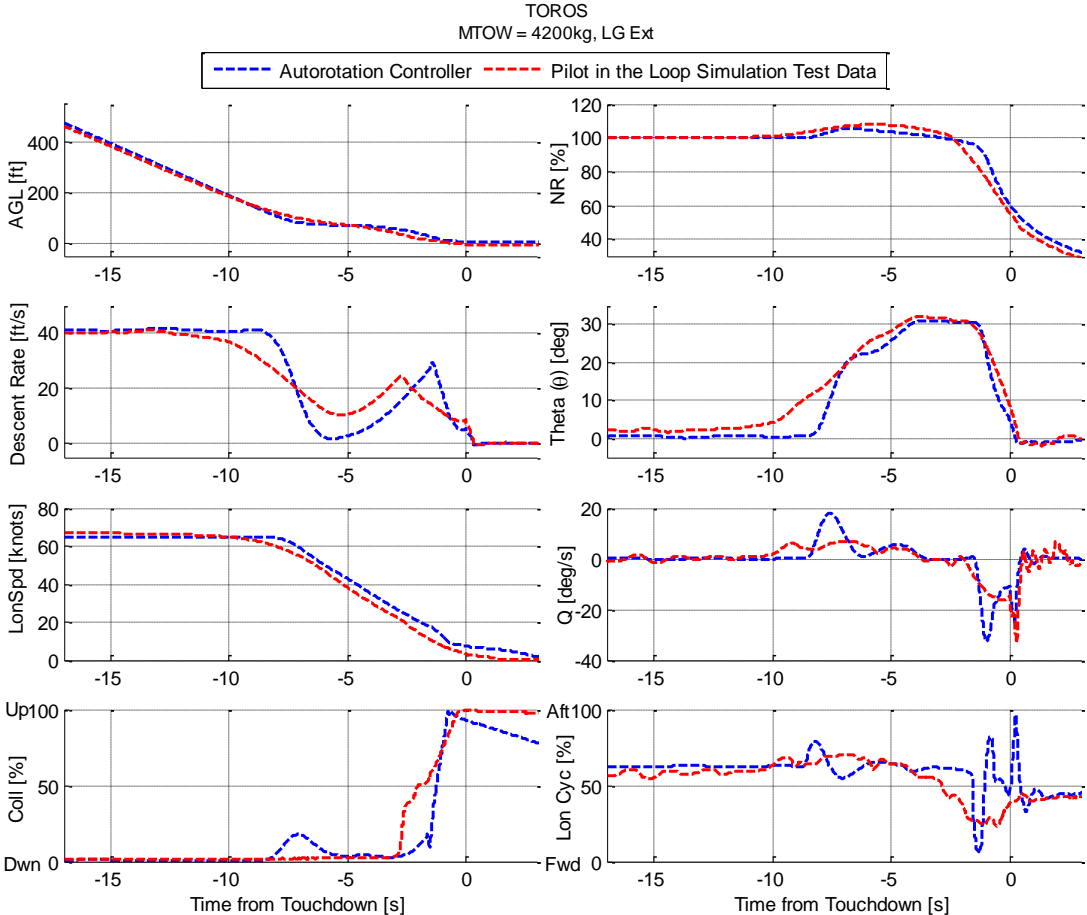


Figure 5-10 Pilot in the Loop Simulations Comparison

From nonlinear simulation results that are provided in this chapter, it can be concluded that using the proposed controller, successful autorotation landings can be performed from various conditions.

CHAPTER 6

CONCLUSION

6.1 Conclusion

In this study an autonomous autorotation controller is proposed and it is implemented to a nonlinear high-fidelity mathematical model of a light utility helicopter. Nonlinear plant model is first linearized around different trim conditions and order of these models are reduced. Comparison results of nonlinear and linear models (both high order and reduced order) show that linear models represent the behavior of the helicopter around these trim points. After linearizing nonlinear plant model, reduced order model is decoupled into lateral and longitudinal dynamics and separate inner loop LQR controllers are designed for these channels. Using performance specifications of ADS-33E-PRF document as a guideline, ACAH and HH controllers are designed as an outer loop to the LQR controller. These controllers are then evaluates as handling quality level 1, using the performance limits defined in [33]. For tracking desired longitudinal velocity during autorotation, a velocity tracking controller, which generates pitch attitude commands to the pitch ACAH controller, is used. In order to perform successful power-off landings, autorotation maneuver is divided into five different phases and different controllers are developed for each of these phases. Outputs of these controllers are blended using trapezoidal membership functions (fuzzy control), which provides smooth transition between controllers. Nonlinear simulation results show that, with the proposed controller, performing realistic, safe and successful power-off landings are possible from various initial conditions.

6.2 Future Work

The study given in this thesis can further be improved with some possible future works that can be done. First of all, during controller design, helicopter model is linearized around 5 different airspeeds and gain scheduling is performed between these points. Other than airspeed, helicopter weight and altitude can also be included as other gain scheduling variables. Secondly, a path planning algorithm, which can generate desired trajectory to the autorotation controller, for safe landing zone selection can be added as an outer loop. Besides that and obstacle avoidance feature can also be included. Additionally, in order to check controller robustness further, sensor models can be implemented to the feedback loops. Finally, this controller can be implemented to and tried on a flight control system of a real helicopter in order to validate simulation results with real flight data.

REFERENCES

- [1] F. Harris, E. Kasper and L. Seler, "U.S Civil Rotorcraft Accidents, 1963 Through 1997," NASA TM-2000-209597, December 2000.
- [2] L. Liu and D. Pines, "Analysis of U.S. Civil Rotorcraft Accidents Caused by Vehicle Failure or Malfunction, 1998-2004," in *61st Annual Forum of American Helicopter Society*, Grapevine, Texas, June 1-3,2005.
- [3] W. Johnson, *Rotorcraft Aeromechanics*, New York: Cambridge University Press, 2013.
- [4] Anon., "Sikorsky S-76 Pilot Training Manual," Flight Safety International, 2000.
- [5] Anon., "Helicopter Flying Handbook," FAA-H-8083-21A, U.S. Department of Transportation, U.S. Federal Aviation Administration,, 2012.
- [6] W. Johnson, "Helicopter Optimal Descent and Landing after Power Loss," NASA TM73244, May 1977.
- [7] T. Wood, "High Energy Rotor System," in *American Helicopter Society 32nd Annual Forum*, Washington, DC, May 10–12, 1976.
- [8] A. Y. Lee, "Optimal Landing of a Helicopter in Autorotation," Ph.D. Thesis, Stanford University, July 1985.
- [9] A. Y. Lee, A. E. Bryson and W. S. Hindson, "Optimal Landing of a Helicopter in Autorotation," *American Institute of Aeronautics and Astronautics, Inc., Journal of Guidance*, vol. 11, no. 1, pp. 7-12, Jan–Feb 1988.
- [10] A. Miele, J. N. Damoulakis, J. R. Cloutier and J. L. Tietze, "Sequential Gradient-Restoration Algorithm for Optimal Control Problems with Non-differential

- Constraints," *Journal of Optimization Theory and Applications*, vol. 13, no. 2, 1974.
- [11] M. W. Floros, "DESCENT Analysis for Rotorcraft Survivability with Power Loss," in *American Helicopter Society 65th Annual Forum*, Grapevine, Texas, May 27–29, 2009.
- [12] L. W. Dooley and R. D. Yeary, "Flight Test Evaluation of the High Inertia Rotor System," USARTL-TR 79-9, U.S. Army Research and Technology Laboratories (AVRADCOM), Fort Eustis, VA, June 1979.
- [13] M. W. Floros, "Application of Sequential Quadratic Programming to Rotorcraft Survivability with Power Loss," in *American Helicopter Society 67th Annual Forum*, Virginia Beach, VA, May 3–5, 2011.
- [14] Y. Okuno and K. Kawachi, "Optimal Control of Helicopter Following Power Failure," *Journal of Guidance, Control and Dynamics*, vol. 17, no. 1, pp. 181-186, Jan–Feb, 1994.
- [15] Y. Okuno, K. Kawachi, A. Azuma and S. Saito, "Analytical Prediction of Height-Velocity Diagram of a Helicopter Using Optimal Control Theory," *Journal of Guidance, Control and Dynamics*, vol. 14, no. 2, pp. 453-459, March–April, 1991.
- [16] P. Abbeel, A. Coates, T. Hunter and A. Y. Ng, "Autonomous Autorotation of an RC Helicopter," in *International Symposium on Robotics*, Athens, Greece, July 14–17, 2008.
- [17] K. Dalamagkidis, K. P. Valavanis and L. A. Piegl, "Autonomous Autorotation of Unmanned Rotorcraft using Nonlinear Model Predictive Control," *Journal of Intelligent and Robotic Systems*, vol. 57, pp. 351-369, 2010.

- [18] S. Tierney and J. W. Langelaan, "Autorotation Path Planning Using Backwards Reachable Set and Optimal Control," in *American Helicopter Society 66th Annual Forum*, Phoenix, AZ, 2010.
- [19] T. Yomchinda, "Real-time Path Planning And Autonomous Control For Helicopter Autorotation," Ph.D. Thesis, The Pennsylvania State University, 2013.
- [20] T. Yomchinda, J. F. Horn and J. W. Langelaan, "Flight Path Planning for Descent-phase Helicopter Autorotation," in *AIAA Guidance, Navigation, and Control Conference*, Portland, Oregon, 08 - 11 August 2011.
- [21] Z. Sunberg and J. Rogers, "A Fuzzy Logic-Based Controller for Helicopter Autorotation," in *51st AIAA Aerospace Sciences Meeting including the New Horizons Forum and Aerospace Exposition*, Grapevine (Dallas/Ft. Worth Region), Texas, 07 - 10 January 2013.
- [22] Z. N. Sunberg, N. R. Miller and J. D. Rogers, "A Real-Time Expert Control System For Helicopter Autorotation," *Journal of the American Helicopter Society*, no. 60, 2015.
- [23] R. B. Mengotti, A. Ragazzi, F. D. Grande, G. Cito and A. B. Zappellini, "AW189 Engine-Off-Landing Certification by Simulation," in *AHS 72nd Annual Forum*, West Palm Beach, Florida, May 17-19, 2016.
- [24] J. Rogers, B. Eberle, M. Jump and N. Cameron, "Time-to-Contact-Based Control Laws for Flare Trajectory Generation and Landing Point Tracking in Autorotation," in *AHS International 74th Annual Forum & Technology Display*, Phoenix, Arizona, May 14-17, 2018.
- [25] Anon., "R44 II Pilot's Operating Handbook and FAA Approved Rotorcraft Flight Manual," Robinson Helicopter Company, Torrance, California, 2014.

- [26] J. G. Leishman, *Principles of Helicopter Aerodynamics*, New York: 2nd ed., Cambridge University Press, 2006.
- [27] K. Şansal, G. Koçak and V. Kargin, "Multi-objective Horizontal Stabilizer Optimization Using Genetic Algorithm," in *AHS International 74th Annual Forum & Technology Display*, Phoenix, Arizona, May 14-17, 2018.
- [28] K. Şansal, K. Volkan and Z. Uğur, "A Generic Ground Dynamics Model for Slope Landing Analysis," in *AHS 72nd Annual Forum*, West Palm Beach, Florida, May 17-19, 2016.
- [29] K. Ogata, "Modern Control Engineering," Prentice Hall, New Jersey, 2010.
- [30] E. Dreier, *Introduction to Helicopter and Tiltrotor Simulation*, Virginia: American Institute of Aeronautics and Astronautics, Inc., 2007.
- [31] G. D. Padfield, *Helicopter Flight Dynamics*, 2nd ed., Blackwell Publishing, 2007.
- [32] MathWorks, "Control System Toolbox For Use With MATLAB: User's Guide (Version 4.2)," January 1999. [Online]. Available: faculty.petra.ac.id/resmana/private/matlab-help/pdf_doc/control/control_tb.pdf. [Accessed 5 11 2017].
- [33] Anon., "ADS-33E-PRF Aeronautical Design Standar Performance Specification Handling Qualities Requirements for Military Rotorcraft," United States Army Aviatiom and Missile Command Aviation Engineering Directorate, Redstone Arsenal, Alabama, 2000.
- [34] C. L. Blanken, R. H. Hoh, D. G. Mitchell and D. L. Key, "Test Guide for ADS-33E-PRF," Commander, U.S. Army Research, Development, and Engineering Command, Moffett Field, CA, 2008.

- [35] D. Karakaş, "Nonlinear Modeling and Flight Control System Design of an Unmanned Aerial Vehicle," MSc. Thesis, Middle East Technical University, September 2007.
- [36] S. J. Shue and J. J. Shillings, "Flight Control System Having a Three Control Loop Design". US Patent 8,473,124 B2, 25 June 2013.
- [37] K. Åström and R. M. Murray, *Feedback Systems: An Introduction for Scientists and Engineers*, New Jersey: Princeton University Press, 2012.
- [38] Anon., "Advisory Circular, AC 29-2C," U.S. Department of Transportation Federal Aviation Administration, 2008.
- [39] N. Grande and J. W. Langelaan, "Safe Autonomous Flare and Landing during Autorotation through Wind Shear," in *AHS 69th Annual Forum*, Phoenix, Arizona, May 21–23, 2013.
- [40] E. A. Fradenburgh, "A Simple Autorotative Flare Index," Sikorsky Aircraft, Stratford, Connecticut.
- [41] Y. Bai, H. Zhuang and D. Wang, *Advanced Fuzzy Logic Technologies in Industrial Applications*, London: Springer, 2006.
- [42] MathWorks, "Fuzzy Logic Toolbox: User's Guide (R2018a)," 2018. [Online]. Available: https://www.mathworks.com/help/pdf_doc/fuzzy/fuzzy.pdf. [Accessed 30 April 2018].

APPENDIX A

AUTOROTATIVE INDEX

Autorotative index, which is based on the physical properties of the rotor system, is used to estimate autorotation flare to landing performance of a helicopter. The index is proportional to rotor kinetic energy and inversely proportional to the product of gross weight and disc loading. In other words, it is the ratio of energy available to energy required. Non-dimensional index can be defined as in [40];

$$AI_{ND} = g\rho_{SL} \frac{(I_R \Omega_N^2)}{W \times DL} \left(\frac{\rho}{\rho_{SL}} \right) \quad (A-1)$$

Notice that this index is based on highly simplified set of assumptions and account for main rotor inertia, rotorcraft gross weight, disk loading and density altitude.

Dropping the dimensional g and ρ_{SL} terms (Sikorsky Aircraft approach) and considering sea level conditions, $\left(\frac{\rho}{\rho_{SL}} \right) = 1$, autorotative index is reduced to;

$$AI = \frac{(I_R \Omega_N^2)}{W \times DL} \quad (A-2)$$

The terms I_R , Ω_N , W and DL given in (A-2) represents main rotor mass moment of inertia, nominal rotor speed, helicopter gross weight and disk loading respectively.

Figure A-1 illustrates the index of various helicopters at sea level. Notice that, for most of the helicopters, autorotative index is given as a single point, which represents the index at nominal gross weight.

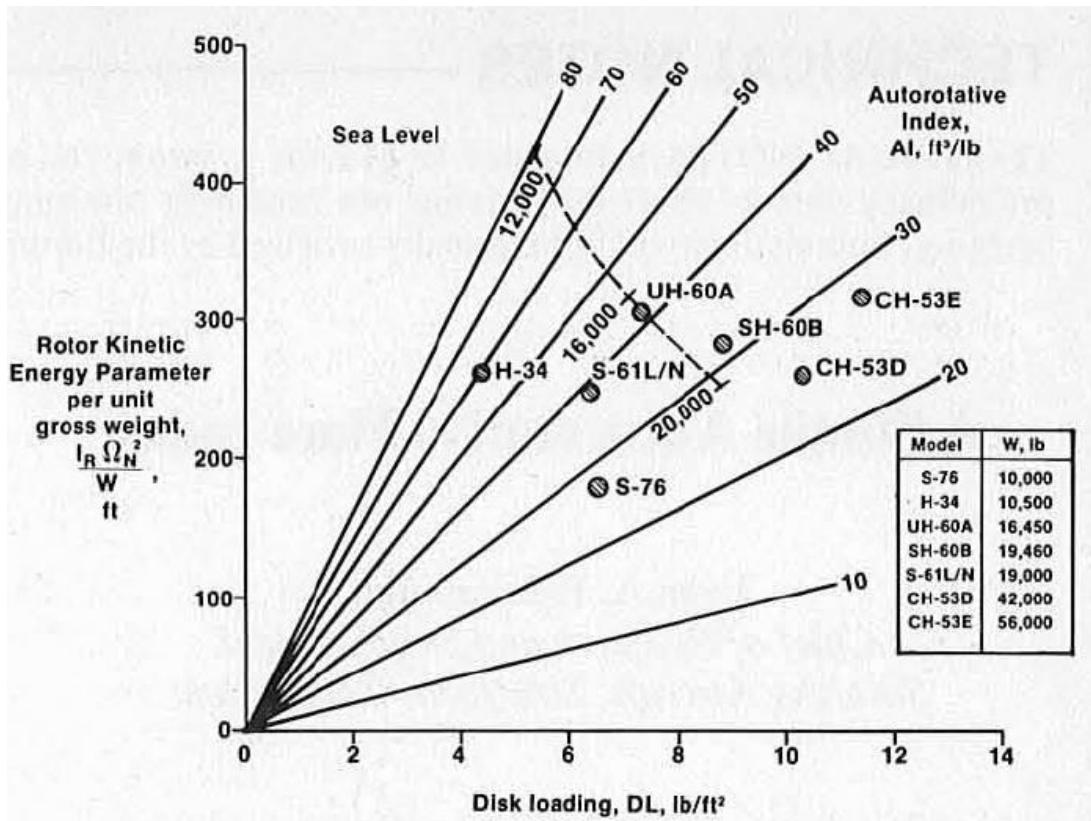


Figure A-1 Autorotative index of various helicopters [40]

Figure A-1 shows that, rotors with high inertia and low disk loadings have higher index which is favorable during flare maneuver. It is also illustrated that, in order to keep the autorotation index constant, rotor kinetic energy per unit gross weight $\left(\frac{I_R \Omega_N^2}{W}\right)$ must be increased with the disk loading.

APPENDIX B

HEIGHT VELOCITY DIAGRAM (DEADMAN'S CURVE)

In case of a power failure, the ability of a helicopter to perform a safe autorotative landing is limited by the structural and aerodynamic design of the helicopter together with the condition it is flying at (i.e. height above ground and airspeed). A height/velocity (H/V) diagram (also called deadman's curve), depicts the critical combinations of airspeed and altitude where successful landing from autorotation is not possible. Figure B-1 represents the examples of height-velocity curves for single and multi-engine helicopters.

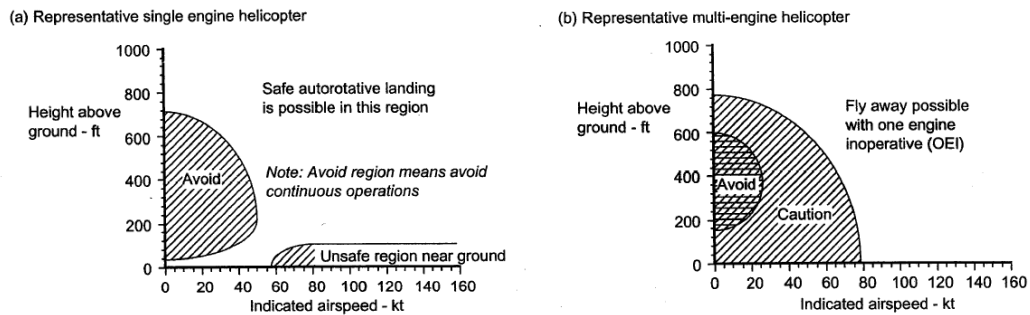


Figure B-1 Representative height-velocity curves for a single-engine and multi-engine helicopters [26]

Notice that continuous operations within the dashed regions must be avoided since power loss inside these regions may result in severe accidents. Although limits of H-V curves depend on many factors like helicopter characteristics, rotor inertia, gross weight, operational density altitude etc. avoid regions are defined such that a pilot with average piloting skills is able to perform safe autorotation.

The main difference between H-V diagram of single and multi-engine helicopters is that, for single engine helicopters there exists a second avoid region at high-speed flight near ground. This low altitude and high-speed region can be marked for the multi

engine helicopters as well to prevent unsafe operations close to the ground. This region (high-speed regime) describes the envelope for both engine and tail rotor failure condition where forward speed is higher than the limit landing speed and the height above ground level is less than required for landing without crash. Moreover, at low altitude high airspeed region of the diagram, there is a great chance that engine failure will shortly result in ground contact without the notice of the pilot.

At low-speed regime (low & high hover) there is no chance to increase the forward speed or reduce the sink speed of helicopter below the forced landing limit. In multi engine H-V diagram there is also a “caution” region in which available power from the remaining engine(s) is less than the required power but successful landing from autorotation is possible.

These H-V curves are identified by test flights during certification and qualification of the helicopter.

APPENDIX C

REDUCED ORDER MODEL STATE AND CONTROL MATRICES

In this section, state (A) and control (B) matrices of the reduced order model, which represents stability and control derivatives of a system, is provided for 80 knots forward flight condition. More information about these derivatives, as well as examples of A and B matrices of different helicopters (Lynx, Puma and Bo105) at various airspeeds, can be found in [31].

V = 80 kts

A Matrix

-0.0288	0.0457	-0.9006	-9.7562	0.0012	-0.3753	0.0000	-0.1034
-0.0119	-0.7758	41.2648	-0.3243	-0.0201	1.8708	0.1787	0.6656
0.0045	0.0054	-1.0169	0.0000	0.0121	0.0665	0.0000	-0.0443
0.0000	0.0000	0.9998	0.0000	0.0000	0.0000	0.0000	0.0172
0.0082	-0.0151	-0.1564	0.0060	-0.1248	1.2873	9.7546	-40.8471
-0.0203	0.1115	-0.4551	0.0001	-0.0747	-2.3697	0.0000	0.0865
0.0000	0.0000	-0.0006	0.0000	0.0000	1.0000	0.0000	0.0326
-0.0159	-0.0019	-0.0110	0.0000	0.0343	-0.3734	0.0000	-0.5829

B Matrix

0.0156	-0.0313	-0.0042	-0.0011
-0.3062	-0.1215	-0.0073	-0.0060
0.0150	0.0401	0.0047	-0.0077
0.0000	0.0000	0.0000	0.0000
-0.0076	-0.0043	0.0103	0.0273
0.0399	-0.0063	0.1145	0.0216
0.0000	0.0000	0.0000	0.0000
0.0195	-0.0045	0.0182	-0.0385

APPENDIX D

CONTROLLER GAINS USED IN THE STUDY

This section summarizes the gains that are used during control law development.

For LQR Controllers

$$K_{LQR_{hover}} = \begin{bmatrix} 2 \times 10^{-7} & 1.2 \times 10^{-6} & 0.16 & 0.04 & 0 & 0 & 0 & 0 \\ 0.025 & 0.015 & 162.7 & 38.81 & 0 & 0 & 0 & 0 \\ 0 & 0 & 0 & 0 & 0.197 & 17.18 & 21.0 & 13.95 \\ 0 & 0 & 0 & 0 & -0.419 & 13.96 & 6.29 & -112.1 \end{bmatrix}$$

$$K_{LQR_{40}} = \begin{bmatrix} 5 \times 10^{-6} & 2 \times 10^{-4} & 0.26 & 0.05 & 0 & 0 & 0 & 0 \\ 0.063 & 0.12 & 122.5 & 27.16 & 0 & 0 & 0 & 0 \\ 0 & 0 & 0 & 0 & 0.01 & 16.99 & 16.65 & 10.02 \\ 0 & 0 & 0 & 0 & 0.02 & 16.06 & 10.39 & -109.4 \end{bmatrix}$$

$$K_{LQR_{80}} = \begin{bmatrix} 1 \times 10^{-4} & 3 \times 10^{-4} & 0.31 & 0.07 & 0 & 0 & 0 & 0 \\ 0.045 & 0.09 & 83.47 & 20.55 & 0 & 0 & 0 & 0 \\ 0 & 0 & 0 & 0 & -0.13 & 19.0 & 13.06 & 12.61 \\ 0 & 0 & 0 & 0 & 0.09 & 14.2 & 12.13 & -107.1 \end{bmatrix}$$

$$K_{LQR_{120}} = \begin{bmatrix} 2 \times 10^{-4} & 6 \times 10^{-4} & 0.39 & 0.09 & 0 & 0 & 0 & 0 \\ 0.052 & 0.14 & 86.35 & 20.33 & 0 & 0 & 0 & 0 \\ 0 & 0 & 0 & 0 & -0.24 & 20.61 & 11.13 & 14.18 \\ 0 & 0 & 0 & 0 & 0.04 & 13.13 & 12.92 & -103.3 \end{bmatrix}$$

$$K_{LQR_{160}} = \begin{bmatrix} 2 \times 10^{-4} & 1 \times 10^{-3} & 0.47 & 0.13 & 0 & 0 & 0 & 0 \\ 0.074 & 0.34 & 93.72 & 25.75 & 0 & 0 & 0 & 0 \\ 0 & 0 & 0 & 0 & -0.29 & 23.17 & 9.74 & 15.63 \\ 0 & 0 & 0 & 0 & -0.144 & 13.74 & 14.52 & -96.38 \end{bmatrix}$$

For PI Controllers

Airspeed (knots)	$K_{P\phi}$	$K_{i\phi}$	$K_{P\theta}$	$K_{i\theta}$	$K_{P\psi}$	$K_{i\psi}$	$K_{p_{LonSpd}}$	$K_{i_{LonSpd}}$
Hover	1.51	1.14	4.28	2.4	-2.51	-0.48	-2.46	-0.03
40	1.51	0.91	3.57	2	-2.44	-1.1	-2.37	-0.03
80	1.41	0.71	2.85	1.14	-1.33	-1.1	-2.46	-0.09
120	1.11	0.56	3.43	1.37	-1.19	-1.65	-2.7	-0.06
160	1.13	0.6	3.43	1.37	-1.46	-3.3	-1.26	-0.05

APPENDIX E

TRAPEZOIDAL MEMBERSHIP FUNCTION

Membership functions are used to represent a fuzzy set graphically. A membership function of a fuzzy set is a curve which is used to map each point of an input space between 0 and 1. There are different types of membership functions which are, triangular, trapezoidal, Gaussian, S-curve waveforms etc... For systems that have rapid dynamic variations over a short period of time, in general, triangular or trapezoidal membership functions are used [41]. Considering different phases of autorotation and significant dynamic changes between these phases, trapezoidal membership functions are utilized in this study. As described in [42], the trapezoidal curve is a function of a vector, x , and depends on four scalar parameters a , d (feet of the trapezoid) and b , c (shoulders of trapezoid) which can be given as;

$$f(x; a, b, c, d) = \begin{cases} 0, & x \leq a \\ \frac{x-a}{b-a}, & a \leq x \leq b \\ 1, & b \leq x \leq c \\ \frac{d-x}{d-c}, & c \leq x \leq d \\ 0, & d \leq x \end{cases} \quad (\text{E-1})$$

MATLAB built-in function *trapmf* can be used to define a trapezoidal shaped membership function as in Figure E-1.

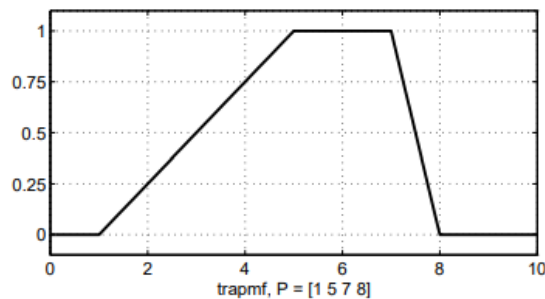


Figure E-1 Example of MATLAB *trapmf* function